Development of an Interferometric Oxygen Analyzer for Precise Measurement of the Atmospheric O_2 Mole Fraction

A thesis presented

by

Ralph Franklin Keeling

to

The Division of Applied Sciences

in partial fulfillment of the requirements
for the degree of
Doctor of Philosophy
in the subject of
Applied Physics

Harvard University
Cambridge, Massachusetts

January, 1988

Abstract

A long-standing challenge in atmospheric science has been the detection of changes in the atmospheric O_2 mole fraction which are believed to occur at the 0.0001 to 0.001 mole % level in background air. A novel optical method for atmospheric oxygen analysis is described. The method relies on measuring changes in the relative refractivity of dry air between 4358 and 2537Å. A prototype analyzer has been constructed which has demonstrated a resolution of 0.00005% on synthetic air samples. Application of the method for accurate measurement of changes in atmospheric oxygen will require the independent measurement or elimination of CO_2 and other variable trace gases which can also cause variations in relative refractivity. Measurements of long-term changes in O_2 will also require the development of highly-stable standards for mixtures of O_2 in air.

The instrument has been used in conjunction with a non-dispersive infrared CO_2 analyzer to measure short-term variations in atmospheric O_2 and CO_2 in Cambridge, Massachusetts. Changes in O_2 were shown to be strongly anticorrelated with changes in CO_2 as expected for combustion processes.

Major questions which can be addressed with this instrument include the following: What are the amplitudes of seasonal variations in atmospheric O_2 which, like CO_2, are expected due to respiratory exchange with land plants and soils? What is the contribution of air-sea exchange to seasonal variations in atmospheric O_2? What is the long-term rate of change in atmospheric O_2, which should be declining annually by 0.0003% from burning fossil fuel, but which also

depends on changes in carbon storage in the land biosphere? Answers to these questions would constrain estimates of primary productivities of land and ocean ecosystems and estimates of long-term changes in biospheric reservoirs.

Estimates are presented for industrial O_2 consumption, and for O_2/CO_2 exchange ratios with the land biosphere. Upper bounds are presented for the net-O_2 fluxes due to imbalances between weathering rates and sedimentation rates and due to long-term changes in oceanic dissolved O_2.

Contents

Abstract iii

List of Figures vii

List of Tables ix

Acknowledgements x

1 Introduction 1

2 The Interferometric Oxygen Analyzer 18
- 2.1 Physical Basis of Measurement 18
- 2.2 Details of Operation 26
- 2.3 Laboratory Test Results 33
- 2.4 Sources of Measurement Error 37
  - 2.4.1 Signal Intensity Stability 37
  - 2.4.2 Scanning-Gas Concentration 38
  - 2.4.3 Sample-Gas Density 38
  - 2.4.4 Temperature 40
- 2.5 References 44

3 Air Measurements in Cambridge 47
- 3.1 Introduction 47
- 3.2 Experimental Method 48
- 3.3 Results and Discussion 49
- 3.4 Comparison with Previous Studies 57
- 3.5 Conclusions 61
- 3.6 References 62

4 The Contemporary Oxygen Budget **64**
4.1 Introduction 64
4.2 The Oxygen Cycle 66
4.3 The Human Imprint on Atmospheric O_2 72
4.4 Industrial Oxygen Consumption 75
4.4.1 Oxygen Consumption Factors for Fossil Fuels 77
4.4.2 Fossil-Fuel Oxygen Consumption 88
4.4.3 Other Industrial Activities 96
4.5 Oxidative Ratios of Terrestrial Carbon 100
4.6 Natural O_2 Sources and Sinks 103
4.6.1 Weathering and Sedimentation 103
4.6.2 Ocean Net Sources or Sinks 104
4.7 Scenarios for Recent O_2 Depletion 115
4.8 Summary 123
4.9 References 124

5 Concluding Remarks **131**

A Derivation of Sensitivity Relation **141**

B Relative Refractivity Measurements **143**
B.1 Introduction 143
B.2 Relative Refractivity Virial Coefficients 145
B.3 Ozone Sensitivity Coefficient of Air 154
B.4 Temperature Sensitivity of N_2 158
B.5 References 160

C Digital Fringe Analysis Algorithm **162**

D Hg Lamp: Use in Interferometry **165**
D.1 Introduction 165
D.2 Interfering Spectral Lines 166
D.3 Continuum Background 171
D.4 Hyperfine Structure 172
D.5 Broadening and Frequency Shifts of ^{198}Hg 175
D.6 References 178

List of Figures

1.1 Profile of CO_2 Mixing Ratio in the Stratosphere 9
1.2 Predicted Stratospheric O_2 Mole Fraction Profiles 11

2.1 Relative Refractivity of Air and O_2 Versus Wavelength 21
2.2 Optical System of the Interferometric Oxygen Analyzer 28
2.3 Raw Fringe Signals 32
2.4 Fringe–Remainder Response to Changing Concentrations 35
2.5 Interferometric Oxygen Analyzer Calibration 36

3.1 Temporal Trends of O_2 and CO_2 Mole Fractions 51
3.2 Temporal Trends, in Detail 52
3.3 Diurnal Trend in O_2 and CO_2 53
3.4 Correlation Plot of CO_2 and O_2 Mole Fractions 55
3.5 O_2 and CO_2 Measurements of Krogh in 1919 60

4.1 The Global Oxygen Cycle 69
4.2 O_2 Consumption Versus API Gravity of Liquid Fuels 84
4.3 Average O_2 Profiles in the Major Ocean Basins 111
4.4 Atmospheric CO_2 Increase from Siple Core Data 118
4.5 Biospheric Releases from Siple Ice-Core Data 120

B.1 Variation of the Relative Refractivity of Air vs $n-1$ 148
B.2 Variation of the Relative Refractivity of N_2 vs $n-1$. 148
B.3 Variation of the Relative Refractivity of Ar vs $n-1$. 149
B.3 Variation of the Relative Refractivity of CO_2 vs $n-1$. 149
B.4 Variation of the Relative Refractivity of CH_4 vs $n-1$. 150
B.6 Variation of the Relative Refractivity of N_2O vs $n-1$. 151
B.5 Variation of the Relative Refractivity of CO vs $n-1$. 152
B.7 Variation of the Relative Refractivity of Air with Trace O_3. . . . 156

B.8 Variation of the Relative Refractivity of O_2 with Trace O_3. . . . 157
B.9 Variation of the Relative Refractivity of N_2 vs Temperature . . . 160

D.1 Energy-Level Diagram of Hg I 167
D.2 2537 Å Fringe-Order Residuals vs 4360 Å Fringe Order. 170
D.3 Hyperfine Splittings of the 2537Å and 4358Å Lines of Hg 173

List of Tables

2.1 Refractivity Data for Air and Its Primary Constituents. 24
2.2 Principal Variable Trace Gases in the Atmosphere 25

3.1 Tabulated O_2 and CO_2 Mole-Fraction Data 54
3.2 Oxidative Ratio for Common Fuels 58

4.1 Primary Reservoirs of O_2 and Organic Matter 67
4.2 Fluxes of O_2 and Organic Matter 68
4.3 Combustion Data for Solids 79
4.4 Combustion Data for Liquids 80
4.5 Combustion Data for Gases 81
4.6 O_2 Consumption Factors and Oxidative Ratios for Fossil Fuels. . 87
4.7 Fossil-Fuel CO_2 Production and O_2 Consumption 90
4.8 Propagating Errors in O_2 Consumption Estimates 94
4.9 Summary of Fossil-Fuel CO_2 Production and O_2 Consumption . 97
4.10 Production of Raw Materials in 1980 98
4.11 Oxidative Ratios of Terrestrial Organic Matter 102
4.12 Ocean Inventories of O_2, Organic C, and P. 105
4.13 Change in Ocean Capacity for Dissolved Gases 108
4.14 Scenarios for Recent and Cumulative O_2 Depletion 122

B.1 Virial Coefficients of the Relative Refractivity of Various Gases . 153

D.1 Hg Lines Near 2537.27 Å and 4359.56 Å. 168
D.2 Continuum Background Intensities of Hg Lamps 172
D.3 Stable Isotopes of Hg 174
D.4 Broadening and Frequency Shifts in ^{198}Hg 177

Acknowledgements

This project had its origins in an obscure conversation with my father, C. D. Keeling, probably more than a decade ago, on the potential use of oxygen measurements for defining biospheric changes. Although many years elapsed between that conversation and the beginning work on this project, the idea stuck in my mind and stimulated many off-beat and, as I will attempt to show in this thesis, a few productive ideas on this subject.

I was very fortunate to have been given the opportunity to work on this project by my advisor, Jim Anderson. I will never forget Jim's immediate grasp of the potential importance of this project, which was quite removed from his primary research interests, and the optimism he showed concerning its technical viability. Jim helped to secure funding for support of this project from the National Science Foundation and allowed generous use of laboratory facilities and personnel in the Atmospheric Research Project. Most of all, his enthusiasm and encouragement were pivotal to the success of this project.

At the early stages, Wes Traub and Nat Carleton spent hours discussing with me the basics of interferometry, a subject which was new to me, and the potential pitfalls which I would face in this work. More recently, Nate Hazen, doing a beautiful work, helped to design key stuctural elements of the interferometer. The correlation studies described in Chapter 3 were made possible only through the use of a carbon-dioxide analyzer and reference gases generously made available by Steve Wofsy. Bill DeRoo developed software which was particularly helpful in working up the Cambridge-air measurements. The

glass parts for gas-handling were marvelously crafted by Bernie Souza, and the countless number of machine-shop parts for the interferometer were built under the expert supervision of George Pisiello.

I benefitted greatly over the years in conversations with Norton Allen, Bill Brune, Joe Demusz, Ed Dobbyn, Bob Heroux, Larry Lapson, Kelley Roney, Craig and Terry Schiller, Danny Spilane, Rick Stimpfle, and Ed Thompson, each of whom contributed greatly to solving the array of technical problems I have encountered. I would like to thank Joyce Makrides and Lenny Solomon for their patience and expertice in administrative matters. I would also like to acknowledge stimulating conversations and camaraderie with the 'old guard' of graduate students including of Jan Bai Nee, Randy Friedl, John Larabee, Lee Lowenstein, and Jim Schwab and the 'newer' guard, consisiting of Jon Abbatt, Manvendra Dubey, Fred Fenter, Pete Haaland, Steve Lloyd, Phil Stevens, Darin Toohey, and Paul Wennberg.

An initial start-up fund for this project was obtained with the help of Peter McKinney of the Division of Applied Sciences. Later, the work was supported by National Science Foundation under Grant AEO-84-12224.

Finally, I would like to thank John Abbatt, Susan Dollar, Pete Haaland, and Darin Toohey for their help in proof-reading this draft.

Chapter 1

Introduction

The purpose of this thesis is to lay the groundwork for a potentially important but recently neglected topic in atmospheric science—namely, the variability in the O_2 mole fraction of air. Dry air contains 20.946 mole percent O_2 (Machta and Hughes, 1970) which is believed to be highly constant over time and space (Benedict, 1912; Krogh, 1919; Carpenter, 1937; Machta and Hughes, 1970). Arguing from analogy with measured variations of CO_2, however, we expect that background concentrations of atmospheric O_2 must vary at the the 0.0001 to 0.001 mole percent level on annual time scales and hemispheric spatial scales. Although such minute variations can hardly be of direct environmental significance, an understanding of the spatial and temporal variability in O_2 would substantially augment the framework for studying global biogeochemical cycles and global change.

Oxygen and carbon are closely coupled through photosynthesis, and respiration:

$$CO_2 + H_2O \rightleftharpoons CH_2O + O_2$$

where CH_2O represents the approximate composition of land-plant organic mat-

ter, and also through burning fossil fuel:

$$C_xH_y + (x + \frac{1}{4}y)O_2 \rightarrow xCO_2 + \frac{1}{2}yH_2O.$$

Based on these couplings and our current knowledge of the distribution of atmospheric carbon dioxide (Keeling et al. 1982, Mook et al. 1983, Keeling et al. 1984, Komhyr et al., 1985; Bischoff et al, 1985) we can anticipate that the distribution of the atmospheric oxygen mole fraction should show the following features (changes in atmospheric O_2 will be expressed in parts-per-million where 1 ppm = 0.0001 mole %):

- A uniform long-term decline in the annual mean oxygen of around 3 ppm/year due to fossil fuel burning;
- A regular seasonal cycle with an amplitude of around 15 ppm in the high northern latitudes and declining to around 2 ppm in the southern hemisphere due to seasonal imbalances in net photosynthesis and respiration of land plants and soils;
- A difference between the mean tropospheric concentration in the northern and southern hemispheres of around 3 ppm due to the burning of fossil the northern hemisphere;
- An excess of approximately 15 ppm O_2 in the middle stratosphere caused by slow penetration of tropospheric air which is depleted in O_2 from burning fossil fuel.

The ability to detect these miniscule variations in atmospheric O_2 mole fraction would provide a sensitive test of our understanding of the global coupled oxygen/carbon cycles. Equally important, however, are differences which might

exist between these predictions and the actual magnitude of the oxygen signals. These differences would provide insights into two of the most important questions faced today in global biogeochemistry.

Question 1: What is the rate of the "new" primary production—i.e., the rate at which carbon is photosynthetically fixed and subsequently exported from the euphotic zone—in the world oceans?

Understanding the magnitude of "new" photosynthetic production in the oceans is important because it is closely tied to the rates of cycling of nutrients and many trace chemicals in the ocean. Recently, there has been considerable debate over the magnitude of "new" production. Estimates based on traditional ^{14}C and ^{15}N incubation studies lead to estimates of new production of around 12 g C $m^{-2}yr^{-1}$ in the central basins (Eppley and Peterson, 1979). This type of estimate has been challenged by researchers who have examined the cycling of oxygen in the mixed layer and upper thermocline (Shulenberger and Reid, 1981; Jenkins, 1982; Jenkins and Goldman, 1985). The oxygen studies lead to estimates of new production of around 50 g C $m^{-2}yr^{-1}$ The oxygen data have raised serious questions concerning the validity of incubation studies, but the oxygen studies have not gone unchallenged (Platt, 1984). One particular problem is the difficulty of interpreting the change in dissolved oxygen in terms of *in situ* production without any firm data for the fluxes of oxygen across the air-sea interface. This controversy and its relationship to the "Global Ocean Flux Study" are reviewed by Brewer et al. (1986).

With *ppm*-level oxygen measurement capability, it would be possible to estimate air-sea O_2 fluxes, not by measuring changes in dissolved O_2, but by detecting corresponding changes in the atmospheric O_2 reservoir. Jenkins and Goldman (1985) estimate that the seasonal (March to January) O_2 surface outgassing flux is around 7 moles/m^2/yr which implies seasonal variations in atmo-

spheric oxygen at the 5 to 10 ppm level. The ocean signals will be superimposed on a seasonal signal from the land biosphere which, from CO_2 data, we expect to have an amplitude of 2 to 15 ppm depending on location (Mook, et al., 1983, Keeling et al., 1984, Komhyr et al., 1985). To a first approximation, the land-biospheric exchanges of O_2 and CO_2 can be inferred from the CO_2 data because seasonal air-sea exchange fluxes of CO_2 are relatively unimportant (Heimann et al., 1986). The land biosphere contribution to seasonal O_2 variation can thus be tied to the CO_2 variations via equation (1). The remaining O_2 variability should then reflect air-sea exchange.

A more sophisticated analysis of seasonal O_2 and CO_2 variations would employ an oceanic mixed-layer model to estimate air-sea fluxes of O_2, CO_2, N_2 and the inert gases coupled to a model of the atmospheric motion field, and to a model of land-biosphere exchange of O_2 and CO_2. With the air motions constrained by independent tracers, the atmospheric CO_2 and O_2 data would simultaneously constrain the land-biosphere and air-sea exchange fluxes. This in turn implies direct constraints on estimates of land and ocean biological productivities. Models of this general character, albeit with simplified treatment of the ocean fluxes, have been used for modeling CO_2 seasonal cycles (Fung et al., 1983; Keeling and Heimann, 1986; Pearman and Hyson, 1980). The short-term changes of O_2 mole fraction in the atmosphere measured at a few carefully well chosen locations would effectively constrain the net O_2 flux into or out of the atmosphere over an entire latitude band, over a hemisphere, or over a continent. Neither *in situ* studies nor satelite-based studies are capable of yielding accurate flux estimates over such broad spatial scales.

Two essential differences between oxygen and carbon cycling in the ocean make it clear that atmospheric oxygen measurements will provide a fundamentally new basis for studying changes in ocean biology and chemistry. Firstly,

although the biologically- and thermally-driven disequilibria of CO_2 and O_2 in sea water are comparable in magnitude (i.e., in moles/kg), the seasonal flux of CO_2 should be significantly smaller than the seasonal flux of O_2 because CO_2 equilibrates more slowly across the air-sea interface than O_2. While O_2 equilibrates between the mixed layer and the atmosphere on a time scale of two to three weeks, CO_2 equilibrates on a time scale of a year or so (see Broecker and Peng, 1982). CO_2 equilibrates slowly because the predominant species of dissolved inorganic carbon in sea water are carbonate and bicarbonate which do not directly influence the CO_2 partial pressure. The second difference is that while the biological and thermal driving-force for O_2 exchange tend to work in parallel (e.g. both driving outgassing in warmer months) the biological and thermal driving-forces for CO_2 tend to oppose each other (e.g. biology drives ingassing flux of CO_2 in summer when temperature is driving outgassing flux).

In summary:

- Seasonal fluxes of oxygen across the air-sea interface should produce detectable changes in the average oxygen mole fraction in the atmosphere which are superimposed on variations induced by the land biosphere.
- The ocean contribution to the measured variations can be isolated by referring to simultaneous data for CO_2.
- With atmospheric data from even just a few land stations, it should be possible to make estimates of hemisphere-scale fluxes of oxygen across the air-sea interface. Such data would fill an important gap in our understanding of the cycling of oxygen and the rates of biological productivity in the world oceans.

Question 2: What is the year-to-year change in the total mass of carbon in the land biosphere?

Recent estimates of the change in the size of land biosphere are only accurate at best to the level of $\pm 1 \cdot 10^{15}$ g C yr^{-1}, and are subject to potentially large systematic errors (Brown and Lugo, 1984; Houghton et al., 1983; Olson, 1982). At this level it is impossible even to answer the question as to whether the biosphere is growing or declining.

Measuring changes in the size of the land biosphere could provide one of the most valuable indices of the impact of human activities on global ecology. Today, slash and burn agriculture is causing the rapid destruction of tropical forests. Also, there is an increase in the concentrations of chemicals such as ozone (Logan, 1985) which are toxic to plants. At the same time, however, some previously farmed land is being reforested today, and the increase in atmospheric CO_2 may be stimulating an increase in global photosynthesis. Today we do not know the relative importance of these processes nor do we know their net impact. Because most of these processes are accelerating, there is a clear need to develop methods for measuring the changes which are likely to occur over the next few decades.

One important reason for knowing the net change in the biosphere is to account for the recent rise in atmospheric CO_2. Atmospheric CO_2 is increasing at a well-established rate of $2.5 \cdot 10^{15}$ g C yr^{-1} (1980 rate estimated from data in Keeling et al., 1982). The annual release rate of CO_2 from burning fossil fuel is also well established at $5.2 \cdot 10^{15}$ g C yr^{-1} (1980 rate from Marland and Rotty, 1984). The question is how to account for the difference of $2.7 \cdot 10^{15}$ g C yr^{-1}.

Initially, it was believed that the dissolution of CO_2 in the ocean accounted for most of the difference. Ocean modelers in the 1970's found that oceanic CO_2 uptake could account for all but about $0.5 \cdot 10^{15}$ g C yr^{-1} of the difference which they assumed was entering the land biosphere (see e.g. Broecker et al., 1979). The notion that the land biosphere was a net sink for CO_2 was met

with scepticism by terrestial ecologists, who, by the late 1970's, had published independent estimates based on land-use statistics indicating that the land biosphere was actually a net source of $1 \cdot 10^{15}$ to $8 \cdot 10^{15}$ g C yr^{-1} (Bolin, 1977, Woodwell et al., 1978) . Although the discrepancy in more recent estimates is smaller—the ocean model studies are now compatible with a biospheric source of 0 to $1 \cdot 10^{15}$ g C yr^{-1} (Siegenthaler and Oeschger, 1987) and the ecological studies are compatible with a net biospheric source of $1 \cdot 10^{15}$ to $2.6 \cdot 10^{15}$ g C yr^{-1} (Houghton et al. 1987)—the inability of ecologists and oceanographers to agree on the size of net biospheric CO_2 source has raised some serious questions. Could the ocean modelers be underestimating oceanic uptake of CO_2? Could the ecologists be neglecting other biospheric CO_2 sinks, such as a global stimulation of net primary production due to higher CO_2 levels or due to higher inputs of nutrients from human activities? Either scenario would have important consequences for the climate and habitability of the earth. To resolve the controversy between the ocean modelers and the ecologists it will be necessary to develop new methods for estimating biospheric changes.

Some time ago, Lester Machta (1980) pointed out that it would be possible to obtain the net biospheric CO_2 source through measurements of the long-term decline in atmospheric oxygen. The burning of fossil fuel decreases atmospheric O_2 by a predictable rate. Oxidation of biomatter also decreases atmospheric O_2. However, the reduction in atmospheric O_2 partial pressure caused by these processes is so slight that it cannot drive a significant flux of dissolved O_2 out of the oceans. Thus, if the change in atmospheric O_2 were measured, the difference between the measured atmospheric O_2 loss and the fossil-fuel O_2 loss would yield the net biospheric oxidation. This method offers two advantages: (1) it would lead to more accurate estimates of biospheric CO_2 source and (2) it would account for the sum of all oxidative processes, including global deforestation,

soil oxidation, and stimulation of net-ecosystem-production (NEP).

There are two experimental requirements for measuring the long-term decline in oxygen. Firstly, one must have the capability of measuring differences of around 1 ppm in oxygen between air samples or between air samples and air standards. Secondly, one must develop standards for O_2 in air which are stable at the level of around 1 ppm per decade. While the first difficulty has been addressed by this thesis, the second difficulty still stands as a very significant experimental challenge.

There is a method, however, for inferring the recent rate of decline in oxygen even before stable standards are developed. Essentially, the method looks at the ratio of total O to total N in the lower stratosphere. The inspiration for this idea comes from the observed CO_2 profile in the stratosphere at 40 N, shown in Figure 1.1, which shows a reduction in the CO_2 level in the 20–30 km region in the stratosphere relative to the troposphere. Stratospheric CO_2 is lower due to the delayed response of stratospheric CO_2 to increasing tropospheric CO_2. The lag time of 5.2 years, based on the CO_2 data, can be fairly well explained by a standard 1-D eddy-diffusion model (Bischoff et al., 1985) calibrated with other tracers.

On the basis of a five-year lag time, one expects the O_2 mole fraction in the stratosphere to be higher than the mean tropospheric value by approximately 15 ppm (assuming 3 ppm/yr decline rate). If the O_2 mole fraction was a conservative tracer, simultaneous O_2 and CO_2 measurements from air samples in the 10–20 km range would define the average rate of depletion of O_2 in the troposphere over the last five years because the CO_2 measurements would effectively date each sample with respect to the time that the air parcel entered the stratosphere.

However, it is clear that the O_2 mole fraction does not behave as a conser-

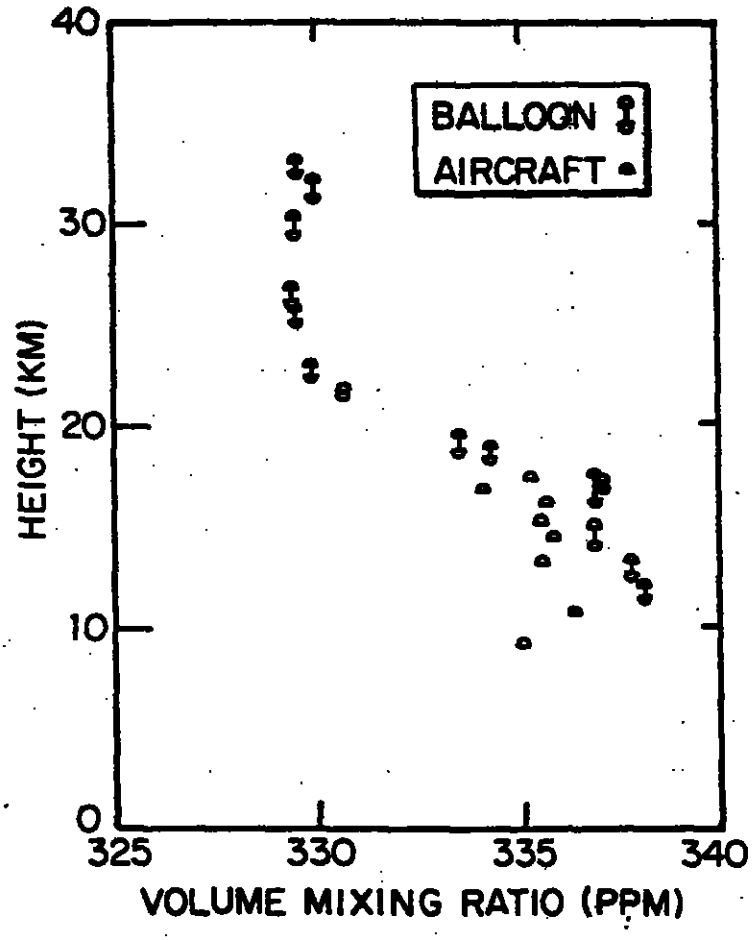

Figure 1.1: Profile of CO_2 mixing ratio in 1982 from Bischoff et al. (1985).

vative tracer at ppm levels in the stratosphere. In addition to chemical losses of O_2 from O_3 formation (maximum loss $\approx$ 15 ppm O_2) and CH_4 oxidation (maximum loss $\approx$ 3 ppm O_2) which could readily be accounted for by backconverting O_3 to O_2 and by measuring CH_4 simultaneously, there is an additional loss due to gravimetric fractionation. Figure 1.2 shows the O_2 profiles predicted by a 1-D eddy diffusion model (neglecting CH_4 oxidation and O_3 formation) in the presence of gravimetric fractionation assuming (1) no surface sink for O_2; (2) a surface sink corresponding to –3 ppm/yr loss (estimated rate for 1986); and (3) a surface sink corresponding to –6 ppm/yr (estimated for 2030 if the current rate of increase in fuel usage continues).

In order to relate stratospheric O_2 and CO_2 measurements to the tropospheric O_2 decrease it will be necessary to quantitatively account for gravimetric fractionation on each sample. This is clearly difficult since the extent of fractionation varies inversely with vertical mixing, which itself is imperfectly understood.

Nevertheless, measurements of stratospheric O_2 and CO_2 mole fractions, in addition to having historical importance in light of the predicted future changes, would serve two immediate purposes:

1. Combined measurements of O_2 and CO_2 mole fraction in the 15–22 km range, where the shape of the O_2 profile is most sensitive to the secular O_2 decline rate, would place constraints on the net O_2 sink over the past five years. Insofar as the uncertainty in the estimated O_2 sink would hinge primarily on uncertainty in vertical mixing rates, the measurements would focus attention on the need for improved understanding of vertical mixing in this range which is of pivotal importance to many aspects of stratospheric chemistry and physics.

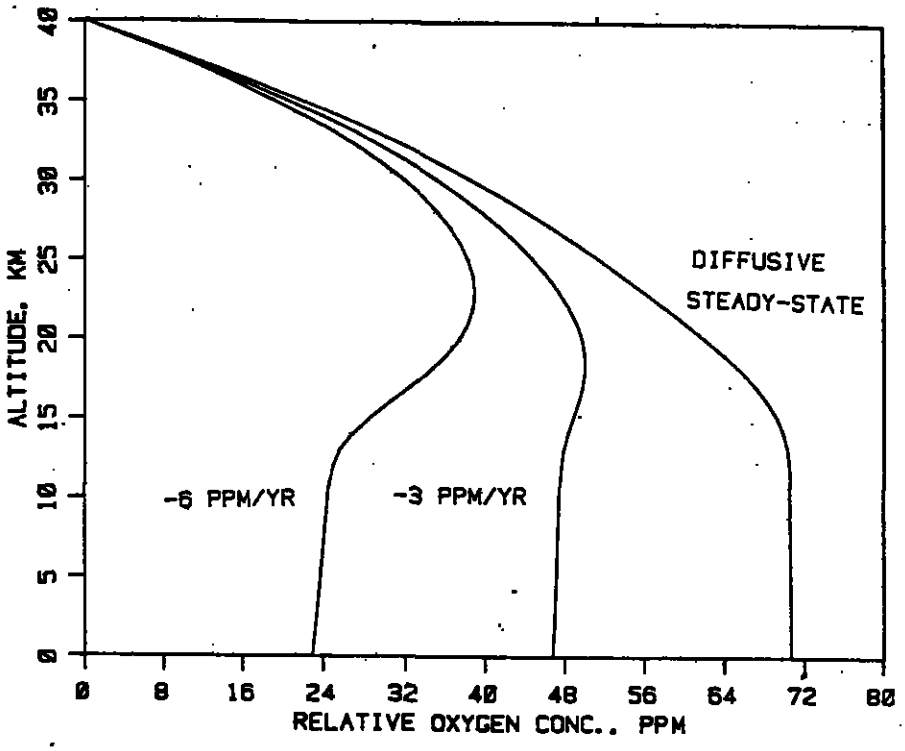

Figure 1.2: Steady state profile of O_2 mole fraction predicted by a 1-D eddy-diffusion/molecular diffusion-model using the composite eddy-diffusion profile of Massie and Hunten (1981) in equation (45) of Lettau (1951). The profile allows for temperature and pressure dependence of the molecular diffusivity of O_2 in N_2. Also shown are profiles predicted in the presence of a constant surface sink for O_2 amounting to –6 ppm/yr and –3 ppm/yr in total atmospheric abundance. The profiles are arbitrarily fixed to 0 ppm at 40 km; only the relative change with altitude is significant.

2. Measurements of O_2 mole fraction in the 30–40 km range where the tropospheric O_2 loss has little influence (see Figure 1.2) would provide a basis for validating models of eddy mixing which are needed for predicting the penetration of source gases such as chlorofluorocarbons which can catalytically destroy O_3 (see, e.g. World Meteorological Org., 1985). As an example of how the O_2 profile could be used, we note that the vertical eddy-diffusion coefficient can be calculated from the vertical O_2 profile according to:

$$\frac{log(1+f)}{log(p_1/p_2)} = \frac{D(R/R'-1)}{D+K}$$

where f is the fractional change in composition (i.e. in the O_2/N_2 ratio) from pressure p_1 to p_2, D is the binary molecular-diffusion coefficient, R and R' are the gas constant (per unit mass) of air and the diffusive tracer (e.g., O_2) respectively, and D and K are the molecular and eddy diffusivities, respectively (Brewer, 1949). The use of the O_2 mole fraction as a tracer has an advantage over existing tracers such as N_2O, CH_4, O_3 (see, e.g., Massie and Hunten, 1981) because its distribution is determined only by physical processes and not by photochemistry.

It is clear that very few atmospheric scientists have given the question of variability in O_2 much thought. This is probably due to a general scepticism that the miniscule atmospheric O_2 changes could ever be detected. Such scepticism is reinforced by the difficulties which have been encountered in detecting changes in atmospheric O_2 using traditional O_2 analysis techniques, such as chemically extracting the O_2 and measuring the weight or volume change, or using commercially available paramagnetic analyzers (Machta and Hughes, 1970).

This thesis introduces a new technique for measuring the O_2 mole fraction of

air which can offer at least a tenfold improvement in resolution over previously available techniques. The resolution which has now been demonstrated for the intercomparison of standards is 0.5 ppm and further improvements appear feasible. The basis of the technique is to resolve changes in the relative refractivity of dried air between the visible and ultraviolet. The relative refractivity $\tilde{r}$ is defined here according to

$$\tilde{r} = \frac{n(\lambda_1) - 1}{n(\lambda_2) - 1} \tag{1.1}$$

where n is the index of refraction of dry air and λ_1 and λ_2 are a pair of suitably chosen wavelengths in the visible and ultraviolet spectrum. Primarily because of the strong absorption of O_2 in the Schumann-Runge continuum around 1500Å, the optical dispersion from 4000 to 2000 Å is greater for O_2 than for N_2 and Ar, and consequently the dispersion of air varies with oxygen abundance. However, the variation is very slight: for pure nitrogen and oxygen at $\lambda_1 = 2537$Å and $\lambda_2 = 4360$Å the relative difference in $\tilde{r}$ is only 3%, which implies that $\tilde{r}$ must be resolved to $3 \cdot 10^{-8}$ to detect ppm changes in the oxygen mole fraction.

Such high resolution in the measurement of the relative refractivity can be achieved interferometrically. The relative refractivity can be directly related to the ratio of the orders of interference at λ_1 and λ_2 in an ordinary dual-arm interferometer:

$$\tilde{r} = \left[\frac{\lambda_1}{\lambda_2}\right]\left[\frac{p_1 + \epsilon_1}{p_2}\right]. \tag{1.2}$$

Here, p_1 and p_2 are the integral orders of interference which elapse upon introducing an air sample into one of the arms of the interferometer (assumed to be initially evacuated) and ϵ_1 is the fractional order at λ_1 for the p_2^{th} integral order at λ_2. It is not difficult to construct an interferometer which yields $p_1 \approx 10,000$, so that a sensitivity of $3 \cdot 10^{-8}$ in $\tilde{r}$ requires resolving ϵ_1 to $3 \cdot 10^{-4}$ of an order. There are many techniques now available for resolving such small fractional

orders.

One slight complication is that relative refractivity is also sensitive to changes in other components of air, most notably H_2O and CO_2. This is not a serious limitation of the method, however, since eliminating or analyzing all potential interfering species to the equivalent of a small fraction of a ppm in O_2 is straightforward.

The subsequent chapters of this thesis address more technical aspects of the detection of changes in O_2 and their interpretation. Chapter 2 discusses the details of the interferometric oxygen analyzer. Chapter 3 discusses the application of the instrument for the detection of short-term O_2 changes in Cambridge, Massachusetts. Chapter 4 reviews what is currently known or can be inferred about contemporary sources and sinks of O_2 with primary emphasis on changes in O_2 brought about by recent human activities. Finally, Chapter 5 ties together the objectives of this thesis with some of the broader issues faced today in global biogeochemistry, and discusses strategies for implementing O_2 measurements in the future.

References

Benedict, F. G., 1912, *The Composition of the Atmosphere with Special Reference to its Oxygen Content*, Carnegie Institution of Washington, Washington, D. C.

Bischoff, W., R. Borchers, P. Fabian, B. C. Kruger, 1985, "Increased concentration and vertical distribution of carbon dioxide in the stratosphere," *Nature* **316**, 708–710.

Bolin, B., 1977, "Changes of land biota and their importance for the carbon cycle," *Science* **196**, 613–615.

Brewer, A. W., 1949, "Evidence for a world circulation provided by the measurement of helium and water vapor in the stratosphere," *Quarterly Journal of the Royal Meteorological Society* **75**, 351–363.

Brewer, P. G., K. W. Bruland, R. W. Eppley, J. J. McCarthy, 1986, "The global ocean flux study (GOFS): status of the U. S. GOFS program," *EOS* **67(44)**, 827–832.

Broecker, W. S., and T. H. Peng, 1982, *Tracers in the Sea*, Eldigio Press.

Broecker, W. S., T. Takahashi, H.J. Simpson, and T. H. Peng, 1979, "Fate of fossil fuel carbon dioxide and the global carbon budget," *Science* **206**, 409–418.

Brown, S., and A. Lugo, 1984, "Biomass of tropical forests: a new estimate based on forest volumes," *Science* **223**, 1290–1293.

Carpenter, T. M., 1937, "The constancy of the atmosphere with respect to carbon dioxide and oxygen content" *J. Amer. Chem. Soc.* **59**, 358–360.

Eppley, R. W., B. J. Peterson, 1979, "Particular organic matter flux and planktonic new production in the deep ocean," *Nature* **282**, 677–680.

Fung, I., K. Prentice, E. Matthews, J. Lerner, and G. Russel, 1983, "Three-dimensional tracer model study of atmospheric CO_2: response to seasonal exchanges with the terrestrial biosphere," *J. Geophys. Res.* **88(C2)**, 1281–1294.

Heimann, M., C. D. Keeling, I. Y. Fung, 1986, "Simulating the atmospheric carbon dioxide distribution with a three dimensional tracer model," in J. R. Trabalka, D. E. Reichle eds., *The Changing Carbon Cycle: A Global Analysis*, 16–49.

Houghton, R. A., J. E. Hobbie, J. M. Melillo, B. Moore, B. J. Peterson, G.R. Shaver, and G. M. Woodwell, 1983. "Changes in the carbon content of terrestrial biota and soils between 1860 and 1980: a net release of CO_2 to the atmosphere," *Ecological Monographs* **53(3)** , 235–262.

Houghton, R. A., R. D., Boone, J. R. Fruci, J. E. Hobbie, J. M. Melillo, C. A. Palm, B. J. Peterson, G. R. Shaver, G. M. Woodwell, B. Moore, D. L. Skole, N. Myers, 1987, "The flux of carbon from terrestrial ecosystems to the atmosphere in 1980 due to changes in land use: geographic distribution of the global flux," *Tellus* **39B**, 122–139.

Jenkins, W. J., 1982, "Oxygen utilization rates in North Atlantic subtropical gyre and primary production in oligotrophic systems," *Nature* **300**, 246–248.

Jenkins, W. J., and J.C. Goldman, 1985, "Seasonal oxygen cycling and primary production in the Sargasso Sea," *J. Marine Res.* **43**, 465–491.

Keeling, C. D., R. B. Bacastow, T. P. Whorf, 1982, "Measurements of the concentration of carbon dioxide at Mauna Loa Observatory, Hawaii, " in W. C. Clark ed., *Carbon Dioxide Review 1982*, Oxford University Press, New York, 375–385.

Keeling, C. D., A. F., Carter, W. G. Mook, 1984, "Seasonal, latitudinal, and secular variations in the abundance and isotopic ratios of atmospheric CO_2. 2. Results from oceanic cruises in the tropical pacific ocean," *Journal of Geophysical Research* **89(D3)**, 4615–4628.

Keeling, C. D., and M. Heimann, 1986, "Meridional eddy diffusion model of the transport of atmospheric carbon dioxide. 2. Mean annual carbon cycle," *J. Geophys. Res.* **91(D7)**, 7782–7796.

Komhyr, W. D., R. H. Gammon, T. B. Harris, L. S. Waterman, T. J. Conway, W. R. Taylor, K. W. Thoning, 1985, "Global atmospheric CO_2 distribution and variations from 1968-1982 NOAA/GMCC CO_2 flask sample data," *J. Geophys. Res.* **90(D3)**, 5567–5596.

Krogh, A., 1919, "The composition of the atmosphere," *Det Kgl. Danske Videnskabernes Selskab.* **1** no. 12.

Lettau, H., 1951, "Diffusion in the upper atmosphere," in T. Malone ed., *Compendium of Meteorology* American Meteorological Society, Boston.

Logan, J. A., 1985, "Tropospheric ozone: seasonal behavior, trends, and anthropogenic influence, " *Journal of Geophysical Research* **90(D6)**, 10463–10482.

Machta, L., E. Hughes, 1970, "Atmospheric Oxygen in 1967 and 1970," *Science* **168**, 1582–1584.

Machta, L., 1980, "Oxygen depletion," in G. C. Jacoby ed., *Proceeding of the International Meeting on Stable Isotopes in Tree Ring Research* 125–127.

Marland, G., R. M. Rotty, 1984, "Carbon dioxide emissions from fossil fuels: a procedure for estimation and results for 1950–1982," *Tellus, 36B*, 232–261.

Massie, S. T., Hunten, D. M., 1981, "Stratospheric eddy diffusion coefficients from tracer data," *Journal of Geophysical Research* **86(C10)**, 9859–9868.

Mook, W. G., M. Koopmans, A. F. Carter, and C. D. Keeling, 1983, "Seasonal, latitudinal, and secular variations in the abundance and isotope ratios of atmospheric carbon dioxide 1. Results from land stations," *Journal of Geophysical Research* **88**, 10915–10933.

Olson, J. S., 1982, "Earth's vegetation and atmospheric carbon dioxide," in W. C. Clark ed., *Carbon Dioxide Review: 1982*, Oxford University Press, New York, 388–398.

Pearman, G. L., and P. Hyson, 1980, "Activities of the global biosphere as reflected in atmospheric CO_2 records," *Journal of Geophysical Research* **85**, 4468–4474.

Platt, T., 1984, "Primary productivity of the central north pacific: comparison of oxygen and carbon fluxes," *Deep Sea Research* **31(11)** , 1311–1319.

Shulenberger, E., and J. L. Reid, 1981, "The Pacific shallow oxygen maximum, deep chlorophyll maximum, and primary productivity, reconsidered," Deep Sea Research *28A(9)*, 901–919.

Siegenthaler, U., H. Oeschger, 1987, "Biospheric CO_2 emissions during the past 200 years reconstructed by deconvolution of ice core data," *Tellus* **39B**, 140–154.

Woodwell, G. M., R. H. Whittaker, W. A. Reiners, G. E. Likens, C. C. Delwiche, D. B. Botkin, 1978, "The biota and the world carbon budget," *Science* **199**, 141–146.

World Meteorological Organization, Global Ozone Research and Monitoring Project–Report No. 16, *Atmospheric Ozone 1985, Assessment of Our Understanding of the Processes Controlling Its Present Distribution and Change.*

Chapter 2

The Interferometric Oxygen Analyzer

2.1 Physical Basis of Measurement

The technique described here for measuring the O_2 mole fraction of air is based on measuring changes in the relative refractivity defined according to

$$\bar{r}(\lambda_1, \lambda_2) = \frac{n(\lambda_1) - 1}{n(\lambda_2) - 1}, \tag{2.1}$$

where λ_1 and λ_2 are two appropriately chosen wavelengths of light and n is the refractive index of air.

Relative refractivity can be measured interferometrically by techniques which are analogous to techniques for intercomparing wavelengths of light. For example, modern laser wavemeters (see e.g. Snyder, 1982) typically rely on measurements of the ratio of the elapsed fringes in a scanning Michelson interferometer which can be expressed according to

$$\frac{p_1}{p_2} = \frac{\Delta L/\lambda_1}{\Delta L/\lambda_2}$$

where p_1 and p_2 refer to the number of elapsed fringes at λ_1 and λ_2 respectively and ΔL is the distance of travel of one of the interferometer end-mirrors. Thus if λ_2 is known, measurement of p_1/p_2 determines λ_1.

Likewise, if a gas cell is present in one of the arms of the interferometer and it is subject to a change in gas pressure, the ratio of the elapsed fringes can be expressed according to

$$\frac{p_1}{p_2} = \frac{L\Delta n(\lambda_1)/\lambda_1}{L\Delta n(\lambda_2)/\lambda_2}$$

where $\Delta n(\lambda)$ is the change in refractive index at wavelength λ and L is the cell length. If both λ_1 and λ_2 are known, measurement of p_1/p_2 determines $\tilde{r}(\lambda_1, \lambda_2) = \Delta n(\lambda_1)/\Delta n(\lambda_2)$.

Modern laser wavemeters readily achieve accuracies at the level of 1 part in 10^8 (Snyder, 1982) and, with care, much higher precision and accuracy can be achieved (Monchalin et al. 1981). Even though the relative refractivity is not strongly sensitive to changes in O_2 mole fraction, as will be discussed below, the extremely high sensitivity that had been demonstrated in modern laser wavemeters argued strongly for the feasibility of ppm-level O_2 detection. This analogy between the interferometric intercomparison of wavelengths and interferometric measurement of relative refractivity was a major consideration in the selection of the relative refractivity from among the many possible physical properties of air that could be used for detecting changes in O_2.

Figure 2.1 shows the spectrum of the relative refractivity normalized to 4359.56Å of air and O_2. The relative refractivities of both air and O_2 are described by smooth, monotonically decreasing functions of wavelength over the wavelength range from 2000 to 8000Å. The change with wavelength for O_2 is more rapid than for air, particularly below 3000Å. This difference is expected on theoretical grounds. The dispersion in a dielectric medium is related to the

location and strengths of absorption features as given by the Kramers-Kronig relations (Jackson, 1975 p. 311). These relations dictate that the refractivity must increase with decreasing wavelength in transparent regions in the spectrum. The rate of increase is more rapid if there are nearby absorption features in the spectrum. Because O_2 exhibits strong absorption in the Schumann-Runge continuum around 1500Å where N_2 is transparent, the relative refractivity of O_2 must increase rapidly as the wavelength decreases towards 1500Å.

In the limit of low number density, the refractivity $n-1$ of a pure gas is given by

$$n - 1 = 2\pi\rho\alpha \tag{2.2}$$

where ρ is the number density (molecules per cm^3) and α is the mean (averaged over orientation and quantum states) molecular polarizibility. Also, the refractivity of a gas mixture is given by

$$n - 1 = 2\pi\rho \sum_i X_i \alpha_i \tag{2.3}$$

where the X_i refers to the mole fraction of species i and ρ is the total number density. From Equations 2.1 and 2.3 it can be shown that the relative refractivity of air will vary with the mole fraction of species i according to

$$\delta\tilde{r} = S_i \cdot \delta X_i \tag{2.4}$$

where

$$S_i = \frac{n_i(\lambda_2) - 1}{n_{air}(\lambda_2) - 1} \cdot \frac{\tilde{r}_i(\lambda_1, \lambda_2) - \tilde{r}_{air}(\lambda_1, \lambda_2)}{1 - X_i} \tag{2.5}$$

and where δX_i is the change in mole fraction of species i under the constraint that the relative abundances of all other species (i.e. the ratio X_j/X_k where $j, k \neq i$) remain constant. The derivation of Eq. 2.5 is left to Appendix A.

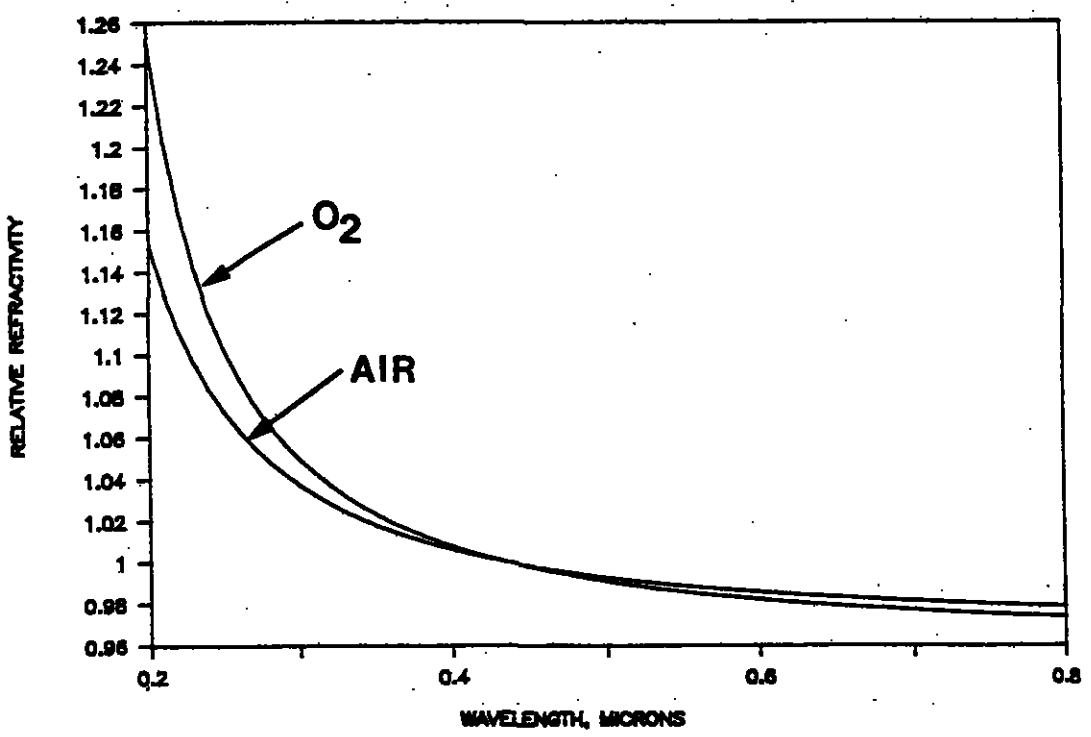

Figure 2.1: Relative refractivity of air and O_2 versus wavelength. Relative refractivities have been normalized to the 4359.56 Å (vacuum) line of Hg. Refractivity data for air from Edlen (1966), for O_2 from equation (7) in Ladenburg and Wolfsohn (1932).

The sensitivity coefficient S_{O_2} of air is maximized by selecting a pair of wavelengths λ_1 and λ_2 which span as much as possible of the wavelength region between the visible and the ultraviolet absorption cut-off of O_2 at around 2000Å. Primarily for reasons of convenience, the wavelengths which were selected are the lines of a low-pressure electrodeless ^{198}Hg lamp at 2537.2688 and 4359.5662Å. Both of these lines have been recommended as absolute length standards (Kaufman, 1962). Although a twofold increase in S_{O_2} could have been achieved by selecting an ultraviolet wavelength shorter than 2537Å, the convenience of deriving both wavelengths from a single source and the remarkable brightness of the 2537Å line seemed to outweigh this advantage. Several other sources were considered, including the argon-ion laser line at 5140Å and its second harmonic at 2570Å. In retrospect, using the ^{198}Hg source appears to have been a wise decision because the coherence and brightness of the ^{198}Hg lamp have now been shown to be adequate for the refractivity measurement and because many additional difficulties (e.g. output-power fluctuations, frequency instabilities, secondary modes, etc.) and much higher costs would have been faced using the laser source.

The sensitivity coefficient for 2537.26 and 4359.56Å can be evaluated based on data in Table 2.1 which yield, according to Eq. 2.5, $S_{O_2} = 3.1 \cdot 10^{-8}$ per ppm. Thus to detect a change of 1 ppm in the oxygen mole fraction of air it is necessary to resolve changes in $\tilde{r}(2537, 4358)$ to 3 parts in 10^{-8}.

At the outset of this project, it was clear that the feasibility of ppm-level O_2 mole fraction measurements would depend on the following questions:

- Could comparable fractional-fringe resolution be achieved with a Hg lamp source as had been achieved with laser wavemeters? High fractional-fringe resolution would be important for reducing the requirements on

cell pressure and cell length which, in a large measure, would dictate the stability and versatility of the analyzer.

- To what extent does the relative refractivity of air depend on density and temperature? The upper limits to such variability set by previous measurements (Svensson, 1960; Erickson, 1962) were insufficient to rule out the possible need for a high level of stabilization of sample pressure and temperature.

- To what extent would variations in relative refractivity of air depend on variations in other gases besides O_2? (Typical variations in trace gases are summarized in Table 2.2) The sensitivity to O_2 was well established based on refractivity data for air from Edlen (1966) and for O_2 from Smith et al. (1976) and Ladenburg and Wolfsohn (1932), which were mutually consistent with refractivity data for N_2 by Koch (1913). However, the refractivity data required to evaluate the sensitivity to CO_2, CH_4, and N_2O, were more than 60 years old, and data for O_3 and H_2O were lacking over the relevant wavelength range.

The latter two questions above have been addressed by refractivity measurements described in Appendix B. These measurements show that the relative-refractivity does depend weakly on density. This can be expressed in terms of a variation in $\tilde{r}$ with $n(\lambda_2)$ which itself is a measure of density. Expanding in a power series about $n(\lambda_2) - 1 = 0$ we can write

$$\tilde{r}(\lambda_1, \lambda_2) = a(\lambda_1, \lambda_2) + b(\lambda_1, \lambda_2)[n(\lambda_2) - 1] + c(\lambda_1, \lambda_2)[n(\lambda_2) - 1]^2 + \ldots \quad (2.6)$$

The measurements for air yield $b(2537, 4360) = 0.015$; the implication of this density dependence on the O_2 measurements is discussed in Section 2.4.

Table 2.1: Refractivity data for air and its primary constituents.

Species	Mole Fraction in dry air, X_i	Relative Refractivity $\bar{r}$(4360Å, 2537Å)	Refractivity at 0°C, 760 torr n(4360Å) − 1	Sensitivity Factor, S_i (ppm^{-1})	Relative Sensitivity S_i/S_{O_2}
Air	—	1.06902[a]	$2.965 \cdot 10^{-4}$ [a]	—	—
N_2	78.084%[b]	1.062023[c]	$3.023 \cdot 10^{-4}$ [d]	—	—
O_2	20.946%[c]	1.09538[f]	$2.758 \cdot 10^{-4}$ [f]	$3.10 \cdot 10^{-8}$	1.00
H_2O	0 to 3%[g]	1.1065[c]	$2.515 \cdot 10^{-4}$ [h]	$3.37 \cdot 10^{-8}$	1.09
Ar	0.934%[b]	1.06126[c]	$2.854 \cdot 10^{-4}$ [i]	$-0.74 \cdot 10^{-8}$	−0.24
CO_2	338 ppm[j]	1.0730[c]	$4.562 \cdot 10^{-4}$ [k]	$0.608 \cdot 10^{-8}$	0.196
Ne	181.8 ppm	1.0245[l]	$6.754 \cdot 10^{-5}$ [m]	$-1.014 \cdot 10^{-8}$	−0.33
He	5.24 ppm[b]	1.0251[k]	$3.508 \cdot 10^{-5}$ [m]	$-0.520 \cdot 10^{-8}$	−0.17
Kr	1.14 ppm[b]	1.0855[n,o]	$4.357 \cdot 10^{-4}$ [o]	$-2.28 \cdot 10^{-8}$	−0.74
CH_4	1.7 ppm[p]	1.0935[c]	$4.475 \cdot 10^{-4}$ [q]	$3.68 \cdot 10^{-8}$	1.19
H_2	0.5 ppm[b]	1.0892[r,c]	$1.416 \cdot 10^{-4}$ [r]	$0.964 \cdot 10^{-8}$	0.31
N_2O	0.30 ppm[s]	1.0992[c]	$5.18 \cdot 10^{-4}$ [t]	$5.25 \cdot 10^{-8}$	1.69
CO	0.02–0.25 ppm[u]	1.1053[c]	$3.416 \cdot 10^{-4}$ [q]	$4.15 \cdot 10^{-8}$	1.34
O_3	0.0 – 0.1 ppm	—	—	$4.9 \cdot 10^{-7}$ [c]	15.8

[a] Edlen, 1966.
[b] US, 1976.
[c] See Appendix B.
[d] Peck and Khana, 1966.
[e] Machta and Hughes, 1970.
[f] Ladenburg and Wolfsohn, 1932.
[g] Typical range in moist air
[h] Zeiss and Meath, 1975.
[i] Peck and Fischer, 1964.
[j] Keeling et al., 1982.
[k] Old et al., 1971.
[l] Cuthbertson and Cuthbertson, 1932.
[m] Mansfield and Peck, 1969.
[n] Smith et al. 1976.
[o] Koch, 1949.
[p] Khalil and Rasmussen, 1986.
[q] Koch, 1909.
[r] Ford and Brown, 1973.
[s] Weiss, R. F., 1981.
[t] Cuthbertson and Cuthbertson., 1914.
[u] Logan et al., 1981.

Table 2.2: Concentration ranges of trace gases at sea level[a]

Spec.	Mean 1984 Level	Secular Change 1975–1985[b]	Seasonal Var. (Range)	Interan. Var. (Range)	N–S Hem. Dif.[c]
CO_2	343.8	+1.4	max. ~ 16	~ 1	+3.0
CH_4	1.67	+0.017 to +0.025	≤ 0.2	< 0.1	+0.14
N_2O	0.30	+0.0007	≤ 0.001	< 0.002	+0.001
CO	0.13	+0.0004 to +0.004	~ 0.022	–	~ +0.09
O_3	0.0–0.05	–	–	–	–

[a]In ppm (mole fraction); References include World Meteorological Organization (1985), Logan (1985), Bacastow et al. (1980), and Keeling et al. (1984).

[b]In ppm/yr.

[c]Difference between mean values in the northern and southern hemispheres. Positive sign indicates higher value in northern hemisphere.

Measurements indicate an upper bound to the temperature sensitivity of $\tilde{r}(2537, 4360)$ for nitrogen at room temperature of $4 \cdot 10^{-7}/°C$. Assuming that this upper bound is appropriate for air as well, it indicates the possible need to stabilize temperature to ca. 0.1 °C for ppm-level O_2 measurements. This is not a stringent requirement.

Relative-refractivity measurements performed on CO, and CO_2 largely confirm the earlier work by Koch (1914) and Smith et al. (1976). Results from the relative-refractivity measurements of other gases are summarized in Table 2.1. Aside from the need to dry the gas to eliminate water vapor, to account for CO_2 variations, and to apply small corrections for CH_4 and CO, the residual corrections for trace-gas variability in background air will generally be smaller than 1 ppm O_2. It appears that all corrections can easily be accounted for with routine trace-gas measurement techniques.

It should be emphasized that the goal of this project was to achieve a high-precision measurement of O_2 mole fraction and not to achieve an absolute measure of O_2 mole fraction. Thus no attempt has been made to reduce constant systematic errors in the measurement of $\tilde{r}$ which would equally affect the measurement of samples and standards. With additional work, high-accuracy measurements of relative refractivity might provide a stable absolute measure of the O_2 content of air. However, this goal lies beyond the scope of the present project.

2.2 Details of Operation

Relative refractivities are measured on a folded-path variant of Jamin interferometer (Born and Wolf, 1975, 309–310) which is uniquely suited for measuring relative refractivity. Both arms of the interferometer are formed between just

two pieces of optics: a 5.3 cm thick parallel fused-silica Jamin plate which serves as the beam splitter and recombining surface, and a corner-cube retro-reflector, as shown in Fig. 2.2.

A stainless-steel cylinder with four parallel bore holes is located between the plate and the corner cube. All four bore holes are sealed with a single pair of fused-silica windows. The light beam corresponding to one arm of the interferometer travels first down one upper bore hole, and returns through the diagonally-opposite lower bore hole. The diagonally-opposite bore holes are connected internally to form a single cell. To first order the optical path difference, OPD, between the two arms depends only on the difference in the refractivity along the two beams and does not depend on the position or orientation of any of the optics. In order to desensitize the interferometer to ambient air currents, all the sensitive beams outside of the cells are enclosed in an evacuated vessel.

The interferometer is illuminated with a low-pressure electrodeless lamp filled with a trace of isotopically pure ^{198}Hg and 3 torr of Ar. The output of the lamp is transmitted through a quartz fiber onto a pinhole placed at the focus of a parabolic mirror. The collimated output of the mirror is stopped down with a circular aperture and is divided into two beams by a beam-splitter coating on the front face of the Jamin plate (Note that the beam-splitter coating only covers half of the front face of the Jamin plate). The two beams then travel complementary paths through the interferometer and are recombined at the Jamin plate. The 4359.56 and 2537.27Å components of the recombined beam are resolved by a quartz prism, isolated with narrow-band interference filters, and detected by photomultipliers. The photomultiplier anode currents are converted to voltages through a 350-hz bandwidth electrometer and are read by a system computer after 12-bit analogue to digital conversion.

Sample gas is introduced into one of the cells (hereafter called the sample

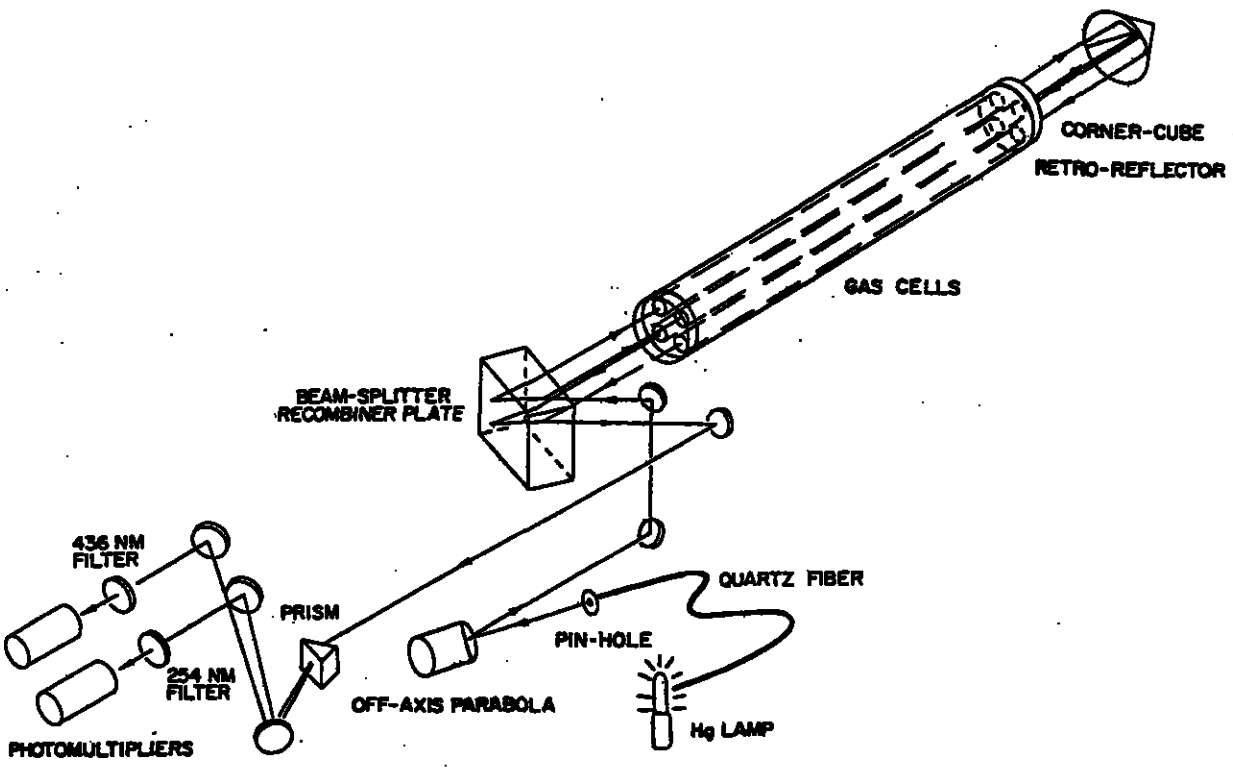

Figure 2.2: Optical System of the Interferometric Oxygen Analyzer.

cell) at an actively-stabilized pressure near 10 atm and under a steady flow of (0.2–0.5) l STP/min. The sample gas introduces an OPD given by

$$OPD_{samp}(\lambda) = \frac{2L}{\lambda}[n_{samp}(\lambda) - 1] \tag{2.7}$$

where $n_{samp}(\lambda)$ is the refractive index of the sample gas, λ is the vacuum wavelength of light and L is the cell length. The relative refractivity is related to the OPD at two wavelengths according to

$$\tilde{r}_{samp}(\lambda_1, \lambda_2) = \frac{n_{samp}(\lambda_1) - 1}{n_{samp}(\lambda_2) - 1} = \frac{\lambda_2 OPD_{samp}(\lambda_1)}{\lambda_1 OPD_{samp}(\lambda_2)} \tag{2.8}$$

In order to resolve small changes in $\tilde{r}_{samp}$, the OPD of the interferometer is modulated by repeatedly admitting dry air at a uniform rate into the second cell (hereafter called the scanning cell), from vacuum to around 20 torr and then re–evacuating. The total OPD of the interferometer is now given by

$$OPD_{tot}(\lambda) = OPD_{samp}(\lambda) - OPD_{scan}(\lambda) + \Delta(\lambda) \tag{2.9}$$

where $\Delta(\lambda)$ allows for any additional contributions to the OPD and where

$$OPD_{scan}(\lambda) = \frac{2L}{\lambda}[n_{scan}(\lambda) - 1] \tag{2.10}$$

where n_{scan} is the refractive index of the scan gas. From Eq. 2.8 and Eq. 2.9, we have

$$OPD_{tot}(\lambda_1) = \frac{\lambda_2}{\lambda_1}\tilde{r}_{samp} OPD_{samp}(\lambda_2) - \frac{\lambda_2}{\lambda_1}\tilde{r}_{scan} OPD_{scan}(\lambda_2) + \Delta(\lambda_1) \tag{2.11}$$

where

$$\tilde{r}_{scan} = \frac{\lambda_2 OPD_{scan}(\lambda_1)}{\lambda_1 OPD_{scan}(\lambda_2)} \tag{2.12}$$

is the relative refractivity of the scan gas.

As scan gas is admitted into the scanning cell, fringes elapse on both the λ_1 and λ_2 detectors. At the instant of occurrence of a particular λ_2 fringe maximum, hereafter known as the reference fringe, we have

$$OPD_{tot}(\lambda_2) = p_2 \tag{2.13}$$

$$OPD_{tot}(\lambda_1) = p_1 + \epsilon_1 \tag{2.14}$$

where $0 \leq \epsilon_1 < 1$ and p_2 and p_1 are exact integers. The parameter ϵ_1, which measures the relative time of occurrence of the reference fringe to an adjacent λ_1 fringe is sensitive to the relative refractivity of the sample gas as can be shown by substituting Eq. 2.14 into Eq. 2.11 and differentiating with respect to X_i, the mole fraction of species i:

$$\frac{d\epsilon_1}{dX_i} = \frac{\lambda_2}{\lambda_1} \cdot S_i \cdot OPD_{samp}(\lambda_2) \tag{2.15}$$

where $S_i = d\tilde{r}_{samp}/dX_i$ is the relative-refractivity sensitivity factor (see Table 2.1). In deriving Eq. 2.15 we have assumed that $OPD_{samp}(\lambda_2)$ is held constant as X_i changes which implies, from Eq. 2.9 and 2.13 that $OPD_{scan}(\lambda_2)$ also remains constant. The sensitivity of ϵ_1 to changes in $OPD_{samp}(\lambda_2)$ is discussed below in Section 2.4.3.

With a cell length of 61 cm (2 ft.) and a sample pressure of 10 atm at 298°C we have from Eq. 2.7

$$OPD_{samp}(\lambda_2) = \frac{(2)(61)}{(4.358 \cdot 10^{-5})}\left(\frac{273}{298}\right)(2.965 \cdot 10^{-4})(10) = 7608 \tag{2.16}$$

and from Eq. 2.15,

$$\frac{d\epsilon_1}{dX_{O_2}} = \frac{(4358)}{(2537)}(7608)(3.10 \cdot 10^{-8}) = 4.05 \cdot 10^{-4}\ \text{ppm}^{-1} \tag{2.17}$$

Thus a resolution of 1 ppm in the oxygen mole fraction requires a resolution in the relative OPD of $4 \cdot 10^{-4}$ of a 2537.27Å fringe.

The fringe remainder ϵ_1 is estimated from the λ_1 and λ_2 fringe signals which are synchronously sampled and stored at a rate 20 to 40 times the fringe rate during the rise in scanning-cell pressure. An example of the raw fringe signals is shown in Fig. 2.3. An algorithm is used for estimating ϵ_1 from the fringe signals which is adapted from the algorithm of Snyder (1980). Details of the fringe algorithm are discussed in Appendix C. In essence, the algorithm first estimates the times of occurrence of all the fringe maxima and minima during the scan (rejecting the first few maxima and minima occurring during the start–up transient) and then uses these times to project an estimate of ϵ_1. While the system computer is occupied with the fringe algorithm, the scanning cell is again evacuated. The entire cycle is repeated automatically after the algorithm is finished and the scanning cell is evacuated to below 0.5 torr. Typically the time required for the entire cycle is around 30 seconds, with around 20 seconds spent on the pressure scan, and 10 seconds spent on the fringe algorithm and other housekeeping tasks. The short-term (scan to scan) reproducibility in ϵ_1 is typically around ± 0.0002 which, under the conditions applying to Eq. 2.17, corresponds to ± 0.5 ppm in the O_2 mole fraction.

The λ_2 reference fringe is unambiguously identified on successive scans on the basis of two independent criteria: (1) The scanning-cell pressure at which the reference fringe occurs should be within a fraction of 1 torr from the pressure at which it occurred on the previous scan and (2) The value of ϵ_1 should lie within ± 0.06 of the value obtained on the previous few scans. The search algorithm for calculating ϵ_1 starts with a default guess for the reference fringe, $p_2^{(0)}$, based on the scanning-cell pressure at which the reference fringe occurred on previous scans. The algorithm then calculates the fringe remainders $\epsilon_1^{(i)}$ for each λ_2

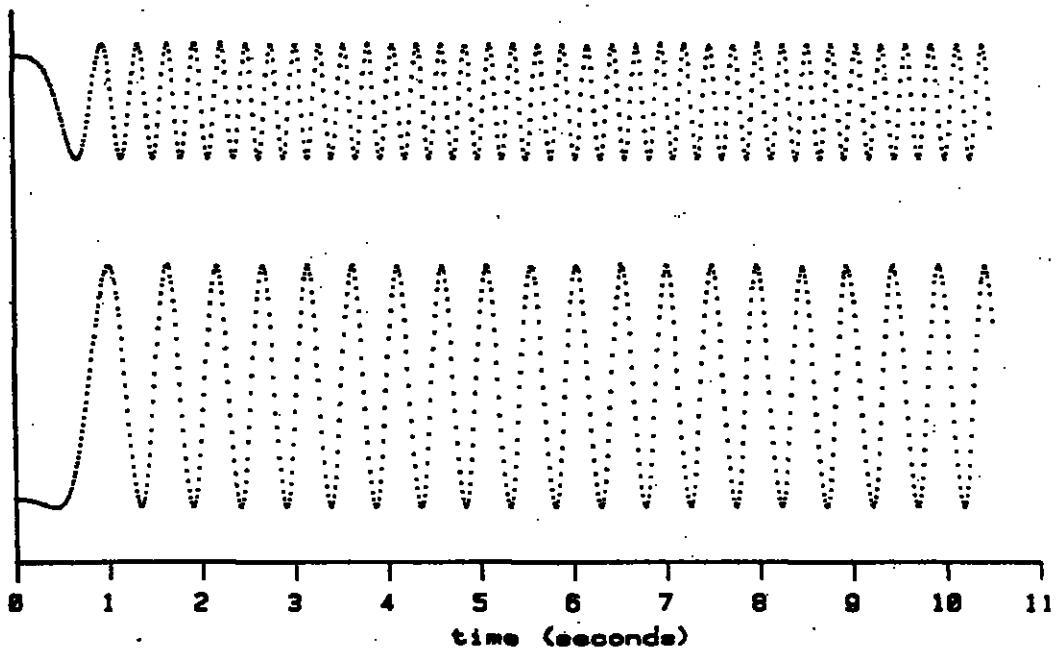

Figure 2.3: Photomultiplier signals versus time at the 2537.27Å (upper) and 4359.56 Å (lower) photomultiplier detectors. The fringes are produced by the controlled admission of gas into the scanning cell. Fringe rate at 4359.56 Å corresponds to approximately 1 fringe per torr scan-gas.

fringe $p_2^{(i)}$ over the range $p_2^{(0)} - 4 \leq p_2^{(i)} \leq p_2^{(0)} + 4$ and seeks i such that $\epsilon_1^{(i)}$ best matches the value of ϵ_1 obtained on the previous few scans. With dry air as the scan gas (for which $(\lambda_2/\lambda_1)\tilde{r}_{scan} = 1.8363$) an incorrect assignment of the reference fringe leads to an error in ϵ_1 of at least 0.180 which is easily distinguished from the typical scan-to-scan reproducibility of ± 0.0002. The search algorithm breaks down if the sample concentration changes too rapidly with time. However, the maximum slew rate of $\delta\epsilon_1 = 0.0060$ per scan or 300 ppm O_2 per minute is certainly adequate for monitoring ambient air.

The calibration of the instrument response depends only on $OPD_{samp}(\lambda_2)$ since the other factors in Eq. 2.15 are constants. $OPD_{samp}(\lambda_2)$ can be measured directly by initially filling the sample cell from vacuum and counting the elapsed fringes. This yields a calibration factor that is accurate to around 1 part in 10^4. For applications involving small deviations between a sample gas and a standard it is only necessary to know the calibration factor to around 1 percent. This can be achieved by using an absolute pressure gauge previously calibrated against the λ_2 fringe count to determine $OPD_{samp}(\lambda_2)$.

2.3 Laboratory Test Results

The physical principles and sub-ppm sensitivity levels of the oxygen analyzer have been verified through a series of calibrations based on proportional mixing of known source gases. The source gases consisted of two cylinders with 21.65% and 21.40% oxygen as supplied by the vendor and certified by comparing to NBS standards with a paramagnetic analyzer. The concentration difference of these cylinders was also verified to be 2500 ± 90 ppm on the basis of the difference in relative refractivity of the samples.

By bleeding small known amounts of the 21.65% mixture into a primary

flow consisting of the 21.40% mixture, concentration shifts at the ppm level could be produced. Fig. 2.4 shows the time trend of the fringe remainder ϵ_1 as the blended gas stream passed through the sample cell. Each data point corresponds to a single fringe analysis cycle. The data show an upward-drifting baseline corresponding to the 21.40% mixture flowing through the interferometer sample cell on which negative offsets corresponding to the injections of the 21.65% mixture are superimposed. The response of the ϵ_1 to the changing concentrations was estimated by interpolating against the drifting baseline, and by scaling the shift in ϵ_1 in units of ppm O_2 according to Eq. 2.15. The concentration shifts derived from the instrument response are plotted against the concentration shifts expected from the proportional mixing in Fig. 2.5.

The linear regression to the data yields a slope of 0.99 ± 0.01 and an intercept of -0.9 ± 0.2 ppm. The standard deviation of the residuals to the fit is ± 0.32 ppm. The intercept of -0.9 ppm between the measured and calculated concentrations is statistically significant and is probably due to slight leakage of the 21.65% mixture into the 21.40% mixture even when the flow of the 21.65% mixture was nominally zero. It is likely that such "leakage" was caused by diffusive mixing of the two source gases from a dead-space between the shut-off valve and the injection point of the 21.65% mixture.

In addition to the response to the changing oxygen concentration, the fringe remainder ϵ_1 exhibits apparently random scan-to-scan variations as well as long-term drift. The origins of these and other errors in the oxygen measurement are discussed in the next section.

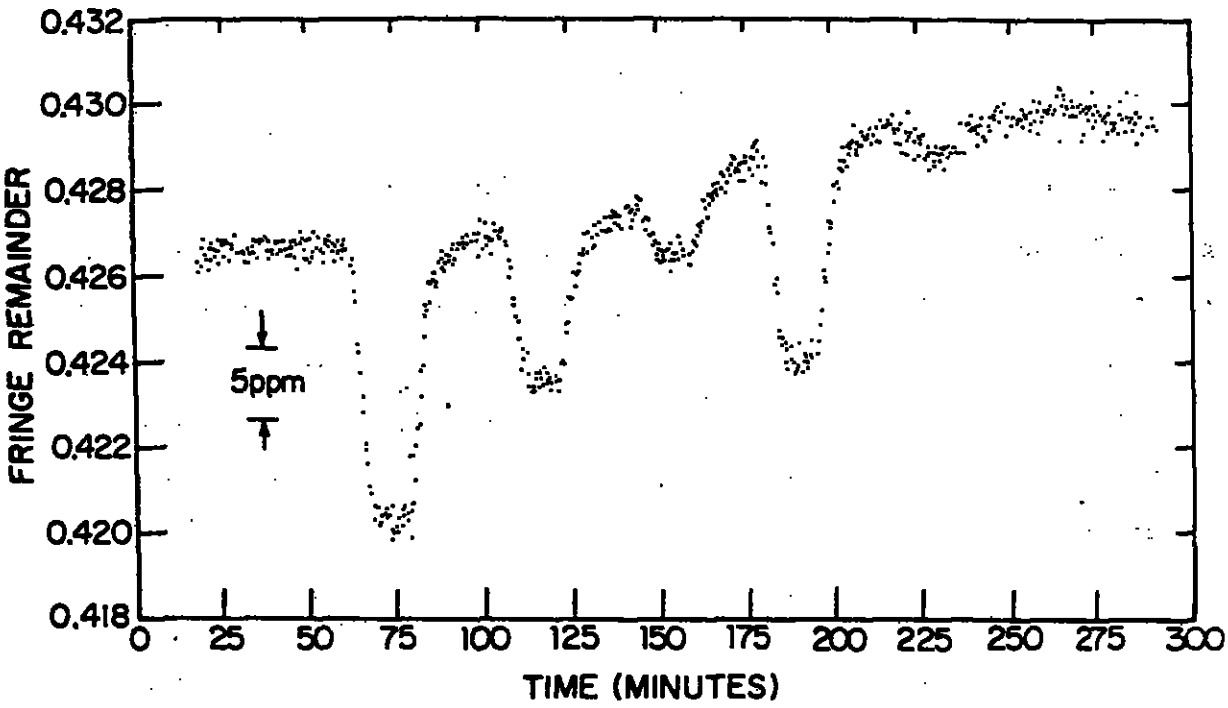

Figure 2.4: Fringe remainder ϵ_1 versus time as differing oxygen concentrations pass through the sample cell. Each data point corresponds to a single fringe-analysis cycle.

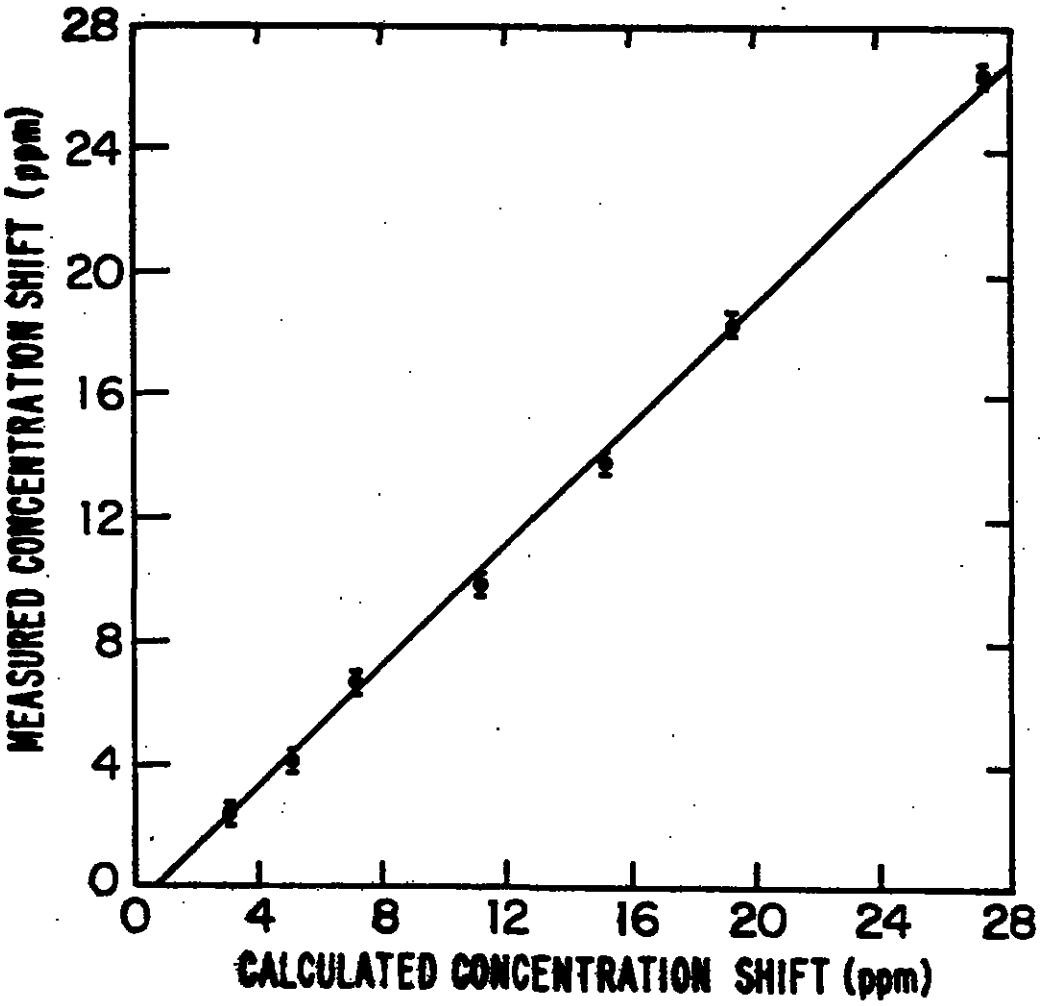

Figure 2.5: Concentration shift as measured from the response in ϵ_1 versus the concentration shift calculated from the known flow proportions.

2.4 Sources of Measurement Error

2.4.1 Signal Intensity Stability

The scan-to-scan repeatability in ϵ_1 is primarily limited, at present, by fluctuations in the intensity of the λ_1 and λ_2 signals. These fluctuations have three origins: Firstly, there is inherent shot-noise which is set by the beam intensity in quantum/sec and the quantum efficiency of the photomultiplier tubes. Secondly, there is additional noise generated by the amplification circuitry in the dynode chain of the photomultiplier and subsequent electronics. Thirdly, there is noise in the emission intensity of the lamp due to fluctuations in the lamp power-supply, or fluctuations in the lamp temperature.

Because the scan-to-scan reproducibility is already as good as ± 0.5 ppm, as discussed above, the noise sources have not been submitted to a detailed study. The photocathode current at the weaker 4359.56Å line is typically $5 \cdot 10^5$ photoelectrons/sec which is the primary source of shot-noise. On the basis of simulations of the fringe-analysis algorithm on signals which contain only shot-noise, it appears that observed reproducibility is within a factor of two of the reproducibility expected on the basis of photomultiplier shot-noise alone. Thus perhaps a two-fold improvement in scan-to-scan reproducibility could be achieved by improving the stability of lamp supply or other electronics. Perhaps an additional two-fold improvement could be achieved by increasing the throughput of the optics which would reduce detector shot-noise. However, a fundamental limit to the scan-to-scan repeatability is set by the finite brightness of the Hg lamp source, and the achieved repeatability is probably no more than a factor of four from this limit.

2.4.2 Scanning-Gas Concentration

Eq. 2.11 indicates that the sensitivity of ϵ_1 to $\tilde{r}_{scan}$ is reduced compared to that of $\tilde{r}_{samp}$ by a factor of $OPD_{scan}(\lambda_2)/OPD_{samp}(\lambda_2) \approx 0.001$. Thus ppm-level fluctuations in the scan-gas composition are negligible.

2.4.3 Sample-Gas Density

In order to evaluate the sensitivity of ϵ_1 to variations in sample-gas density it is convenient to use Eq. 2.13, Eq. 2.14, and Eq. 2.9 in order eliminate $OPD_{scan}(\lambda_2)$ from Eq. 2.11 to yield

$$p_1 + \epsilon_1 = \frac{\lambda_2}{\lambda_1}(\tilde{r}_{samp} - \tilde{r}_{scan})OPD_{samp}(\lambda_2) + \frac{\lambda_2}{\lambda_1}\tilde{r}_{scan}p_2 + \Delta' \tag{2.18}$$

where

$$\Delta' = \Delta(\lambda_1) - \frac{\lambda_2}{\lambda_1}\tilde{r}_{scan}\Delta(\lambda_2). \tag{2.19}$$

The first term on the right-hand side of Eq. 2.18 gives the direct response of ϵ_1 to a change in $OPD_{samp}(\lambda_2)$ which, at constant composition, is equivalent to a change in density. The rate at which ϵ_1 will drift for a drift in $OPD_{samp}(\lambda_2)$ is given by

$$\delta\epsilon_1 = \frac{\lambda_2}{\lambda_1}\left[(\tilde{r}_{samp} - \tilde{r}_{scan}) + OPD_{samp}(\lambda_2) \cdot \frac{d\tilde{r}_{samp}}{dOPD_{samp}(\lambda_2)}\right]\delta OPD_{samp}(\lambda_2) \tag{2.20}$$

where the second term in brackets allows for the variation of $\tilde{r}_{samp}$ with density at constant composition. By properly adjusting the scan-gas composition it is possible to adjust $\tilde{r}_{scan}$ so that the right-hand side of Eq. 2.20 vanishes.

A special case, which is convenient in practice, is to use a scan gas which has virtually the same composition as the sample gas. In this case Eq. 2.20 can

be simplified to yield

$$\delta\epsilon_1 = 2 \cdot \frac{\lambda_2}{\lambda_1} \cdot b \cdot [n_{samp}(\lambda_2) - 1] \cdot \delta OPD_{samp}(\lambda_2) \tag{2.21}$$

where the approximations $\tilde{r}_{samp} = a + b[n_{samp}(\lambda_2) - 1]$, and $\tilde{r}_{scan} = a$ have been used. With the sample cell at 10 atm pressure we have $n(\lambda_2) - 1 \approx 0.003$ which yields

$$\frac{d\epsilon_1}{dOPD_{samp}(\lambda_2)} = (2)\frac{(436)}{(254)}(.014)(.003) = 1.4 \cdot 10^{-4} \tag{2.22}$$

This shows that if the sample-cell pressure drifts by the equivalent of one 4359.56Å fringe the error in the estimate of the oxygen mole fraction is $0.00014/0.0004 = 0.3$ ppm.

The errors induced by density changes in the sample gas are reduced by actively stabilizing $OPD_{samp}(\lambda_2)$. A two-level feedback-control loop is used for this purpose. At the inner level, the pressure in a buffer volume upstream of the sample cell is actively stabilized using a capacitance differential-pressure gauge to generate an error signal proportional to the difference between the buffer- and reference-volume pressures. The error signal is fed back through a control circuit (MKS Instruments 250B controller) which makes settings on an automatic regulating valve at the inlet to the buffer volume. The inner feedback loop typically achieves a short-term stability of better than ± 0.01 torr out of a total pressure of around 7600 torr. The outer control loop relies on an error signal consisting of the deviation of the $OPD_{samp}(\lambda_2)$, detected as described below, from a setpoint to make adjustments in the pressure setpoint of the inner control loop. The outer loop operates once per fringe-analysis cycle and can either be operated by making manual adjustments to the pressure setpoint or by using the system computer to make automatic adjustments.

The technique for measuring changes in $OPD_{samp}(\lambda_2)$ relies on Eq. 2.9 and Eq. 2.13 which can be rearranged to yield

$$OPD_{scan}(\lambda_2) = OPD_{samp}(\lambda_2) - p_2 + \Delta(\lambda_2) \tag{2.23}$$

which indicates that changes in $OPD_{samp}(\lambda_2)$ can be detected via changes in $OPD_{scan}(\lambda_2)$. Changes in $OPD_{scan}(\lambda_2)$ can be detected through scan-to-scan changes in the value of scanning-cell pressure at which the reference fringe occurs. Since, for a 61 cm cell, one λ_2 fringe corresponds to roughly one torr change in pressure, the scanning-cell pressure only needs to be determined to 0.1 torr out of 10 torr in order to determine $OPD_{samp}(\lambda_2)$ to 0.1 of a fringe. Using this technique, it has been possible to stabilize $OPD_{samp}(\lambda_2)$ for several hours to within ± 0.2 fringe corresponding to an error in X_{O_2} of ± 0.06 ppm (see Eq. 2.22).

2.4.4 Temperature

Temperature changes in the interferometer optics and in the gas cells are the primary cause of long-term variations in ϵ_1 through the Δ' term of Eq. 2.18. Unfortunately, the form given for Δ' in Eq. 2.19 is not very helpful for understanding sources of drift in Δ' because the terms are not easily measured. However, considerable insight has been gained into the factors contributing to changes in Δ' by studying how ϵ_1 responds to systematic changes in ambient temperature.

Changes in ambient temperature cause changes in the OPD of the cell windows due to thermal expansion and the increase in the refractive index of the glass with temperature. The change induced in a 1.6 cm fused-silica cell window amounts to 0.37 $\lambda/°C$ and 0.77 $\lambda/°C$ at 4359.56Å and 2537.27Å respectively

(calculated from specifications of Corning 7940 fused silica). A uniform change in window temperature, however, does not induce changes in the OPD of the interferometer because both beams in the interferometer are transmitted the same number of times (twice) through each window optic. Only temperature gradients in the windows can cause shifts in the OPD through this mechanism, and the temperature gradients induced by changes in ambient temperature are probably not significant.

The initial cell-window design called for a high parallelism specification (1 arc-second) in order to reduce prismatic separation of the two wavelengths. Through a mechanism which was not anticipated, however, this parallelism of the window apppears to cause significant variations in the OPD of the interferometer through variations in window temperature. This mechanism operates because a plane-parallel window acts like a low-finesse etalon.

The amplitude of a light beam transmitted through a plane-parallel window consists of the sum of a directly-transmitted and multiply-reflected components (which have suffered one or more reflections on each face of the window). The amplitude of the transmitted beam is given by (see e.g. Born and Wolf, 1975, pages 323–325)

$$A^{(t)} = \frac{1-r}{1-re^{i\delta}} A^{(i)} \tag{2.24}$$

where $A^{(i)}$ is the incident amplitude, r is the (intensity) reflection coefficient, and where

$$\delta = \frac{4\pi}{\lambda} nh$$

where n and h are the refractive index and window thickness respectively. For $r \ll 1$, Eq. 2.24 can be simplified to

$$A^{(t)} = [1 - r(1 - cos\delta)]\ e^{irsin\delta} A^{(i)} \tag{2.25}$$

which indicates that the phase of the transmitted beam varies sinusoidally with δ, i.e. with the window temperature. For an uncoated window, $r \approx 0.05$ so that the phase can vary over a range of $\pm 0.05/2\pi = \pm 0.008\lambda$ over temperature changes as small as 0.5 °C.

The OPD of the interferometer is affected by the etalon phase-shifts at each of the four window orifices for each of the two arms of the interferometer. Furthermore, the quantity ϵ_1 is affected by the shifts in the OPD at both wavelengths with the 4359.56Å shifts scaled by the factor $(\lambda_1/\lambda_2) \cdot \tilde{r}_{scan} \approx (436/254)(1.06) = 1.8$ as indicated by the coefficient of the $\Delta(\lambda_2)$ term in Eq. 2.18. Assuming all these components add randomly, one expects the root-mean-square deviation of ϵ_1 with small temperature changes to be around ± 0.023.

If the windows of the interferometer were perfectly parallel and flat, one would expect the etalon phase-shifts on both arms of the interferometer to complement one another and thus produce no change in the OPD. This is because both arms of the interferometer pass the same number of times through each window optic and thus would experience identical phase-shifts. However, in order for phase-shifts of one arm to compensate the phase-shifts in the other arm it would be necessary to hold the window-parallelism specification to better than $\lambda/8$ at 2537.27Å between the orifices. With the present window orifice separation of 3.2 cm, this corresponds to a parallelism of 0.15 arc-seconds, a specification which is not satisfied with the present window optics.

The etalon action of the cell windows can be eliminated by giving the window a slight wedge angle. However, this introduces prismatic separation of the λ_1 and λ_2 beams which can also cause temperature sensitivity through the interaction between variable density gradients in the gas and misalignment of the λ_1 and λ_2 beam components. It was assumed, in deriving Eq. 2.8, that

the λ_1 beam and the λ_2 beam exactly overlap. If the beams do not exactly overlap, the ratio $OPD_{samp}(\lambda_1)/OPD_{samp}(\lambda_2)$ is sensitive to any difference in the average density of the sample gas between the λ_1 beam and the λ_2 beam. For example, for the 61 cm cell at 10 atm, a uniform misalignment of 1mm between the 2537.27 and 4359.56Å components subject to a temperature gradient along the direction of misalignment of 10^{-3} $^{\circ}C$/cm yields an offset in ϵ_1 of around 0.004. This offset would change if the magnitude or direction of the temperature gradient changed.

The prismatic separation of the beams can be avoided, however, by introducing a wedged compensation plate which counteracts the window wedge angle. In the near future, I am planning to install cell windows with a 120 arc-second wedge with compensating plates which should significantly reduce the sensitivity of the interferometer to changes in ambient temperature.

Temperature changes can be caused by heating or cooling in the gas itself. Under adiabatic expansion or contraction, the temperature of an ideal gas varies with pressure according to

$$T \propto P^{\frac{\gamma-1}{\gamma}} \tag{2.26}$$

where $\gamma \doteq C_p/C_v = 1.4$ for air. The most serious consequence of fluctuations in sample pressure is the inducement of temperature changes in the cell windows. The fringe positions are particularly sensitive to temperature changes originating in the gas because the heating or cooling is initially communicated to window orifices in only one arm (the sample-cell arm) of the interferometer.

A sudden increase in the sample-cell pressure of, for example, 0.01 atm. out of 10 atm. total pressure increases the gas temperature by $9 \cdot 10^{-2}$ $^{\circ}C$. As the gas cools back into equilibrium with the cell walls a certain amount of the excess heat is conducted into the window. As a very rough estimate we can assume

that the excess heat produced up to distance r from the window, where r is the sample-cell bore radius, will be conducted into the window. By conservation of energy, this implies that the average temperature of the orifice will increase by roughly $(r/h) \cdot (C_p/C_{glass})$ times the temperature increase in the gas where h is the window thickness, C_p is the heat capacity of the gas (expressed per unit volume) and C_{glass} is the heat capacity of the glass (also expressed per unit volume). Taking $r/h = 0.4$ and $C_p/C_{glass} = 0.01$ (values for air at 10 atm. and fused silica), yields a ratio of $3 \cdot 10^{-3}$. For the pressure fluctuation of 0.01 atm this yields an average temperature increase in the window orifice of $2.7 \cdot 10^{-4}$ $^{\circ}C$. This same increase will occur in each window orifice of the sample-cell, i.e. at four locations in total. Thus the change in the OPD of the sample-cell at 2537.27Å is estimated to be $8 \cdot 10^{-4}$ λ. This thermal perturbation will relax on a time scale given approximately by $h^2/D_{glass} = (1.6\text{cm})^2/(0.008\text{cm}^2/\text{sec}) = 320$ seconds where D_{glass} is the thermal diffusivity of the window material (here Corning 7940 fused silica).

Oxygen measurements are particularly sensitive to pressure fluctuations which occur in sample cell at the instant when the reference gas and sample gas are exchanged. Such pressure fluctuations can produce relatively long-lived temperature transients in the cell windows which can obscure the signature of concentration difference between samples. This difficulty has been eliminated by the active feedback-control loop discussed above which readily reduces short-term fluctuations in sample-cell pressure to below one part in 10^5 of the total pressure.

2.5 References

Born, M. A., E. Wolf, 1975, *Principles of Optics*, Pergamon, Oxford.

Cuthbertson C., M. Cuthbertson, 1914, *Phil. Trans. Royal Soc. London.* **62**, 213.

Cuthbertson C., M. Cuthbertson, 1932, "The refraction and dispersion of neon and helium," *Proc. Roy. Soc. London Ser. A.* **135**, 40-47.

Edlèn, B., 1966, "The refractive index of air," *Metrologica* **2(2)**, 71-80.

Erickson, K. E., 1962, "Investigation of the invariance of atmospheric dispersion with a long-path refractometer," *Journal of the Optical Society of America* **52(7)**, 777-780.

Ford, A., J. C. Brown, 1973, "Direct-resolvent-operator computations on the hydrogen-molecule dynamic polarizibility, Raleigh and Raman scattering," *Phys. Rev. A.* **7(2)**, 418.

Jackson, J. D., 1975, *Classical Electrodynamics, 2nd Ed.*, John Wiley & Sons, New York.

Kaufman, V., 1962, "Wavelengths, energy levels, and pressure shifts in mercury 198," *Journal of the Optical Society of America* **52**, 866–870.

Keeling C. D., R. B. Bacastow, T. P. Whorf, 1982, "Measurements of the concentration of carbon dioxide at Mauna Loa Observatory, Hawaii," W. C. Clark ed., *Carbon Dioxide Review: 1982*, Oxford University Press, New York, 377–385.

Koch, J.,1909,"Dispersionsmessungen an Gasen im Sichtbaren und im Ultraroten Spektrum.", *Nova Acta Regiae Societatis Scientiarum Upsaliensis*, **4(2)**, no. 5.

Koch, J., 1949, "On the refraction and dispersion of the noble gases krypton and xenon," *Kungl. Fysiografiska Sällskapets i Lund Förhandlingar* **19(13)**, 173–187.

Khalil, M. A. K., R. A. Rasmussen, 1986, "Interannual variability of atmospheric methane: possible effects of the El Niño–Southern Oscillation," *Science* **232**, 56–57.

Ladenburg, R., Wolfsohn, G., 1932, "Untersuchungen über die Dispersion von Gasen und Dämpfen und ihre Darstellung durch die Dispersionstheorie. III. Die Dispersion des Sauerstoffs zwischen 6000 und 1920 Å," *Zeitschrift für Physik* **79**, 42–61.

Logan, J. A., M. J. Prather, M. B. Wofsy, M. B. McElroy, 1981, "Tropospheric chemistry: a global perspective," *Journal of Geophysical Research* **86**, 7210–7254.

Machta L., E. Hughes, 1970, "Atmospheric Oxygen in 1967 and 1980," *Science* **168**, 1582–1584.

Mansfield, C. R., E. R. Peck, 1969, "Dispersion of helium," *J. Opt. Soc. Am.* **59(2)**, 199-204.

Monchalin, J.-P., M. J. Kelly, J. E. Thomas, N. A.Kurnit, A. Szöke, F. Zernike, P. H. Lee, A. Javan, 1981, "Accurate laser wavelength measurement with a precision two–beam scanning Michelson interferometer," *Applied Optics* **20(5)**, 736–757.

Old, J. G., K. L. Gentili, E. R. Peck, 1971, "Dispersion of carbon dioxide," *Journal of the Optical Society of America* **61(1)**, 89–90.

Peck, E. R., D. J. Fisher, 1964, "Dispersion of Argon," *Journal of the Optical Society of America* **54(11)** 1362–1364.

Peck, E. R., B. N. Khanna, 1966, "Dispersion of Nitrogen," *Journal of the Optical Society of America* **56(8)**, 1059–1063.

Smith, P. L., M. C. E. Huber, W. H. Parkinson, 1976, "Refractivities of H_2, He, CO, and Kr for $168 \leq \lambda \leq 288$ nm," *Physical Review A* **13(4)**, 1422–1434.

Snyder, J. J., "Algorithm for fast digital analysis of interference fringes," *Applied Optics* **19(8)** 1223–1225.

Snyder, J. J., 1982, "Laser wavelength meters," *Laser Focus*, May 1982, 55–61.

Svensson, K.-F.,1960, "Measurement of the dispersion of air for wavelengths from 2302 to 6907 Å," *Arkiv för Fysik* **16(35)**, 361–384.

US, 1976, *U. S. Standard Atmosphere, 1976*, National Oceanic and Atmospheric Administration, National Aeronautics and Space Administration, United States Air Force, U. S. Printing Office, Washington, D. C.

Weiss, 1981, "The Temporal and Spatial Distribution of Tropospheric Nitrous Oxide," *Journal of Geophysical Research* **86(C8)**, 7185–7195.

Zeiss, G. D., W. J. Meath, 1975, "The H_2O–H_2O dispersion energy constant and the dispersion of the specific refractivity of dilute water vapour," *Molecular Physics* **30(1)**, 161–169.

Chapter 3

Air Measurements in Cambridge

3.1 Introduction

In this chapter I report measurements of the atmospheric O_2 mole fraction in Cambridge, Massachusetts using the interferometric oxygen analyzer. These measurements were conducted with simultaneous CO_2 measurements on the same air stream. The purpose of these measurements was twofold:

- To test the instrument on real air.
- To explore the correlation between CO_2 and O_2 in urban air.

Urban air is a useful testing ground for the oxygen analyzer because local fuel combustion causes the atmospheric O_2 mole fraction to vary at the 10 to 100 ppm level on a relatively short time scale of a day or less. Insofar as the dominant fuels—natural gas, fuel oil, and gasoline—span a limited range of oxidation states, simultaneous measurements of CO_2 provide an important consistency test for the O_2 measurements.

3.2 Experimental Method

Air was drawn from outside a first-floor window located about 10m from Oxford St., a moderately busy street. The air was drawn through an inlet system into a manifold and from the manifold into the oxygen analyzer. The inlet system consisted successively of a 12m inlet line, a cold trap at −78°C, a membrane filter for removing particulates, a diaphram compressor pump, and a second cold trap at −78°C. Previous tests (involving saturating, drying, and then analyzing for differences in O_2 mole fraction) showed that this procedure did not detectably alter the O_2 mole fraction. The manifold allowed ambient air or reference gas to be introduced into the interferometer alternately. When a reference gas was used, the ambient air stream was vented to the room through a back-pressure regulator in order to maintain a constant flow rate and a steady pressure in the inlet system at all times. This was necessary because it was found that pressure fluctuations could lead to fluctuations in O_2 mole fraction (presumably due to differential physisorption of O_2 and N_2).

Between the manifold and the interferometer the flow passed successively through a cold trap at −78°C, a sub-micron filter, an automatic flow-control valve, a ballast volume, and a fine metering valve. The ballast volume served to isolate the interferometer sample cell against upstream pressure variations and to stabilize the flow. The pressure in the ballast volume was stabilized by feedback from an electronic controller (MKS 250B) to an automatic flow-control valve. The materials exposed to the gas included stainless steel, glass, and teflon, and trace amounts of viton and Apiezon N vacuum grease. The sample attained a pressure of 1935 torr in the sample cell at a flow rate of 680 cm^3 STP/min. The time required to flush the volume spanned by inlet manifold and sample cell (combined volume estimated to be 380 cm^3) was roughly 1.3

minutes.

Carbon dioxide concentrations were measured in the exhaust line of the interferometer with a non-dispersive dual-cell infrared analyzer (Binos) operated at ambient pressure. The infrared analyzer was operated at all times with a nominal 340-ppm reference gas flowing through the carbon dioxide analyzer reference cell at ambient pressure. Carbon dioxide concentrations are reported on a scale linear in instrument response which was based on a two-point calibration with reference gases with 340.0±0.5 ppm and 380.0±0.5 ppm respectively. The imprecision of replicate readings on the adjusted scale was ±0.1 ppm.

To correct for thermal drift, the interferometer sample cell was flushed with a reference gas at intervals of around 2 hours. The reference gas, containing 343.9 ppm CO_2, was derived from a cylinder of air compressed at the Scripps Pier in La Jolla, California during conditions when the wind was blowing off the ocean. The interferometer response from three or four consecutive calibrations was fitted in a least-squares sense to a second- or third-order polynomial. This established a calibration baseline which was subtracted from the interferometer readings with ambient air on a point-for-point basis. Tests using polynomials of different orders and using different consecutive sets of readings indicated that the baseline could be interpolated with a precision of approximately ±2.0 ppm O_2.

3.3 Results and Discussion

Ambient air was monitored on the evening of 25 Oct. 1986 and throughout the next day. Fig. 3.1 shows the output of the CO_2 and O_2 analyzers over a selected time interval on 26 Oct. which spans three calibrations intervals. Fig. 3.2 shows a fraction of this interval in closer detail. The output of both analyzers is

expressed in units of ppm mole fraction difference between ambient air and the reference gas. The individual readings of the oxygen and carbon dioxide analyzer, taken at 30-second intervals, have been smoothed with a four-point *running mean*. The output of the oxygen analyzer has been scaled according to the sensitivity factor in Eq. 2.5 but has not been corrected for the interference of carbon dioxide and other gases. The CO_2 corrections are the wrong sign and four times too small to account for the observed response. Other gases, most notably CO and hydrocarbons, which can be present in the 0 to 10 ppm level in urban air, might also account for a fraction of the response of the O_2 analyzer. However, since these gases would tend to increase with increasing CO_2, their contribution to the change in dispersion is, again, of the wrong sign. The observed decrease in dispersion with increasing CO_2 must be caused by changes in O_2 mole fraction.

The data show fluctuations in CO_2 and O_2 mole fraction that are strongly anticorrelated on time scales ranging from minutes to hours. The level of instrumental noise on the oxygen analyzer is evident from the scale of fluctuations during the calibration intervals.

A summary of the diurnal trends in O_2 and CO_2 is shown in Fig. 3.3. These data represent the average concentration recorded between calibration intervals on both 25 and 26 Oct. These O_2 data have been corrected for the instrumental CO_2 interference according to

$$\delta X_{O_2} = \delta X_{O_2}^{(\text{uncorrected})} - \frac{S_{CO_2}}{S_{O_2}} \delta X_{CO_2}. \qquad (3.1)$$

On the evening of 26 Oct., the atmosphere was relatively still, and ambient CO_2 increased from 350 to 410 ppm overnight while O_2 decreased by a similar amount. A storm system moved in on 26 Oct. accompanied by increasing winds, a decrease in CO_2 towards background levels, and a comparable increase in O_2.

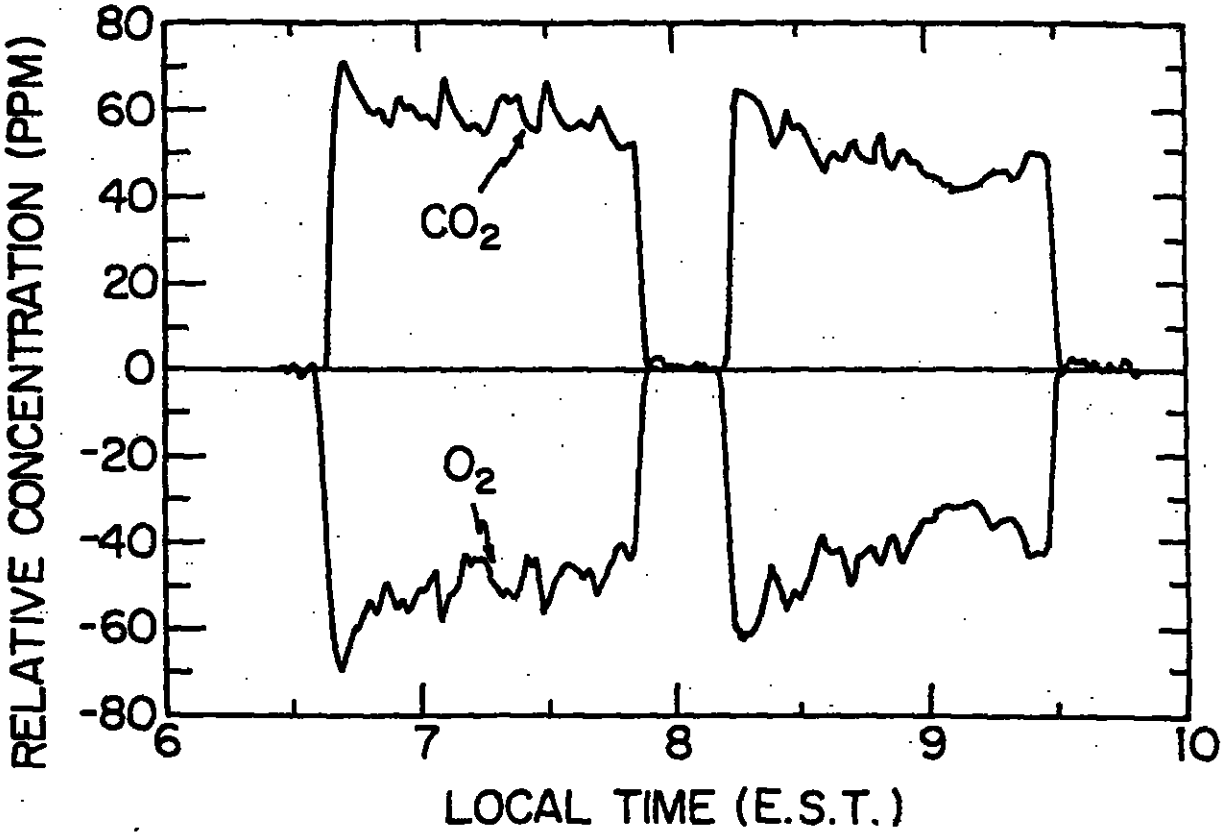

Figure 3.1: Temporal trends of the response of the O_2 and CO_2 analyzers expressed as the difference between ambient air and the reference gas in ppm (mole fraction). Oxygen data has not been corrected for interferences of CO_2, CO, and hydrocarbons.

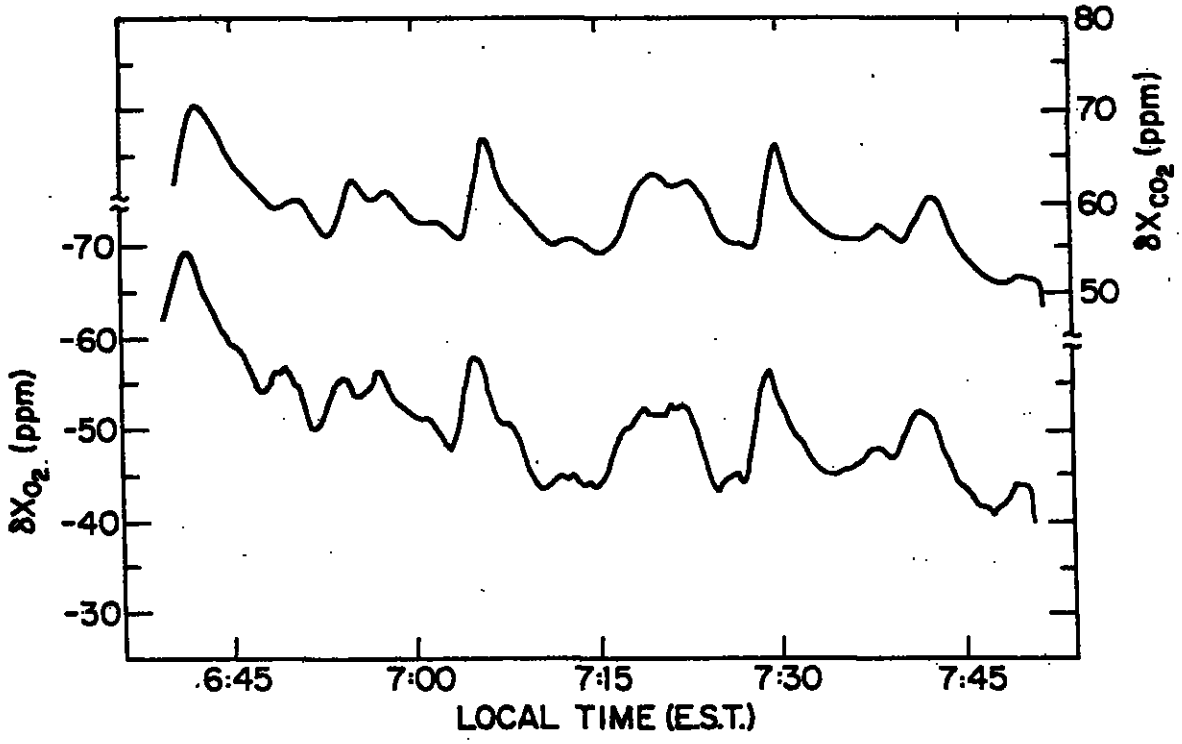

Figure 3.2: Detail from Figure 3.1. O_2 axis has been inverted to allow better visualization of correlations.

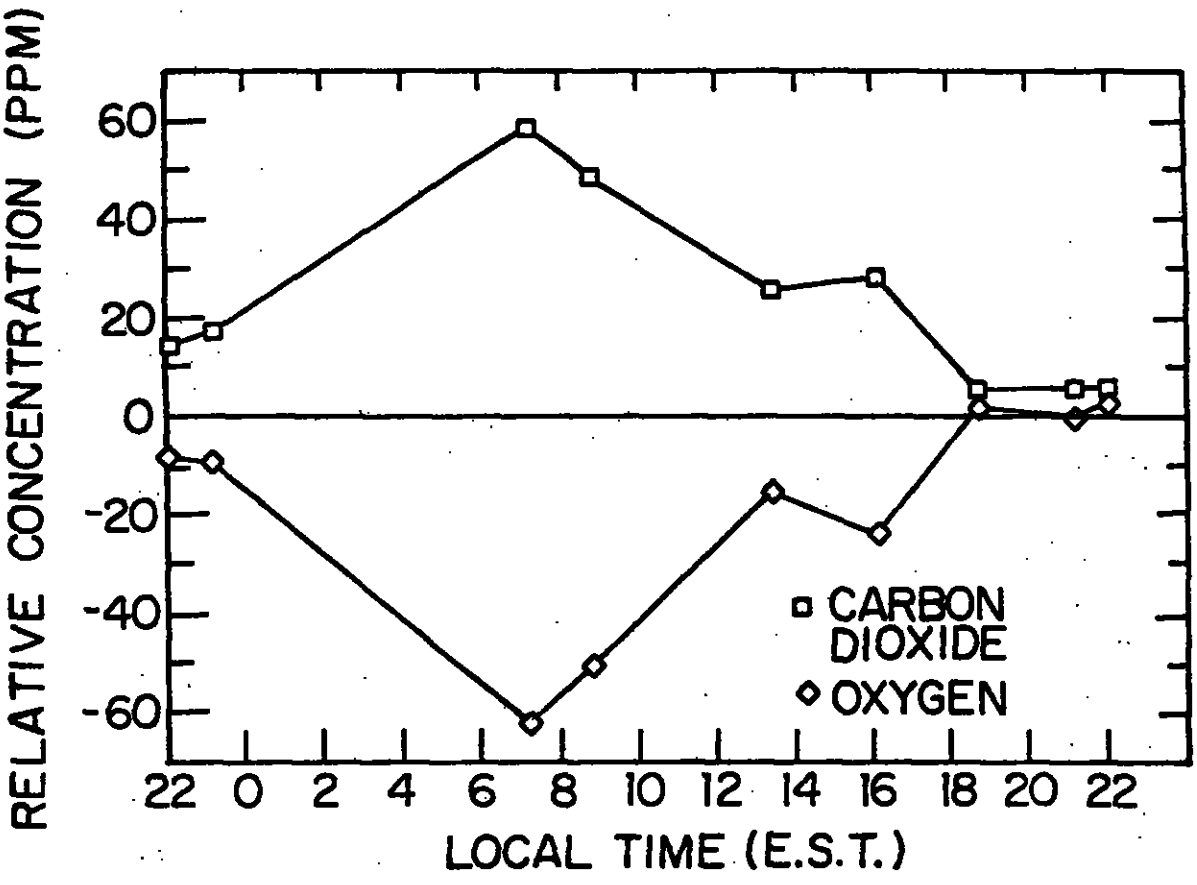

Figure 3.3: Diurnal trend in O_2 and CO_2. The data represent averages of the ambient levels of the oxygen and carbon dioxide recorded between calibration intervals. The data are expressed in units of ppm (mole fraction) difference between ambient air and reference gas. The O_2 data has not been corrected for possible interferences of CO and hydrocarbons.

Table 3.1: Measured difference between ambient oxygen and carbon dioxide mole fractions and reference gas in ppm.

Date	Time	CO_2	O_2	Date	Time	CO_2	O_2
25 Oct. 86	22:44	12.5	-5.9	26 Oct. 86	14:21	28.8	-20.9
	23:31	17.0	-8.9		15:14	33.1	-31.9
	23:17	13.5	-6.7		16:16	24.3	-18.0
26 Oct. 86	0:16	18.3	-10.2		16:52	17.0	-8.4
	6:50	60.0	-67.0		18:14	4.4	1.3
	7:13	55.8	-55.2		18:35	7.0	-1.4
	7:21	62.2	-64.5		19:07	3.9	7.2
	7:36	56.2	-56.7		20:26	9.3	-1.1
	8:46	49.3	-51.7		20:43	14.1	-7.7
	9:09	42.1	-39.5		21:02	2.8	7.0
	10:58	27.6	-19.8		22:09	4.9	5.3
	11:16	21.4	-13.0		22:23	4.9	7.8
	13:33	26.2	-15.7				

In order to explore the extent of the correlation between O_2 and CO_2 mole fractions, time intervals of approximately five minutes were selected during which stable readings were recorded on both analyzers. The CO_2 and O_2 readings were averaged over each interval, and the O_2 readings were corrected for CO_2 interference as outlined above. These data are summarized in Table 3.1 and the CO_2-corrected O_2 readings are plotted against CO_2 readings in Fig. 3.4. A least-squares fit to the data yields a linear correlation coefficient of 0.991 which is valid at better than the 99.9% confidence level, and a slope of -1.218 ± 0.025 (1σ) ppm O_2 per ppm CO_2. Based on the imprecision for replicate scans of ± 2 ppm, the imprecision for a five-minute average is estimated to be ± 0.6 ppm. The ambiguity of the calibration baseline leads to an additional error of around ± 2 ppm, as discussed above. The standard deviation of the residuals to the fit is ± 2.5 ppm which is an independent upper estimate to the total error since some of the variance in the fit could be due to atmospheric variability.

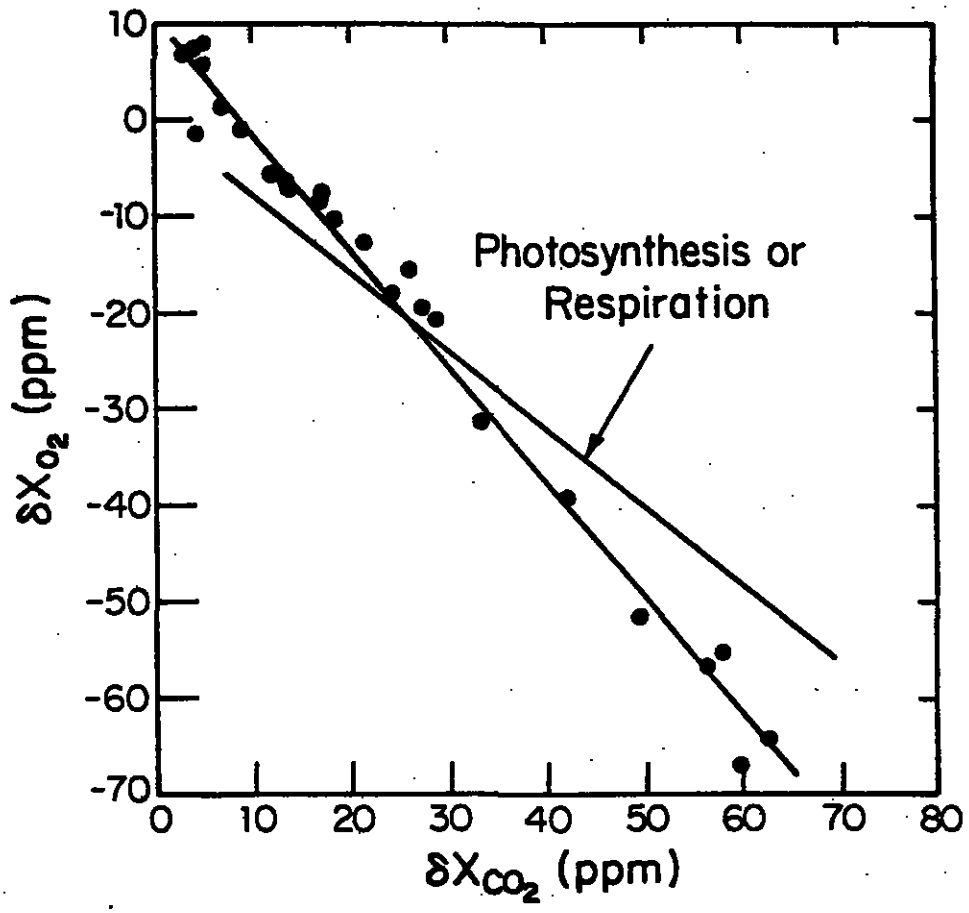

Figure 3.4: Measured ambient O_2 versus CO_2 concentrations measured on 25 and 26 Oct. 1986. Concentrations reported in mole-fraction difference between ambient air and reference gas in ppm. The O_2 data have not been corrected for possible interferences of CO and hydrocarbons. The line through the data is a linear least-squares fit. The line labeled "photosynthesis or respiration" corresponds to an oxidative ratio of 1 mole O_2 per mole CO_2.

The slope of the correlation plot contains information about the average composition of material oxidized in the local environment at the time of the measurements. Quantitative interpretation of the correlation, however, requires an assessment of the magnitude of CO and hydrocarbon interferences. CO levels often achieve 10 ppm or more in urban air, and significant CO interference during the measurements appears likely. Although non-methane hydrocarbon (NMHC) levels in Boston as high as 5 ppm have been observed in the summer, a typical summer value is around 400 ppb (Sexton and Westberg, 1984) and lower NMHC levels would be expected under the cool ($\approx 10°C$) conditions under which these measurements were carried out. The following analysis neglects possible interferences from NMHCs.

Allowing for formation of CO, we can represent the combustion of fuel according to

$$CH_x + (1 - \frac{y}{2} + \frac{x}{4}) \cdot O_2 \longrightarrow (1-y) \cdot CO_2 + y \cdot CO + \frac{x}{2} \cdot H_2O. \qquad (3.2)$$

where CH_x represents the composition of the fuel and y represents the fraction of C emitted as CO. The oxidative ratio of the fuel, i.e. the ratio of O_2 consumed to CO_2 emitted in the full oxidation of the fuel, is given by

$$(OR) = 1 + \frac{x}{4}. \qquad (3.3)$$

If changes in the atmospheric abundances of O_2, CO_2, and CO are determined only by Eq. 3.2, then the atmospheric mole fractions of these species are related according to

$$\delta X_{O_2} = -(1 - X_{O_2}) \cdot \left[\frac{1 - \frac{y}{2} + \frac{x}{4}}{1-y}\right] \cdot \delta X_{CO_2} \qquad (3.4)$$

$$\delta X_{CO} = \left[\frac{y}{1-y}\right] \cdot \delta X_{CO_2} \qquad (3.5)$$

where X_{O_2} is the O_2 mole fraction on a constant CO_2 and CO basis.

We now define the quantity r to be the ratio of the change in the relative refractivity of air scaled in units of ppm O_2 according to Eq. 2.4 to the change in X_{CO_2}. It follows that

$$r \cdot \delta X_{CO_2} = \delta X_{O_2} + \frac{S_{CO_2}}{S_{O_2}} \cdot \delta X_{CO_2} + \frac{S_{CO}}{S_{O_2}} \cdot \delta X_{CO}. \tag{3.6}$$

From Eq. 3.3 to 3.6 it follows that

$$(OR) = \frac{1-y}{1-X_{O_2}} \left[-r + \frac{S_{CO_2}}{S_{O_2}} + \frac{y}{1-y} \cdot \frac{S_{CO}}{S_{O_2}} \right] + \frac{y}{2}. \tag{3.7}$$

Eq. 3.7 has been used to calculate the observed oxidative ratio listed in Table 3.2 where $r - S_{CO_2}/S_{O_2}$ has been identified with the least-squares slope in Fig. 3.4. The uncertainty in the oxidative ratio allows for experimental uncertainties and assumes $y = 0.085 \pm 0.085$. This latter assumption allows CO/total C emission ratios to range from 0% to 17% where the high value corresponds to the emission factors for automobiles in an urban environment (Holey, 1987). The observed oxidation ratio agrees with the ratio expected for gasoline burning to within the uncertainties (see Table 3.2). This is consistent with automobiles being the dominant local CO_2 source and O_2 sink.

3.4 Comparison with Previous Studies

A landmark in the study of atmospheric O_2 is the work of Benedict (1912). Benedict performed numerous analyses of air drawn from outside the Nutrition Laboratory of the Carnegie Institution of Washington located in Boston in order to assess the level of variability in atmospheric O_2. These measurements spanned a period of nearly three years and were conducted during different

Table 3.2: Comparison of oxidative ratio for common fuels compared with oxidative ratio implied by the measured O_2/CO_2 correlations.

Observed oxidative ratio[a]	$1.60 \pm .07$
gasoline[b]	$1.52 - 1.56$
natural gas[c]	$1.83 - 2.00$
fuel oil[d]	$1.39 - 1.44$

[a]Computed according to Eq. 3.7. The calculation assumes that $8.5 \pm 8.5\%$ of the C is emitted as CO and the stated uncertainty allows of the variance to the least-squares fit between the scaled instrument response and measured CO_2 concentrations, the inaccuracy of scaling of carbon dioxide analyzer response, and the uncertainty in the CO emission factor, assuming errors are statistically independent.

[b]Based on range of composition spanned by the two types of gasoline listed in Mark's Handbook (1967).

[c]Based on range of composition spanned by fuels, Index 1 and Index 7 from Cardwell and Benton (1971).

[d]Based on range of composition spanned by the three types of fuel oil listed in Mark's Handbook, (1967).

weather conditions and different seasons. These measurements relied on chemically extracting O_2 from air and observing the volume contraction, a technique which formed the primary basis for virtually all atmospheric O_2 measurements prior to 1970. Several modifications in the analysis procedure were carried out in an endeavour to improve the measurements. Benedict was concerned with random errors arising in the measurements and performed replicate measurements on air drawn from a steel cylinder as a control. A latter set of measurements from April, 1911 to January, 1912 achieved a standard deviation of 0.06% (60 ppm) while measurements on air from the steel cylinder over the same period achieved a comparable standard deviation. Benedict's work provided strong evidence that fluctuations in oxygen in Boston over a wide range of conditions did not exceed 0.06%. Concurrent measurements of atmospheric CO_2 yielded a mean of 0.030% (see footnote in Krogh, 1919) and a standard deviation of 0.0025%. Although Benedict did not examine correlations between

the atmospheric CO_2 and O_2 measurements, his study is significant because it demonstrated that the fluctuations in O_2 did not greatly exceed the fluctuations in CO_2.

Krogh (1919) reports simultaneous measurements of CO_2 and O_2 in Copenhagen. This study employed a volumetric technique, which Krogh claimed achieved a standard deviation for replicate measurements of an identical air sample of 0.00025% (2.5 ppm) for CO_2 and 0.0005% (5 ppm) for O_2. Krogh reported a series of 14 measurements from October, 1917 to January, 1918 which showed that CO_2 levels in Copenhagen were usually increased 10 to 70 ppm above the background (then about 300 ppm), and that there was roughly an equal deficit in O_2 corresponding to the increase in atmospheric CO_2. The correlation plot of these data is shown in Figure 3.5. Krogh's data yields a linear correlation coefficient of 0.83 which is significant at greater than the 99.9% level. A linear least-squares fit yields a slope corresponding to an oxidative ratio of 1.39 ± 0.23. The scatter of Krogh's data about the least-squares line is greater than allowed by his stated precision. Because Krogh's study was conducted over several months, this scatter might very likely be due to true atmospheric variability, although analytic errors may also be a factor. Note that the oxidative ratio implied by Krogh's measurements is slightly larger than one would expect from coal burning or from photosynthesis/respiration, presumably the major O_2 and CO_2 sources and sinks at that time, although this difference probably is not statistically significant.

Carpenter (1937), using apparatus similar to Benedict's, reports measurements of atmospheric O_2 and CO_2 in Baltimore, Boston, and Durham. Each series yielded a virtually constant atmospheric O_2 concentration with the standard deviations of individual measurements being typically 0.04% (40 ppm). Concurrent measurements of atmospheric CO_2 yielded a standard deviation of

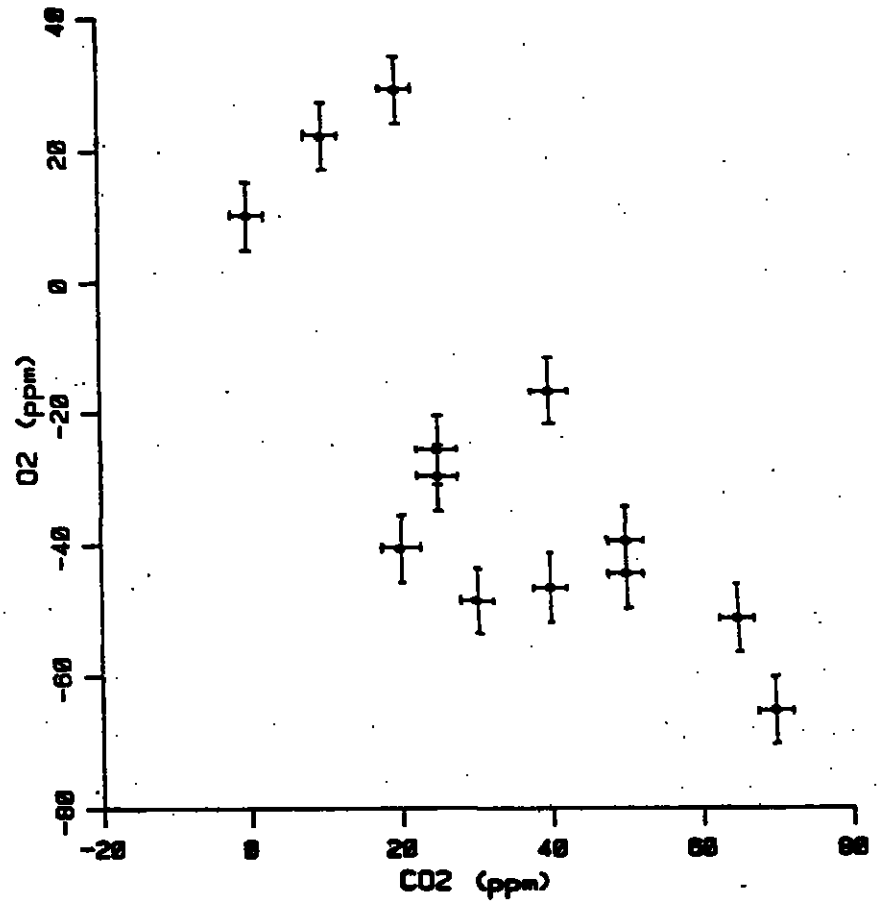

Figure 3.5: O_2 and CO_2 measurements of Krogh (1919). O_2 concentrations are reported on a mole-fraction basis which includes CO_2 as opposed to a CO_2–free basis used in Fig. 3.4.

0.0016%. Carpenter does not address the possibility of correlations between atmospheric O_2 and CO_2 and does not present tabulations of the individual analysis.

The only additional survey of atmospheric O_2 conducted since 1910 appears to be the work of Machta and Hughes (1970). Samples of dried air were taken in stainless-steel flasks and analyzed in the laboratory by comparison with a cylinder of compressed air with a paramagnetic O_2 analyzer. Samples were taken only in "clean" air, mostly over the oceans. Examination of the tabulated shipboard samples yields a standard deviation of 15 ppm. Any variability in O_2 was generally smaller than the uncertainty of the measurements. This study was not accompanied by simultaneous measurements of CO_2.

In addition to the studies mentioned above, a few isolated measurements of atmospheric O_2 have been reported: Lockhart and Court (1942), Shepherd (1935), and Hughes (1968). These studies, however, do not address the question of short-term variability in atmospheric O_2.

Only one previous study by Krogh (1919) demonstrated sufficient precision in simultaneous O_2/CO_2 measurements to detect coherent variations. Krogh's data is qualitatively consistent with the data presented here; however, the comparison is not very meaningful because of the relatively large uncertainties in Krogh's data.

3.5 Conclusions

Short-term fluctuations in atmospheric oxygen mole fraction have been detected in the air in Cambridge, Massachusetts by interferometric detection of changes in relative refractivity. The fluctuations in oxygen are strongly anti-correlated with changes in carbon dioxide, and the amplitude ratio of the changes is con-

sistent with that expected from gasoline burning. The precision of the oxygen measurements is ±2 ppm in the mole fraction. This study represents a significant improvement in analytic precision over the previous study of Krogh (1919) which is apparently the only previous study in which variations in atmospheric O_2 have been positively detected.

Although this study reports only measurements in urban air, the results are significant because they demonstrate the feasibility of detecting variations in atmospheric oxygen at the level expected in background air. There are many important biogeochemical questions which could be addressed with this technique including the magnitude of seasonal variations and the ratio of O_2 exchange to CO_2 exchange from different ecosystems.

3.6 References

Benedict, F. G., 1912, *The Composition of the Atmosphere with Special Reference to its Oxygen Content*, Carnegie Institution of Washington, Washington, D. C.

Carpenter, T. M., 1937, "The constancy of the atmosphere with respect to carbon dioxide and oxygen content," *J. Amer. Chem. Soc.* **59**, 358-360.

Cardwell, L.E., L. F. Benton, 1971, "U. S. Bureau of Mines Information Circular 8518, Analysis of Natural Gases."

Holey, T., Environmental Protection Agency, Air Management Division. Personal communication.

Hughes, E. E., 1968, "A simple technique for the absolute determination of atmospheric oxygen," *Environmental Science and Technology* **2(3)**, 201-203.

Krogh, A., 1919, "The composition of the atmosphere," *Det Kgl. Danske Videnskabernes Selskab.* **1** no. 12.

Lockhart E. E., A. Court, 1942, "Oxygen deficiency in Antarctic air," *Monthly Weather Review* **70(5)**, 93-96.

Machta, L., E. Hughes, 1970, "Atmospheric Oxygen in 1967 and 1970," *Science* **168**, 1582-1584.

Marks, L. S., 1967, *Standard Handbook for Mechanical Engineers, 7th ed.*, New York, McGraw–Hill.

Sexton K., H. Westberg, 1984, "Nonmethane hydrocarbon composition of urban and rural atmospheres," *Atmospheric Environment* **18(6)**, 1125–1132.

Shepherd M., 1935, "The composition of the atmosphere at approximately 21.5 kilometers," *U. S. Army stratosphere flight of 1935 in Balloon Explorer II* National Geographic Soc., Washington D. C., 117-133.

Chapter 4

The Contemporary Oxygen Budget

4.1 Introduction

One feature which clearly distinguishes the earth from the other planets of the solar system is the presence of oxygen in the atmosphere. The oxygen content of the earth's atmosphere is remarkable given the overall oxidation state of the upper crust and mantle, and the origin of atmospheric O_2 must ultimatly be a consequence of its production by photosynthesis. The O_2 in the earth's atmosphere is testimony to to the strong impact of life on the overall chemistry of the earth.

Recent studies of atmospheric O_2 have centered around the questions of the origin and long-term stability of atmospheric O_2; questions which are fundamental to the study of the coevolution of climate and life (see e.g. Holland, 1984; Garrels and Lerman, 1981; Walker, 1977; Lovelock and Lodge, 1972, Van Valen, 1971). The time scales of interest to these studies has ranged from tens

of millions to billions of years.

Little scientific effort has gone into the study of changes in O_2 on time scales shorter than a million years. This is in part because changes in O_2 on such short time scales must of necessity be very slight and thus of little direct environmental consequence (see e.g. Broecker, 1970). A more fundamental reason, however, is the lack of evidence for changes in atmospheric O_2 on shorter time scales. Small changes in O_2 would be virtually impossible to discern in the geologic record, and even the depletion in atmospheric O_2 over the last century caused by burning fossil fuel has been too slight to detect with previously available oxygen analyzers (Machta and Hughes, 1970).

This latter difficulty has recently been overcome: with the development of the interferometric O_2 analyzer, discussed above, it should now be possible to resolve short-term seasonal, secular, and interannual variations in the atmospheric O_2 mole fraction. (Changes in O_2 mole fraction essentially record changes in O_2 because the changes in N_2 and Ar, the other dominant species in air, are much smaller than changes in O_2.) Other techniques to measure the O_2 mole fraction (or equivalently the O_2/N_2 ratio) such as Raman scattering or conventional mass spectrometry may soon achieve similar resolution. Also, past changes in O_2 may be detectable through measurements of air trapped in ice cores. It is appropriate, therefore, to review what is known about short-term sources and sinks of O_2.

The purpose of this chapter is to review what is presently known or can be inferred about contemporary sources and sinks of O_2. Principal concerns are the sources and sinks of O_2 from human activities such as burning fossil fuel and deforestation. Also of interest is the application of atmospheric O_2 measurements for deriving changes in size of the biosphere, an idea first put forth by Machta (1980). Section 4.2 outlines the primary terms in the global

O_2 cycle. Section 4.3 discusses the coupling between the sources and sinks of O_2 and sources and sinks of CO_2 from burning fossil fuel and changing biomatter reservoirs, and discusses the possibilty of estimating biospheric CO_2 sources from atmospheric O_2 data. Section 4.4 discusses the oxygen consumption from industrial activities. Included in Section 4.4 are estimates of O_2 consumption factors for solid, liquid, and gaseous fuels and tabulations of the yearly O_2 consumption from 1860 to 1982. Section 4.5 discusses the O_2/CO_2 exchange ratios with terrestrial organic matter. Section 4.6 assesses the magnitude of various natural sources and sinks of O_2. Finally, Section 4.7 discusses the likeliest scenarios for recent atmospheric O_2 depletion. These scenarios will form a basis for comparing measurements of future or past changes in atmospheric O_2.

4.2 The Oxygen Cycle

Tables 4.1 and 4.2 summarize the principal reservoirs and fluxes of O_2 and organic matter. Fig. 4.1 depicts the O_2 cycle.

Atmospheric oxygen is coupled to the terrestrial reservoirs of organic matter via photosynthesis and respiration

$$CO_2 + H_2O \rightleftharpoons H_2CO + O_2 \qquad (4.1)$$

where CH_2O represents the approximate composition of terrestrial organic matter (see Section 4.5 below). Atmospheric O_2 is also coupled to the reservoir of dissolved O_2 in the ocean via air–sea exchange. Dissolved O_2 in the ocean is coupled to the marine reservoirs of organic matter via photosynthesis and respiration which proceed according to

$$106CO_2 + 16NO_3^- + H_2PO_4^- + 17H^+ + 122H_2O \rightleftharpoons C_{106}H_{263}O_{110}N_{16}P + 138O_2 \qquad (4.2)$$

Table 4.1: Primary reservoirs of O_2 and organic matter.

O_2 Reservoirs	Moles O_2
Atmosphere[a]	$3.705 \cdot 10^{19}$
Total ocean[b]	$2.25 \cdot 10^{17}$
Surface ocean (0–100m)[c]	$8.3 \cdot 10^{15}$

Organic Reservoirs	Moles C	Est. Average Oxidative Ratio	Potential O_2 sink
Terrestrial Reservoirs:			
Living Biomass	$4.7 \cdot 10^{16}$[d]	1.05	$5.0 \cdot 10^{16}$
Soils	$1.3 \cdot 10^{17}$[e]	1.07	$1.4 \cdot 10^{17}$
Ocean Reservoirs:			
Dissolved Organic Carbon	$8.3 \cdot 10^{16}$[f]	$1.0 - 1.3$	$8.3 - 11 \cdot 10^{16}$
Particulate Organic Carbon	$2.5 \cdot 10^{15}$[e]	1.3	$3.2 \cdot 10^{15}$
Plankton	$2.5 \cdot 10^{14}$[e]	1.3	$3.2 \cdot 10^{14}$
Fossil Fuel:[g]			
Coal	$5.7 \cdot 10^{17}$	1.17	$6.7 \cdot 10^{17}$
Crude Oil	$2.1 \cdot 10^{16}$	1.44	$3.0 \cdot 10^{16}$
Natural Gas	$1.2 \cdot 10^{16}$	1.95	$2.3 \cdot 10^{16}$
Oil Shale	$2.4 \cdot 10^{16}$	1.44[h]	$3.5 \cdot 10^{16}$
Oil Sands	$8 \cdot 10^{16}$	1.44[g]	$1.2 \cdot 10^{16}$
Total fossil fuel	$7.1 \cdot 10^{17}$		$7.7 \cdot 10^{17}$
Sedimentary rocks[i]			$1.6 \cdot 10^{21}$

[a]Based on total mass of dry air of $5.124 \cdot 10^{21}$g (Trenberth, 1981), mean molecular weight of dry air of 28.97g/mole (US, 1976), and O_2 mole fraction of .20946 (Machta and Hughes, 1970).

[b]Derived using 3.90 ml/l average O_2 concentration and $1.299222 \cdot 10^9$ km^3 total ocean volume, from Table 65 in Levitus (1982).

[c]Derived from Levitus (1982) tables 59a and 61 taking totals for standard levels 1 through 6 plus half of standard level 7.

[d]From Olson (1982).

[e]From Schlesinger (1984).

[f]From Mopper and Degens. (1979)

[g]Ultimately recoverable reserves. Values for C reserves from Sundquist (1985) based on fuel reserves from WEC (1980).

[h]Oxidative ratio for crude oil is assumed to apply for oil shale and oil sands.

[i]Includes oxygen demand of both organic carbon and pyrite in sedimentary rocks and in metamorphic rocks of sedimentary composition, from Garrels and Perry (1974).

Table 4.2: Fluxes of O_2 and organic matter.[a]

Atmosphere, terrestrial biosphere:	
Net primary production (NPP)	4.4–5.5
Gross primary production (GPP)	$\approx 2 \cdot$ NPP
Litter fall	4.2
Decay of organic matter	$= -$NPP
Anthropogenic deforestation (net)	-0.08 ± 0.04
Agriculture (net)	-0.12 ± 0.08
Fossil fuel burning (1980):	-0.610 ± 0.061
Iron ore reduction (1980):	$+0.0066 \pm 0.00007$
Air–sea exchange[b]	140
Ocean, marine biota:	
Primary production	4.3
Detritus fallout from surface	0.4
Lithosphere[c]:	
Sedimentation	$+0.010 \pm 0.002$
Weathering	-0.012 ± 0.003
Oxidation of volcanic gases	0 to -0.003
Hydrogen escape (i.e from H_2O)[d]:	$+0.00004$

[a] In units of 10^{15} moles O_2 or O_2 equivalent (i.e. O_2 required to fully oxidise the material) per year, . Adapted from Bolin (1983) unless otherwise indicated.

[b] Based on invasion rate of 379 mole/m^2/yr from Broecker and Peng (1982) and ocean surface area of $362 \cdot 10^6$ km^2 from Dietrich et al. (1980). Invasion rate used is the average of the rates listed for 0°C and 24°C.

[c] Fluxes from Holland (1978).

[d] Calculated from rate of $3 \cdot 10^8$ atoms/cm^2 sec cited in Holland (1984).

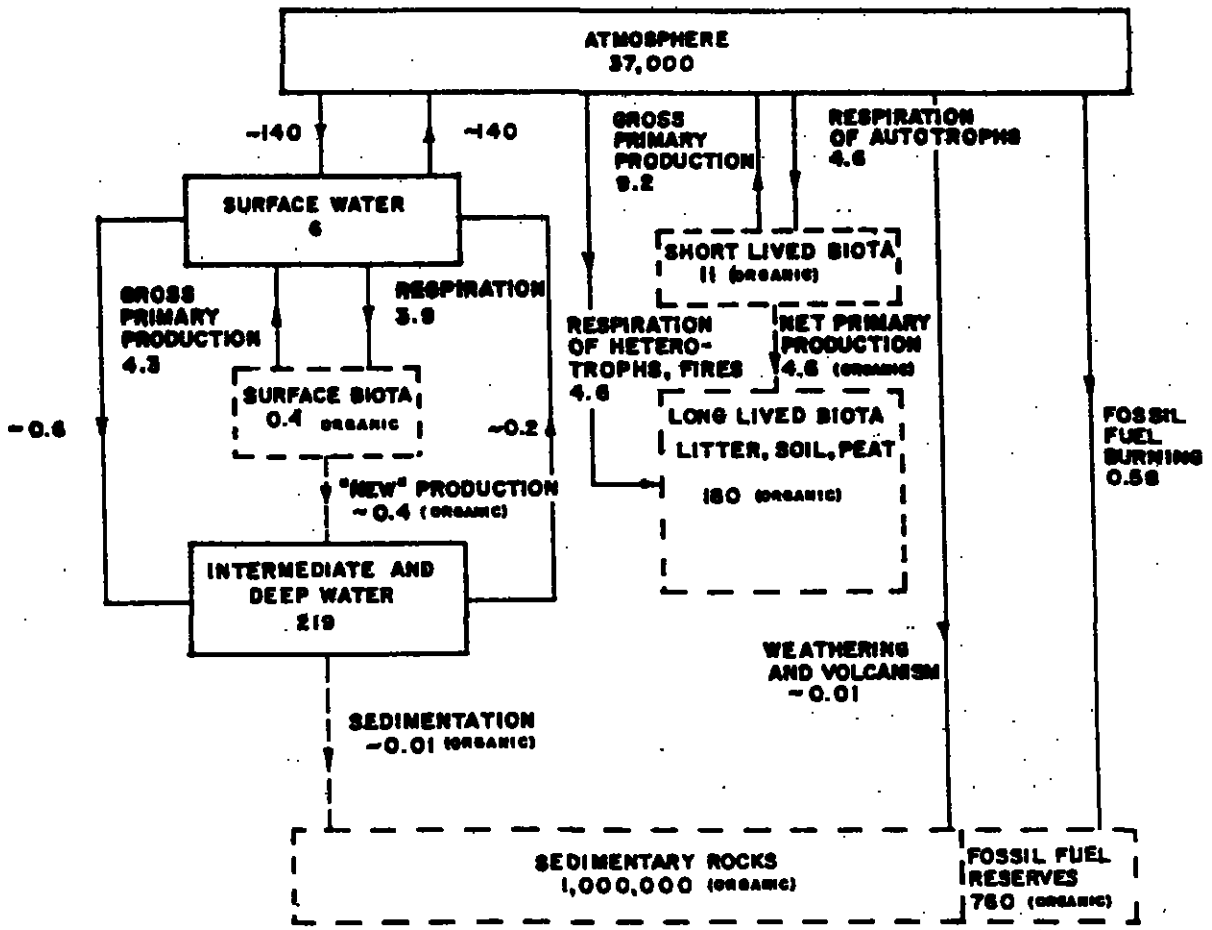

Figure 4.1: The global oxygen cycle showing short-term and long-term sources and sinks and coupling with the carbon cycle in units of 10^{15} moles and 10^{15} moles/yr. Oxygen fluxes and reservoirs are denoted by solid lines, and solid boxes, respectively. Organic fluxes and reservoirs are denoted by dashed lines and dashed boxes, respectively. Organic matter is expressed in terms of O_2 equivalent, i.e. the amount of O_2 required to fully oxidize the material. Organic reservoirs and fluxes are adapted from Bolin (1983). Advective fluxes of O_2 in the ocean are determined by the assumption of steady state consistent with an assumed 1000-year turnover time for the intermediate and deep-water reservoir. Other reservoirs and fluxes are consistent with Tables 4.2 and 4.1

where $C_{106}H_{263}O_{110}N_{16}P$ represents the approximate composition of plankton (Redfield et al. 1962).

Most organic matter produced photosynthetically on land and in the ocean is rapidly recycled. Net O_2 is produced only by that small fraction of organic matter which escapes oxidation and is buried 'permanently' in sediments. It appears that most organic carbon in sediments is of marine origin, terrestrial organic matter being of secondary importance (Holland, 1978, pp. 221–222). Some of the organic matter is oxidized at the expense of sulfate during the formation of sediments, although this process is probably only of secondary importance to the balance of atmospheric O_2. Net O_2 is consumed by the weathering of re-exposed sediments and by the oxidation of volcanic gases. These processes effectively couple the atmospheric O_2 reservoir to the reservoir of reduced material cycling through the crust and mantle.

The estimated abundance of reduced material in the crust and mantle would consume, if fully oxidized, 40 times the present atmospheric level (PAL) of O_2. With the cycling time of atmospheric O_2 with respect to coupling with the lithosphere estimated at four million years, it is clear that the processes of weathering, volcanism, and sedimentation must exert a major influence on the atmospheric abundance of O_2 on time-scales longer than a few million years. Because the deposition rate of reduced sediments is a sensitive function of dissolved-O_2 and nutrient levels in the ocean, it is possible that marine biological cycles have served to stabilize atmospheric O_2 on time-scales longer than 4 million years (see e.g. Holland, 1978. McElroy, 1976). Mechanisms for stabilizing atmospheric O_2 through biological or abiological control of the escape of hydrogen have also been proposed (Lovelock and Lodge, 1972; Brinkmann, 1969). Such feedback mechanisms could hardly be expected to prevent significant variations in atmospheric O_2 over geologic time. Indeed, studies of the isotopic composition of

carbonates suggest that there has been substantial variability in the fraction of carbon deposited as organic matter over the past 600 million years, although studies of the isotopic composition of sulfates suggest that variations in the deposition rate of reduced sulfur compounds may have partially compensated for variations in the deposition rate of organic carbon (Holland, 1984; Veizer et al. 1980). Probably the most significant boundary condition on the variabilty of atmospheric O_2 over the past 600 million years is the continuity of aerobic life.

On time-scales much shorter than 4 million years the overall oxidation state of the atmosphere-ocean-biospheric system must remain nearly constant. Thus changes in atmospheric O_2 must be balanced by changes in the organic reservoirs or in the dissolved-O_2 reservoir of the oceans. Over time-scales of 10,000 years or more we might expect substantial variations in the reservoirs of terrestrial organic carbon or in the reservoir of dissolved O_2 in the ocean. Based on the present sizes of these reservoirs, we would expect the corresponding variations in atmospheric O_2 to amount to at most 1% of PAL.

On time-scales of a few years or less we expect the dominant natural variability in atmospheric O_2 to be caused by seasonal or interannual imbalances in the exchange with land plants and ocean surface waters. The regular seasonal variations which have been detected in atmospheric CO_2 (see e.g. Keeling et al. 1982, Kohmyr et al. 1985) are attributed primarily to exchange with the land biosphere, and it is expected that atmospheric O_2 must undergo complementary variations. Dissolved O_2 in the ocean mixed-layer equilibrates with the atmosphere on a time-scale of approximately 3 weeks. Plankton blooms, the seasonal warming and cooling of surface waters, and the rapid weakening of the thermocline in winter could drive substantial seasonal fluxes of O_2 across the air–sea interface. Indeed, the study of Jenkins and Goldmann (1985) of a site off Bermuda indicates seasonal net fluxes as large as 7 moles m^{-2} yr^{-1} which

implies hemispheric-scale variations of roughly 0.002–0.005% of PAL (4 to 8 ppm in the O_2 mole fraction)

4.3 The Human Imprint on Atmospheric O_2

Burning fossil fuels depletes atmospheric O_2 according to

$$C_xH_y + (x + \frac{1}{4}y)O_2 \rightarrow xCO_2 + \frac{1}{2}yH_2O \tag{4.3}$$

At the present rate of fuel consumption atmospheric O_2 would be exhausted in 64,000 years; however, the known fuel reserves will be exhausted long before this happens. The oxidation of known fuel reserves would reduce atmospheric O_2 by 2%. The consequences of a 2% loss in O_2 are probably not serious since the reduction in O_2 partial pressure is equivalent to only a 160-m rise in elevation.

Although the loss of O_2 from burning fossil fuel is apparently not a serious environmental issue, knowledge of the net changes in atmospheric O_2 could be of importance for defining sources and sinks of CO_2. In particular, as noted by Machta (1980), atmospheric O_2 data could potentially be used to determine the net CO_2 source from biospheric changes.

Assuming that the burning of fossil fuel and the oxidation of biospheric organic matter are the only significant sources and sinks of O_2, we can express the change in atmospheric O_2 according to

$$A_{O_2} = F_{O_2} + B_{O_2} \tag{4.4}$$

where A_{O_2} is the net decrease in atmospheric O_2, F_{O_2} is the net O_2 sink from burning fossil fuel, and B_{O_2} is the net O_2 sink from oxidation of biospheric

organic matter, all in units of moles O_2/yr. Likewise, we can express changes in atmospheric CO_2 according to

$$A_{CO_2} = F_{CO_2} + B_{CO_2} - O_{CO_2} \tag{4.5}$$

where A_{CO_2} is the net increase in atmospheric CO_2, F_{CO_2} is the CO_2 source from burning fossil fuel, B_{CO_2} is the net CO_2 source due to oxidation of biospheric organic matter, and O_{CO_2} is the net CO_2 sink due to dissolution of inorganic carbon in the ocean, all in units of moles C/yr

The fossil-fuel CO_2 source can be linked to the fossil-fuel O_2 sink according to

$$F_{O_2} = (OR)_F \cdot F_{CO_2} \tag{4.6}$$

where $(OR)_F$ is the average ratio of moles O_2 consumed per mole CO_2 produced by burning fossil fuel. (OR_F) accounts, not only for the C content of the fuel, but also for H, S, N, or O which are important for the determining oxygen consumption. Likewise, the net biospheric CO_2 source can be linked to the net biospheric O_2 sink according to

$$B_{O_2} = (OR)_B \cdot B_{CO_2} \tag{4.7}$$

where $(OR)_B$ is the average oxidative ratio, (also known as photosynthetic quotient) for biospheric organic matter.

If the change in atmospheric O_2 is measured and the loss of O_2 from burning fossil fuel is accounted for, the net biospheric CO_2 source can be estimated from Eqs. 4.4–4.7 according to

$$B_{CO_2} = (OR)_B^{-1} [A_{O_2} - F_{O_2}] . \tag{4.8}$$

The determination of the net biospheric CO_2 source from Eq. 4.8 requires, in addition to measurements of atmospheric O_2, the following information:

- Accurate accounting of the O_2 sink from burning fossil fuel and other industrial processes.
- An estimate of the appropriate world-mean oxidative ratio of biospheric organic matter.
- Accounting of any additional sources and sinks of O_2 and CO_2 which have been neglected in this analysis.

The primary purpose of the subsequent sections is to discuss these terms.

For some applications the magnitude of the net oxidative CO_2 source,

$$S_{CO_2} = F_{CO_2} + B_{CO_2}, \tag{4.9}$$

is more relevant rather than the magnitude of either component F_{CO_2} or B_{CO_2} separately. The net oxidative CO_2 source is required for estimating the airborne fraction

$$(AF) = \frac{A_{CO_2}}{S_{CO_2}} \tag{4.10}$$

which is an important constraint on models used to forcast the uptake of fossil-fuel CO_2 by the ocean. (see e.g. Clark et al., 1982). From Eq. 4.8 and 4.9 we can write

$$S_{CO_2} = F_{CO_2} + \frac{A_{O_2} - F_{O_2}}{(OR)_B} \tag{4.11}$$

which from Eq. 4.6 can be rearranged to yield

$$S_{CO_2} = +\frac{A_{O_2}}{(OR)_B} - \left[\frac{(OR)_F}{(OR)_B} - 1\right] \cdot F_{CO_2}. \tag{4.12}$$

Since $(OR)_B \approx 1$, the second term on the right-hand side is nearly equal to $[(OR)_F - 1]F_{CO_2}$, which is simply the O_2 loss owing to the oxidation of elements other than carbon (e.g. H, S, N, etc.) in fossil fuel.

Using Eq. 4.12 to estimate the net oxidative CO_2 source has two potential advantages. Firstly, Eq. 4.12 does not require knowing the net biospheric CO_2 source. Secondly, the term in Eq. 4.12 which is proportional to fossil-fuel consumption is smaller than the corresponding term in Eq. 4.9. This means that errors in estimated fossil-fuel consumption will propagate to smaller errors in the net oxidative CO_2 source using Eq. 4.12 than using Eq. 4.9.

4.4 Industrial Oxygen Consumption

In this section, I have outlined a procedure for calculating the historical industrial oxygen consumption. These estimates use, where possible, the same data sets that have been used for calculating industrial production of CO_2. Included in this section are estimates of the year-by-year oxygen consumption from 1860 to the present. This work should be viewed as a preliminary set of estimates, and I have tried to show where refinements may be needed if more accurate estimates are to be made.

The procedure for estimating fossil-fuel CO_2 emissions used by Keeling (1973a), Rotty (1983), and Marland and Rotty (1984) is based on calculating separately the CO_2 emissions from solid, liquid, and gaseous fuels according to

$$F_{CO_2}^{(i)} = (P^{(i)})(FO^{(i)})(C^{(i)}) \tag{4.13}$$

where $F_{CO_2}^{(i)}$ is the annual CO_2 emissions in units of mass of carbon, $(P^{(i)})$ is the fuel-production data, $(FO^{(i)})$ is the fraction of the fuel produced which is oxidized, and $(C^{(i)})$ is the average carbon content of a particular fuel group. The factor $(P^{(i)})$ is derived from the global fuel-production figures published by the United Nations (UN, 1982). The factor $(FO^{(i)})$ is derived from estimates of the fraction of 'fuel' diverted into non-fuel uses or incompletely oxidized

in combustion. The factor $(C^{(i)})$ is derived from statistical summaries of the average elemental abundance of carbon in each fuel group.

The same procedure can be used for estimating oxygen consumption if, instead of the factor $(C^{(i)})$, a factor is substituted which accounts for the quantity of oxygen required to fully oxidize the fuel. Oxygen consumption is then estimated according to

$$F_{O_2}^{(i)} = (P^{(i)})(FO^{(i)})(O^{(i)}) \tag{4.14}$$

where $F_{O_2}^{(i)}$ is the mass of oxygen consumed, and $(O^{(i)})$ is the mass of oxygen consumed per unit of fuel burnt and $(P^{(i)})$ and $(FO^{(i)})$ are the same as in Eq. 4.13.

The factor $(O^{(i)})$ depends on the carbon, hydrogen, oxygen, sulfur, and nitrogen content of the fuel. Oxygen consumption is calculated according to

$$\begin{aligned} &CH_wO_xS_yN_z + \left(1 + \frac{w}{4} - \frac{x}{2} + \frac{3}{2}y + \frac{5}{4}z\right) O_2 \longrightarrow \\ &CO_2 + \left(\frac{w}{2} - y - \frac{z}{2}\right) H_2O + yH_2SO_4 + zHNO_3 \end{aligned} \tag{4.15}$$

which assumes that the final oxidation states of sulfur and nitrogen are S^{VI} and N^{V} respectively. Although this assumption requires more careful consideration, the sulfur and nitrogen content of fuels is virtually insignificant compared to the hydrogen and carbon content.

Some justification is required for using the same efficiency factor $(FO^{(i)})$ for estimating O_2 consumption as well as CO_2 emissions. Fuels which are diverted into non-fuel usages or incompletely burnt may be partly oxidized such that O_2 is consumed even though CO_2 is not released. An example of this is the formation of carbon monoxide during combustion (although CO formation is not accounted for in CO_2 emission estimates because CO undergoes relatively rapid oxidation in the atmosphere). I am neglecting such processes in the

present analysis because I am assuming that only a small fraction of diverted or incompletely-burnt fuels remain for very long in a partly-oxidized state, and the fractions of fuel diverted or incompletely burnt are not large enough to justify applying small corrections to them. A more thorough examination of this assumption should be carried out at some point.

4.4.1 Oxygen Consumption Factors for Fossil Fuels

The United Nations reports fuel production in energy equivalent units in order to account for variations in fuel quality. The use of energy equivalent units has been advantagous for the purpose of calculating CO_2 emission factors because, for a given fuel type, the energy content of fuel is usually nearly proportional to carbon content. This same advantage applies to the estimation of oxygen consumption.

Tables 4.3–4.5 summarize the higher heating values of different fuels normalized per mole of O_2 consumed. (Higher heating value is the heat released upon oxidation of the fuel to carbon dioxide, water, sulfuric acid, and nitric acid followed by the condensation of all condensible products to liquid.) For the remainder of this discussion the heating value normalized per mole of O_2 consumed will be refered to as the normalized higher heating value, NHHV. Oxygen consumption is computed according to Eq. 4.15. For some of the fuels listed it is not clear at what temperatures the heating values are measured or whether they are measured at constant pressure or at constant volume. This is not of great concern because the adjustments which would apply to correct for a temperature difference of 10°C or from constant pressure to constant volume are typically 0.5% or smaller. The NHHV of virtually all the fuels listed in Tables 4.3–4.5 lies between 101 and 110 kcal/mole which indicates that energy

production is nearly proportional to oxygen consumption over a broad range of fuels.

Solid Fuels

The NHHVs for the different ranks of bituminous coal from Brame and King (1975) listed in Table 4.3 range from 99 to 103 kcal/mole with an average 101.5 kcal/mole. Since bituminous grades comprise the bulk of world coal production, we can take the value of 101.5 ± 1.5 kcal/mole, which corresponds to an oxygen consumption factor of

$$(7\text{kcal/gm})(32\text{gm/mole})/(101.5\text{kcal/mole}) = 2.187 \pm 0.032$$

tons O_2 per ton coal equivalent, as valid for world-average coal (calculated based on the United Nations definition of a coal equivalent of 7000 calories per gram).

The United Nations tabulations for energy production from solid fuels also include contributions from lignite production, which in 1980 comprised around 16% of the total for coal equivalent. The NHHV of brown lignite from Brame and King (1975) listed in Table 4.3 of 119.0 kcal/mole is 15 kcal/mole higher than the value derived above for world-average coal. However, the the NHHV values of the two lignites from Marks' Handbook (Marks, 1967) of 103.4 and 103.8 kcal/mole are much closer values for world-average coal, and I suspect there is an error in the composition data for lignite listed in Brame and King (1975). Assuming that the world-average NHHV for lignites lies in the range 103–105 kcal/mole, I have adopted a world-average NHHV for coal equivalent of 102 ± 2 kcal/mole corresponding to an O_2 consumption factor of $(O_s) = 2.20 \pm 0.04$ ton O_2 per ton coal equivalent. The question of the correct world-average NHHV for lignite should be examined more closely in the future.

Table 4.3: Combustion data for solids

solids	elemental abundances (wt. %)						heat of combustion	heat of combustion	oxidative
	H	C	O	S	N	other	kcal/gm fuel	kcal/mole O_2	ratio
sucrose[a]	6.48	42.01	51.42	0	0	0	-3.939	-112.4	1.00
graphite[b]	0	100	0	0	0	0	-7.803	-94.0	1.00
sulfur[a]	0	0	0	100	0	0	-3.918	-83.7	∞
wood[c]	6.5	50	43	0.05	–	.45	-4.4	-100.2	1.06
peat[c]	6	60	32	2	–	0	-5.6	-99.6	1.12
brown lignite[c]	5.5	67	26	1.5	–	0	-7.33	-118.7	1.11
black lignite[c]	5.4	74	19	1.6	–	0	-7.72	-110.6	1.13
bituminous 1[c]	5	77	16	2	–	0	-7.44	-102.8	1.13
bituminous 2[c]	5	84	8	3	–	0	-8.89	-103.3	1.16
bituminous 3[c]	5	85.6	5.4	4	–	0	-8.44	-100.7	1.18
bituminous 4[c]	5.3	87	4.7	3	–	0	-8.5	-99.4	1.18
carbonaceous[c]	4	92	2	2	–	0	-8.5	-101.1	1.13
anthracite[c]	3	94	2	1	–	0	-8.78	-101.3	1.09
lignite (N. Dakota)[d]	6.7	42.4	43.3	0.7	–	6.9	-4.01	-103.5	1.10
lignite (Texas)	6.8	42.5	42.1	0.5	–	9.0	-4.83	-103.8	1.11

[a]Chemical Rubber Company (1974).
[b]Rossini et al. (1952).
[c]Brame and King (1967).
[d]Marks (1967).

Table 4.4: Combustion data for liquids

liquids	elemental abundances (wt. %)						heat of combustion	heat of combustion	oxidative
	H	C	O	S	N	other	kcal/gm fuel	kcal/mole O_2	ratio
n-pentane[a]	16.76	83.23	0	0	0	0	-11.63	-104.9	1.60
n-hexane[a]	16.37	83.63	0	0	0	0	-11.55	-104.8	1.58
n-heptane[a]	16.09	83.91	0	0	0	0	-11.48	-104.5	1.57
n-octane[a]	15.88	84.12	0	0	0	0	-11.40	-104.2	1.56
cyclo–hexane[a]	14.37	85.63	0	0	0	0	-11.13	-104.1	1.50
benzene[a]	7.74	92.26	0	0	0	0	-10.00	-104.1	1.25
Calif. crude[b]	12.7	84	1.2	0.75	1.7	–	-10.51	-104.2	1.47
Kansas crude[b]	13	84.15	–	1.9	0.45	0.5	-10.64	-104.8	1.48
Oklahoma crude (1)[b]	13.11	85.7	–	0.4	0.3	0.49	-10.84	-106.1	1.46
Oklahoma crude (2)[b]	12.9	85	–	0.76	–	1.34	-10.83	-107.2	1.46
Penn. crude[b]	13.88	86.06	0	0.06	0	0	-10.84	-104.4	1.48
Texas[b]	12.3	85.05	0	1.75	0.7	0.2	-10.82	-107.4	1.45
Mexidan crude[b]	10.2	83.7	-	4.15	–	1.95	-10.43	-109.5	1.39

[a]Chemical Rubber Company (1974).
[b]Marks (1967).

Table 4.5: Combustion data for gases

gases	volume fraction %						heat of combustion	heat of combustion	oxid.
	CH_4	C_2H_6	C_3H_8	HCs[a]	CO_2	other	kcal/mole fuel	kcal/mole O_2	ratio
methane[b]	100	0	0	0	0	0	-212.8	-106.4	2.00
ethane[b]	0	100	0	0	0	0	-372.8	-106.5	1.75
n-propane[b]	0	0	100	0	0	0	-530.6	-106.1	1.667
iso-butane[b]	0	0	0	100	0	0	-683.4	-105.1	1.625
n-pentane[b]	0	0	0	–	0	0	-845.3	-105.6	1.60
1976 US ref. gas[c]	88.32	4.65	2.12	1.53	0.92	2.46	-229.4	-107.4	1.923
1970 wtd. US mean[c]	89.32	4.66	2.04	1.56	0.65	2.33	-230.2	-106.9	1.928
unwtd. US mean[c]	86.63	5.02	2.57	1.88	0.63	3.26	-233.5	-108.1	1.919
wtd. world mean[c]	89.24	4.52	1.95	1.54	0.78	2.42	-229.2	-107.0	1.927
1976 adj. dry gas[c]	92.88	3.91	0.62	–	–	2.59	-215.5	-107.9	1.980

[a]Includes other hydrocarbons taken as butane.
[b]Chemical Rubber Company (1974).
[c]Marland and Rotty (1984).

Marland and Rotty (1984) note that the United Nations has recently switched from basing its definition of coal equivalent from a higher-heating-value basis to a lower- or net-heating-value basis while retaining the 7000 cal/g standard. They estimate a factor of 1.055 to convert from the lower-heating-value basis to the higher basis for world-average coal based on data for United States coals. They adjust their emission factor for coal upward by a factor of 1.055 in order to account for the coal-equivalent basis used by the United Nations. Because the oxygen consumption factor estimated above is also based on higher heating values, the same upward adjustment is necessary for the the oxygen consumption factor. Thus the corrected consumption factor is $(O_*) = (1.055)(2.20 \pm 0.04) = 2.32 \pm 0.04$ ton O_2 per ton coal equivalent.

Liquid Fuels

The NHHVs of the crudes listed in Table 4.4 range from 105 to 110.6 kcal/mole. In comparison to the NHHVs of the liquid hydrocarbons listed in Table 4.4, which vary between 104 and 105 kcal/mole, the NHHVs for the crudes appear to be too high. The origin of this discrepancy is unclear, and the possibility that the caloric content of the crudes listed in Table 4.4 are systematically too high by around 3% cannot be ruled out. An additional difficulty with the heating values in Table 4.4 is noted in comparing the heating values for crudes, ranging from 10.51 to 10.84 kcal/gm with the basis for oil equivalency used by the United Nations (UN, 1981) of 10.180 cal/gm. Here the discrepancy is probably due to the usage of a lower-heating-value basis by the United Nations.

Because of the difficulties in reconciling the various heating value bases for liquid fuels, I have followed the procedure of Marland and Rotty (1984) of estimating the world-average composition of liquid fuel from the world-average specific gravity crude. The specific gravity of crudes is usually expressed in

terms of API gravity where

$$\text{API gravity} = \frac{141.5}{\text{specific gravity}} - 131.5. \tag{4.16}$$

and where the specific gravity refers to the value at 15 °C. The API gravity can be taken as a rough indicator of the composition of a crude because denser crudes tend to have a higher carbon fraction, and thus a lower hydrogen fraction. Marland and Rotty (1984) estimate the world-average API gravity of crudes is $32.5° \pm 2°$ by considering the average value for the 10 largest crude–producing countries in 1978 and other published estimates for the world average.

Fig. 4.2 shows a plot of the number of grams of oxygen consumed per gram of fuel versus the API gravity for the crudes in Table 4.4. There is a rough linear relation between API gravity and oxygen consumption, with the API gravity of $32.5° \pm 2°$ suggesting the value of 3.26 ± 0.05 grams O_2 per gram crude where the uncertainty allows for the uncertainty in the world-average specific gravity of crude as well as the uncertainty in the relation between specific gravity and oxygen consumption.

The United Nation tabulations for liquid fuels include contributions from crude petroleum and natural-gas liquids. A factor of 1.06 is applied to convert natural-gas liquids into oil equivalents in order to account for the higher energy content per unit mass of natural-gas liquids. In 1980 natural-gas liquids contributed around 3% to the total liquid fuel production. Because Marland and Rotty (1984) did not wish to take into account this weighting factor for the calculation of CO_2 emission, they based their estimates on an unweighted sum of petroleum and natural-gas liquids rather than on the United Nations totals. For the purpose of calculating oxygen consumption, however, it is logical to use the weighted-sum figures from the United Nations because of the the general proportiality between oxygen consumption and heating values. I have,

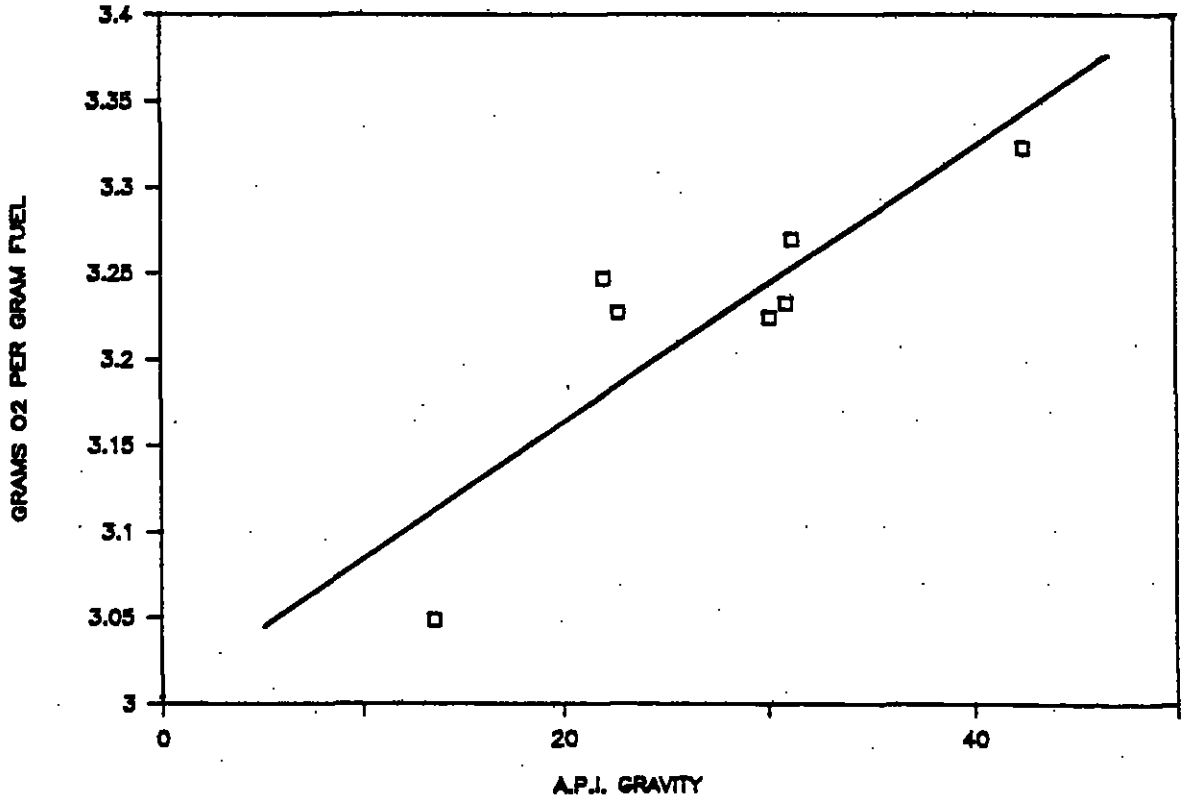

Figure 4.2: Oxygen consumed per gram of fuel burnt versus API gravity for various crudes listed in Marks' Handbook (Marks, 1967)

nevertheless, used the tabulated liquid-fuel tonnages of Marland and Rotty (1984) because they are the most up-to-date year-by-year tabulation of liquid production since 1950 that has been published. (The 1980 Yearbook of World Energy Statistics, lists production figures at five year intervals before 1970). The weighted and unweighted sums differ by only 0.2% (product of 0.03 and 0.06) which is negligible compared to other sources of error.

Based on the above considerations, I have taken the oxygen consumption factor to be $(O_l) = 3.26 \pm 0.05$ ton O_2 per ton crude oil.

Gaseous Fuels

Table 4.5 lists NHHVs for the gaseous hydrocarbons and for several estimates of the average composition of natural gas, as compiled by Marland and Rotty (1984). The NHHVs of the natural gases span the range of 107.4 to 108.1 kcal/mole with an average value of 107.5 kcal/mole. This value is around 1 to 2 kcal/mole higher than the value for the constituent hydrocarbons also listed in Table 4.5. Part of the discrepancy may come from the assumption that there are no hydrocarbons heavier than butane in the fuels and from disparate temperature or pressure conditions in the caloric measurements. As was the case for the liquids discussed above, however, it is possible that the heating values reported for the natural gases are systematically too high, in this case by around 1%. I have adopted a NHHV of 107.5 ± 1 kcal/mole corresponding to a consumption factor of 71.1 ± 0.6 tons O_2 per terajoule as valid for world-average natural gas. Note that the use of perhaps a more theoretically-correct NHHV of 106 kcal/mole would be inconsistent with the CO_2 emission calculation of Marland and Rotty (1984) leading to an oxidative ratio for world-average natural gas of around 1.98 which lies at the extreme range of the values for the compilations in Table 4.5.

Natural-Gas Flaring

I have followed the assumption of Marland and Rotty (1984) that the composition of flared natural gas is close to that of the compilation for dry marketed gas in the United States included in Table 4.5 as 1976 adjusted dry gas. This gas has a carbon content 525 g C/m^3 and an oxidative ratio of 1.980 corresponding to a consumption factor of 2.77 tons oxygen per thousand cubic meters. The uncertainty figure of 3% assumed by Marland and Rotty (1984) for carbon content should be valid for oxygen consumption as well.

Summary of O_2 Consumption Factors

Table 4.6 summarizes the O_2 consumption factors $O_2^{(i)}$ derived above. To be consistent with the errors estimates of Marland and Rotty (1984), I have estimated errors in the oxygen consumption factors such that there is a 90% probability that the true value lies within the specified range. It should be kept mind, however, that both the error estimates and the confidence limits are rough guesses.

Table 4.6 also lists world-average excess-O_2 consumption factors defined according to

$$\Delta O^{(i)} = O^{(i)} - \frac{32.00}{12.01} C^{(i)} \tag{4.17}$$

which yields the oxygen consumed in the oxidation of elements other than carbon in the fuel, and also lists world-average oxidative ratios calculated according to

$$OR^{(i)} = \frac{12.01\, O^{(i)}}{32.00\, C^{(i)}}. \tag{4.18}$$

The factors $C^{(i)}$ used in Eq. 4.17 and Eq. 4.18 are given in Marland and Rotty (1984).

Table 4.6: Oxygen consumption factors and oxidative ratios for fossil fuels.

From natural gas

$O^{(g)} = 0.0711$ ($\pm 1\%$); in 10^6 tons O_2 per thousand 10^{12} J.
$\Delta O^{(g)} = 0.0346$ ($\pm 3\%$); in 10^6 tons excess O_2 per thousand 10^{12} J.
$OR^{(g)} = 1.95 \pm 0.04$[a]; in moles O_2 per mole C.

From crude oil and natural gas liquids

$O^{(l)} = 3.26$ ($\pm 1.5\%$); in tons O_2 per ton crude.
$\Delta O^{(l)} = 0.988$ ($\pm 5\%$); in tons excess O_2 per ton crude.
$OR^{(l)} = 1.44 \pm 0.03$[b]; in moles O_2 per mole C.

From coal production

$O^{(s)} = 2.32$[c] ($\pm 2\%$); in tons O_2 per ton coal equivalent.
$\Delta O^{(s)} = 0.33$[c] ($\pm 30\%$); in tons excess O_2 per ton coal equivalent.
$OR^{(s)} = 1.17 \pm 0.03$[d]; in moles O_2 per mole C.

From natural gas flaring

$O^{(f)} = 2.77$ ($\pm 3\%$); in tons O_2 per thousand m^3.
$\Delta O^{(f)} = 1.37$ ($\pm 6\%$); in tons O_2 per thousand m^3.
$OR^{(f)} = 1.98 \pm 0.07$; in moles O_2 per mole C.

[a] Error estimated from range of oxidative ratios for gases in Table 4.5.
[b] Error estimated from range of oxidative ratios for crudes in Table 4.4.
[c] Includes heating value adjustment to account for the lower heating value basis used in production data in UN (1982).
[d] Error estimated from range of oxidative ratios for coals in Table 4.3.

I have estimated errors in the excess-O_2 consumption factors $\Delta O_2^{(i)}$ and oxidative ratios $OR^{(i)}$ based on the range in composition of the particular fuels (listed in Tables 4.3 through 4.5) which were used to derive the oxygen consumption factors $O_2^{(i)}$. (Note that errors in $\Delta O_2^{(i)}$ and $OR^{(i)}$ cannot be estimated by assuming errors in $O_2^{(i)}$ and $C^{(i)}$ are uncorrelated because both $O_2^{(i)}$ and $C^{(i)}$ are derived from the same estimates of the world-average composition of fuels.)

4.4.2 Fossil-Fuel Oxygen Consumption

Table 4.7 lists yearly oxygen consumption and carbon dioxide consumption from 1860 to 1982. Oxygen consumption from 1950–1982 is derived according to Eq. 4.14 where the factors $(O^{(i)})$ are listed in Table 4.6 and the factors $(P^{(i)})$ and $(FO^{(i)})$ are listed in Marland and Rotty (1984). O_2 consumption from 1860 to 1950 is estimated by scaling the CO_2 emission estimates of Keeling (1973) by the oxidative ratios listed in Table 4.6. CO_2 emissions in Table 4.7 for 1950–1982 are taken from Watts (1982).

In constructing estimates for CO_2 production for these earlier years, Keeling (1973) used the fuel-production tabulations in UN (1955) with overlapping data for the years 1929, 1937, 1949, from UN (1951-1969). The estimates of Keeling (1973) have apparently never been revised, and the more recent tabulations of CO_2 production listed in Watts (1982) for the years before 1950 are identical to those of Keeling (1973). Scaling the emission estimates of Keeling (1973) based on oxidative ratios which were derived, in part, from the emission factors used by Marland and Rotty (1984) is justified because the emission factors used by Keeling (1973) and Marland and Rotty (1984) are mutually consistent to within quoted uncertainties (Marland and Rotty, 1984). Also, although Keeling (1973) classifies natural-gas liquids differently from Marland

and Rotty (1973) (Keeling (1973) classifies them as gasous fuel whereas Marland and Rotty (1984) classify them under liquid fuel), this leads to a negligible error in total O_2 consumption in the earlier years because natural-gas liquids are not very important. Note that there is probably not enough information to account for changes in oxidative ratios of fuels before 1950, and that, in any case, the assumption of time-invariant oxidative ratios is fully consistent with the assumption of time-invariant CO_2 emission factors by Keeling (1973).

Taking the suggestion in the note added in proof by Keeling (1973), I have accounted for the flaring of natural gas before 1950 by assuming that the carbon produced by flared gas amounted to 5.7% of the carbon produced from crude petroleum. Oxygen consumption from flaring before 1950 is based on scaling the CO_2 emmisions by the oxidative ratio of 1.980, the same factor which is used for the years after 1950.

The principal errors and approximations which have been introduced in estimating O_2 consumption are identical to those introduced in estimating CO_2 emissions by Keeling (1973) and Marland and Rotty (1984) and are discussed further in these references. Errors in O_2 consumption per unit fuel derived above are relatively minor. The most serious errors are in the estimates of world fuel production derived from the United Nations compilations. Other errors are introduced in estimating how fuels produced are ultimately used, and in assuming that fuel produced in a given year can be equated to the fuel consumed in that year.

Table 4.7: Fossil fuel CO_2 production and O_2 consumption (10^6 tons C or O_2).

	CO_2 production				O_2 consumption				total CO_2	total O_2
year	solid fuels	liquid fuels	gas fuels	gas flaring	solid fuels	liquid fuels	gas fuels	gas flaring	prod-uction	cons-umption
1860	93	0	0	0	290	0	0	0	93	291
1861	98	0	0	0	307	1	0	0	99	308
1862	98	0	0	0	306	1	0	0	98	307
1863	106	0	0	0	329	1	0	0	106	330
1864	115	0	0	0	358	1	0	0	115	359
1865	122	0	0	0	379	1	0	0	122	330
1866	128	0	0	0	400	2	0	0	129	402
1867	138	0	0	0	429	2	0	0	138	430
1868	136	0	0	0	425	2	0	0	137	426
1869	141	1	0	0	440	2	0	0	142	442
1870	144	1	0	0	450	2	0	0	145	453
1871	161	1	0	0	503	2	0	0	162	505
1872	175	1	0	0	546	3	0	0	176	549
1873	187	1	0	0	584	5	0	0	189	589
1874	183	1	0	0	569	5	0	0	184	574
1875	188	1	0	0	586	4	0	0	189	591
1876	190	1	0	0	593	5	0	0	192	598
1877	194	2	0	0	606	6	0	1	196	613
1878	195	2	0	0	607	7	0	1	197	614
1879	205	2	0	0	639	10	0	1	208	650
1880	224	3	0	0	698	12	0	1	227	711
1881	241	3	0	0	751	13	1	1	245	766
1882	258	4	0	0	806	15	2	1	263	823
1883	276	3	0	0	862	12	2	1	280	877
1884	278	4	1	0	866	15	3	1	282	884
1885	272	4	1	0	847	15	4	1	277	867
1886	273	5	1	0	850	19	5	2	279	876
1887	291	5	1	0	908	19	7	2	298	936
1888	315	6	2	0	982	21	8	2	322	1012
1889	320	6	2	0	998	25	9	2	329	1034
1890	340	8	2	1	1059	31	10	2	350	1103
1891	354	10	2	1	1103	37	10	3	366	1153
1892	357	9	2	1	1114	36	11	3	369	1163
1893	350	10	2	1	1090	37	11	3	362	1142
1894	365	9	2	1	1139	36	12	3	378	1190
1895	385	11	2	1	1201	42	12	3	399	1259
1896	397	12	3	1	1237	46	14	4	412	1301
1897	416	13	3	1	1296	49	16	4	432	1364
1898	438	13	3	1	1366	51	17	4	455	1437
1899	480	14	4	1	1496	53	18	4	498	1571
1900	505	16	4	1	1576	61	19	5	526	1660
1901	518	18	4	1	1616	68	21	5	541	1711
1902	529	19	4	1	1650	73	23	6	554	1752
1903	581	20	5	1	1812	79	24	6	608	1921
1904	586	23	5	1	1826	88	26	7	615	1946

Table 4.7: Fossil fuel CO_2 production and O_2 consumption (10^6 tons C or O_2).

year	CO_2 production from:				O_2 consumption from:				total CO_2 production	total O_2 consumption
	solid fuels	liquid fuels	gas fuels	gas flaring	solid fuels	liquid fuels	gas fuels	gas flaring		
1905	618	23	6	1	1927	87	29	7	648	2050
1906	667	23	6	1	2080	86	32	7	697	2205
1907	737	28	6	2	2297	107	33	8	773	2446
1908	700	30	6	2	2183	116	33	9	738	2340
1909	730	32	8	2	2276	121	39	10	771	2445
1910	762	35	8	2	2376	132	42	10	807	2560
1911	777	36	8	2	2423	139	42	11	824	2616
1912	820	37	9	2	2557	142	46	11	868	2756
1913	879	41	9	2	2739	158	48	12	932	2958
1914	786	43	9	2	2451	165	48	13	841	2677
1915	776	45	10	3	2418	174	51	14	833	2657
1916	835	48	12	3	2603	184	61	15	898	2863
1917	880	53	13	3	2742	204	65	16	948	3027
1918	867	53	11	3	2704	205	59	16	935	2983
1919	758	60	12	3	2362	229	61	18	832	2669
1920	870	76	13	4	2712	293	67	23	963	3093
1921	735	83	10	5	2291	317	54	25	833	2687
1922	786	92	12	5	2451	354	62	28	896	2895
1923	881	109	16	6	2745	417	82	33	1012	3278
1924	872	109	18	6	2718	417	93	33	1005	3261
1925	873	114	19	6	2722	439	98	34	1013	3293
1926	868	118	21	7	2705	451	108	35	1013	3299
1927	940	135	23	8	2930	517	119	40	1105	3606
1928	924	142	25	8	2881	543	129	43	1099	3596
1929	983	159	30	9	3063	610	157	48	1181	3878
1930	898	151	28	9	2799	580	148	46	1086	3572
1931	795	146	28	8	2478	559	143	44	976	3224
1932	709	139	26	8	2210	533	134	42	882	2919
1933	741	152	26	9	2311	582	135	46	927	3073
1934	807	160	29	9	2516	614	153	48	1006	3331
1935	827	174	30	10	2579	669	156	52	1042	3456
1936	923	188	35	11	2878	723	181	57	1157	3838
1937	972	215	39	12	3030	826	202	65	1238	4123
1938	914	210	37	12	2850	805	192	63	1173	3911
1939	974	220	40	12	3035	842	207	66	1245	4150
1940	1033	224	43	13	3220	861	223	68	1313	4372
1941	1077	215	45	12	3358	823	236	64	1349	4481
1942	1083	202	49	12	3375	776	257	61	1346	4469
1943	1087	222	55	13	3390	850	286	67	1377	4592
1944	1043	249	60	14	3252	956	311	75	1366	4593
1945	875	263	66	15	2728	1009	340	79	1219	4157
1946	914	289	68	17	2848	1109	352	87	1287	4396
1947	1028	318	75	18	3205	1222	390	96	1440	4912
1948	1073	360	85	21	3346	1381	439	108	1538	5274
1949	1022	358	89	20	3186	1375	463	108	1490	5132

Table 4.7: Fossil fuel CO_2 production and O_2 consumption (10^6 tons C or O_2).

	CO_2 production from:				O_2 consumption from:				total CO_2	total O_2
year	solid fuels	liquid fuels	gas fuels	gas flaring	solid fuels	liquid fuels	gas fuels	gas flaring	prod-uction	cons-umption
1950	1077	423	97	23	3351	1620	501	122	1620	5594
1951	1137	479	115	24	3536	1832	596	127	1755	6091
1952	1127	504	124	26	3504	1930	644	138	1781	6217
1953	1132	533	131	27	3522	2044	681	141	1823	6388
1954	1123	557	138	27	3490	2134	714	144	1845	6482
1955	1215	625	150	30	3780	2394	776	161	2020	7110
1956	1281	679	161	32	3982	2600	838	169	2153	7589
1957	1317	714	178	35	4096	2734	923	186	2244	7939
1958	1344	732	192	35	4178	2803	996	183	2303	8160
1959	1380	790	214	36	4290	3024	1114	191	2420	8619
1960	1430	850	235	39	4449	3254	1219	208	2554	9130
1961	1341	906	253	41	4171	3469	1315	219	2541	9174
1962	1373	981	276	44	4272	3759	1435	233	2674	9698
1963	1431	1054	300	47	4449	4037	1558	249	2832	10294
1964	1481	1138	328	51	4607	4357	1704	269	2998	10936
1965	1503	1220	351	55	4673	4670	1824	288	3129	11455
1966	1524	1323	380	60	4739	5068	1973	319	3287	12097
1967	1466	1421	409	66	4556	5444	2125	349	3362	12475
1968	1497	1551	445	73	4654	5940	2308	385	3566	13288
1969	1524	1669	487	80	4739	6392	2527	421	3760	14078
1970	1577	1833	516	88	4903	7022	2678	463	4014	15066
1971	1572	1944	553	90	4889	7443	2871	474	4159	15677
1972	1584	2054	583	95	4928	7865	3023	499	4316	16314
1973	1604	2238	608	112	4989	8570	3155	590	4562	17304
1974	1613	2245	616	107	5017	8597	3197	565	4581	17375
1975	1683	2131	621	96	5233	8160	3221	507	4531	17122
1976	1727	2311	645	110	5370	8851	3347	582	4793	18150
1977	1779	2391	668	108	5532	9156	3465	571	4946	18723
1978	1795	2423	695	106	5582	9281	3605	557	5019	19025
1979	1892	2527	730	105	5885	9675	3789	554	5254	19903
1980	1935	2412	718	102	6017	9236	3724	537	5167	19514
1981	1947	2270	727	93	6056	8692	3771	493	5037	19012
1982	1999	2162	727	92	6217	8280	3774	485	4980	18756

The procedure used to estimate the propagation of errors is outlined in Table 4.8. Following Marland and Rotty (1984), I have assumed that errors in product $F_{O_2}^{(i)} = (P^{(i)})(FO^{(i)})(O^{(i)})$ for a given fuel type can be estimated by the usual procedure (square root of the sum of squares) for addition of random errors. This is justified because the different factors are derived from independent data bases and therefore should have independent biases. Also following Marland and Rotty (1984), I have estimated the errors in the sum $\sum F_{O_2}^{(i)}$ in two ways: firstly assuming errors add randomly, which yields a lower estimate of the error, and secondly assuming the errors add systematically, which yields an upper estimate of the error. The latter assumption allows for the possibility that production data for different fuel types compiled by the same sources have similar biases. (It is plausible, for example, that all production data is too low because of incomplete reporting, or too high because of over–reporting.) The uncertainty in O_2 consumption since 1950 is estimated by this procedure to be 7% to 10.5% at the 90% confidence level. This represents a best effort to combine errors from various sources. However, it should be kept in mind that such errors are only approximately known.

The uncertainty in the O_2 consumption data before 1950 is more difficult to estimate. Keeling (1973) notes that the production figures before 1950 are likely to be systematically too low due to incomplete reporting but that the carbon content of fuels was likely to be higher. Presumably the O_2 consumption per ton of fuel was also higher. Keeling (1973) suggests that the CO_2 production data before 1950 could be in error by as much as 20%. Comparable errors may be present in the O_2 consumption data before 1950.

Taking the figures for CO_2 production and O_2 consumption, one can derive the excess-O_2 consumption i.e. the O_2 consumed consumed owing to the

Table 4.8: Propagating errors in O_2 consumption. Errors in percent (%).

	gases	liquids	solids	gas flared
E_1, error in $P^{(i)a}$	10	8	11.2	20
E_2, error in $FO^{(i)a}$	1	3	2	1
E_3, error in $O^{(i)}$	1	1.5	2	3
$\sqrt{\sum E_j^2}$	10.5	8.2	11.6	20.2
f_i, fraction of total cons.				
in 1950	0.09	0.30	0.59	0.02
in 1980	0.19	0.48	0.30	0.03

Total uncertainty:	If uncertainties for the individual fuels are mutually independent $\sqrt{\sum \left(f_i \sqrt{\sum E_j^2} \right)^2}$	If uncertainties for the individual fuels are not independent $\sum f_i \sqrt{\sum E_j^2}$
in 1950	7.3	10.6
in 1980	6.8	10.5

[a]From Marland and Rotty (1984).

oxidation of elements other than carbon according to

$$F^{(i)}_{\Delta O_2} = \left(F^{(i)}_{O_2} - \frac{32.00}{12.01} F^{(i)}_{CO_2} \right) \tag{4.19}$$

where $F^{(i)}_{\Delta O_2}$ is the excess-O_2 consumption, F_{CO_2} is the total oxygen consumption (column 11 in Table 4.7) and, $F^{(i)}_{CO_2}$ is the total fossil-fuel CO_2 production (column 10 in Table 4.7). For example, this yields $1.28 \cdot 10^9$ tons O_2 ($0.40 \cdot 10^{14}$ moles O_2) and $5.75 \cdot 10^9$ tons O_2 ($1.80 \cdot 10^{14}$ moles O_2) in 1950 and 1980 respectively. The uncertainty in excess-O_2 consumption is estimated to be 13% to 19% in 1950 and 8% to 14% in 1980 at the 90% confidence level. These uncertainties estimates have been derived by combining errors in $\Delta O^{(i)}$ (see Table 4.6) with errors in $(P^{(i)})$ and $(FO^{(i)})$ according to the same assumptions used in Table 4.8. The change in the uncertainty over time primarily reflects the change in the relative importance of coal, the fuel with greatest uncertainty in excess-O_2 consumption per ton of fuel. The percentage uncertainty in excess-O_2 consumption before 1950 is even larger. Allowing an uncertainty of 30% for the excess-O_2 consumption factor for coal and allowing for 20% uncertainty in the fuel-production data, I estimate the uncertainty in excess-O_2 consumption to be 36% in the earlier years when coal burning dominates.

Oxygen consumption before 1860 can be estimated by assuming that fuel production grew exponentially according to

$$F_{O_2}(t) = F_{O_2}(1860) e^{0.0435(t-1860)} \tag{4.20}$$

where t is the calendar year and $F_{O_2}(1860) = 291 \cdot 10^6$ tons O_2. The growth rate of 4.35%/yr is based on Keeling's (1973) estimate for the growth in CO_2 production over the period 1860 to 1900. Since coal was the only fuel of significance over this period, the same growth rate applies to O_2 consumption. Based

on Eq. 4.20 the integrated O_2 consumption through 1859 amounts to $6.69 \cdot 10^9$ tons O_2 or $2.09 \cdot 10^{14}$ moles O_2.

Table 4.9 summarizes the CO_2 production, O_2 consumption, and excess-O_2 consumption in 1950, 1980, as well as the cumulative totals through 1980. The cumulative totals include the estimated contributions before 1860.

4.4.3 Other Industrial Activities

The reduction of metal ores, fixation of iron, and other industrial activites besides burning fossil fuel involve a consumption or production of oxygen. Table 4.10 gives figures for the global production of raw materials in 1980 as listed in the United Nations Statistical Yearbook (UN, 1981). Generally, the total tonnages produced are negligible in comparison to oxygen consumption from burning fossil fuel. I shall consider here only the contributions from the iron production and nitrogen fixation.

Iron Production

Iron ore, which consists of various mixtures of hematite Fe_2O_3 and magnetite Fe_3O_4, is reduced to elemental iron either by a blast furnace or by direct reduction. In either case the overall chemistry is given by

$$2Fe_2O_3 + 3C \rightarrow 2Fe + 3CO_2$$

and

$$Fe_2O_3 + 3H_2 \rightarrow 2Fe + 3H_2O$$

where the C and H_2 are obtained from coke, a derivative of coal (Encyclopedia of Chemical Technology, 1984). It is evident that the reduction of iron ore

Table 4.9: Summary of Fossil-Fuel CO_2 Production and O_2 Consumption

Total CO_2 Production			
1950	$1.62 \cdot 10^9$ tons C	or	$1.35 \cdot 10^{14}$ moles C (±10%)
1980	$5.17 \cdot 10^9$ tons C	or	$4.30 \cdot 10^{14}$ moles C (±10%)
cumulative[a]	$163.8 \cdot 10^9$ tons C	or	$136.4 \cdot 10^{14}$ moles C (±10%)
Total O_2 Consumption			
1950	$5.59 \cdot 10^9$ tons O_2	or	$1.75 \cdot 10^{14}$ moles O_2 (±11%)
1980	$19.51 \cdot 10^9$ tons O_2	or	$6.10 \cdot 10^{14}$ moles O_2 (±10%)
cumulative[a]	$577.7 \cdot 10^9$ tons O_2	or	$180.5 \cdot 10^{14}$ moles O_2 (±10%)
Total Excess-O_2 Consumption			
1950	$1.28 \cdot 10^9$ tons O_2	or	$0.40 \cdot 10^{14}$ moles O_2 (±17%)
1980	$5.75 \cdot 10^9$ tons O_2	or	$1.80 \cdot 10^{14}$ moles O_2 (±13%)
cumulative[a]	$136.1 \cdot 10^9$ tons O_2	or	$42.5 \cdot 10^{14}$ moles O_2 (±16%)
Oxidative Ratio[b]			
1950	1.30		
1980	1.42		
cumulative[a]	1.32		

[a]Includes cumulative total from preindustrial times through 1980.
[b]Total O_2 Consumption/Total CO_2 Production.

Table 4.10: Production of raw materals in 1980[a].

Pig Iron	525.8
Sulfuric Acid (as H_2SO_4)	132.4
Nitrogenous fertilizers (as N)	67.7
Nitric Acid (as HNO_3)	29.7
Aluminum	18.7
Copper	8.1
Lead	3.4

[a]From United Nations Statistical Yearbook, 1981 (UN, 1981). Units are in millions of metric tons (10^3 kg).

represents an oxidative use for coal in which the oxygen comes from iron ore rather than from the atmosphere.

The United Nations pig-iron production figure for 1980 of $526 \cdot 10^6$ tons Fe corresponds to the production of $213 \pm 23 \cdot 10^6$ tons O_2 ($6.65 \pm 0.72 \cdot 10^{12}$ moles O_2) or 1.1% of fossil-fuel production in 1980 where the error estimate allows for both a 10% uncertainty in the United Nations production figures as well as a uncertainty in whether the iron is derived from hematite or magnetite.

Industrial Nitrogen Fixation

Atmospheric N_2 is fixed in the production of nitrogenous fertilizers and in the combustion of fossil fuels. These processes directly affect the abundance of atmospheric O_2 in two ways:

1. because the nitrogen changes its oxidation state when it is fixed, and

2. because the incorporation of industrial nitrogen in organic form implies a net accumulation of organic matter.

To estimate the first effect it is sufficient to know the final oxidation state of the nitrogen after it is released into the environment. Because nitrogen can exist in such a wide range of oxidation states (–3 to +5) and undergo such a wide range of transformations in the environment this is not an easy problem. Nevertheless, comparing the $5 \cdot 10^{12}$ moles N/yr of fixed as fertilizer and the $1.4 \cdot 10^{12}$ moles N/yr of NO_x released from fossil fuel burning (Söderland and Svensson, 1975) with the $6.1 \cdot 10^{14}$ moles O_2/yr consumed from fossil burning, we see that the maximum possible effect is only about 2% of fossil-fuel O_2 consumption.

To estimate the second effect one must know what fraction of the nitrogen ends up in organic matter and one must know the C/N ratios of this organic matter. C/N ratios in terrestrial organic reservoirs range from 12:1 to 150:1 (Peterson and Melillo, 1985) and the standard value for marine organic matter is 7:1. (Redfield et al., 1963). The potential carbon storage due to eutrification by anthropogenic nitrogen is quite large. If all of the $6.4 \cdot 10^{12}$ moles N/yr of fixed nitrogen is assimilated in organic matter with a C/N ratio of 15:1, this implies a net C sink or O_2 source of about $1 \cdot 10^{14}$ moles/yr. There are large uncertainties in making this kind of estimate, and it is likely that the estimate of $1 \cdot 10^{14}$ moles C/yr storage is too high. Peterson and Melillo (1985) have recently considered the question of the eutrophication caused by anthropogenic nutrients by examining separately the potential storage in forests, rivers, coastal sediments, the open ocean, and the deep-sea sediments. They estimate a maximum storage of $1.7 \cdot 10^{13}$ moles C/yr due to eutrophication.

We can conclude from this analysis is that the changes in oxidation state of the industrial nitrogen, in terms of the consequences for atmospheric O_2, are about ten times less important than changes in carbon storage caused by eutrification. Therefore the consequences of industrial nitrogen fixation should be viewed as part of the biological term in the oxygen budget rather than as part of the industrial consumption term.

4.5 Oxidative Ratios of Terrestrial Carbon

An important aspect of the coupling between the oxygen and carbon cycles is the O_2/CO_2 exchange ratio between the atmosphere and the terrestrial biosphere. It is often assumed that land biomatter can be adequately described by the formula CH_2O corresponding to an oxidative ratio of 1 mole O_2 produced per mole CO_2 fixed. While this formula may accurately describe organic matter consisting predominantly of carbohydrates such as starches and cellulose, the formula is only approximately valid for lignins, lipids, and humic substances, all of which are important geochemically. Also, one must consider not only the exchange fluxes from formation and destruction of organic matter, but also the exchange fluxes from material transformation between one organic form and another (e.g. the transformation of litter into humic material). For material transformations what matters is the *difference* in the oxidation states of the starting and ending material. The purpose of this section is to define the range of oxidative ratios for terrestrial organic matter.

For terrestrial matter, just as for fossil fuels, the estimation of oxidative ratios requires knowledge of the elemental abundances of C, H, O, N, and S in the material. Unfortunately, although a vast number of studies of biotic materials have been carried out, a large percentage of these studies fail to include analy-

sis of O which is essential for determining the oxidation state of the material. Often O is estimated by subtracting the weight of other elements from the total dry weight (Bowen, 1966 p. 46) which does not inspire great confidence in the results.

Table 4.11 summarizes results from elemental analysis of a (haphazard) selection of organic substances and organisms. Although the elemental composition of different woods listed in Table 4.11 vary significantly, the computed oxidative ratios are remarkably consistent—ranging only from 1.03 to 1.07 (moles O_2 per mole CO_2). An oxidative ratio of 1.05 ± 0.02 appears to characterize the composition of wood globally, although this result must be treated cautiously because the data in Table 4.11 do not include tropical samples. Since most of the carbon present in living organisms is stored in forests (Atjay et al., 1979; Olson, 1982), the oxidative ratio 1.05 should be a reasonable estimate for the living biosphere as a whole.

Soil organic matter is usually classified according into incompletely decomposed organic matter and humus (Schlesinger, 1985). Humus, in turn, is classified based on solubility in weak acids and bases into three fractions: (1) fluvic acid, (2) humic acid, and (3) humins (Schnitzer and Khan, 1971). The composition of newly-decomposing matter should have an oxidative ratio close to that of wood (O.R. ≈ 1.05) whereas the oxidative ratios of various types of soil organic matter vary considerably, from around 0.9 for some fluvic acids to 1.15 for peat (Table 4.11). Based on the model of Schlesinger (1985), humic acids and humins appear to comprize the bulk of humus. Since peat comprises only 10% of global soil carbon (Bolin, 1983), the world-average oxidative ratio for soil carbon can be assumed to lie in the range 1.07 ± 0.05 (mean and standard deviation of the humic acids and humins listed in Table 4.11).

Based on the above discussion, it is clear that the O_2/CO_2 exchange ratios

Table 4.11: Elemental abundances and oxidative ratios of terrestrial organic matter.

	% Dry Weight						
	C	H	O	S	N	O.R.[a]	references
Living Organisms							
"Wood"	50	6.5	43	0.05	0.1	1.07	Brame and King (1967)
Typical nonresinous	37.9	7.2	53.8	0	0.1	1.03	Marks (1971)
Charcoal, willow	85	2.7	10.1	0.1	0.3	1.05	Marks (1967)
California redwood	26.5	8.5	64.8	0	0.2	1.04	Marks (1967)
Western hemlock	21.2	8.9	69	0	0	1.03	Marks (1967)
Douglas fir	33.5	8	57.9	0	0.1	1.06	Marks (1967)
Tanbark	14.2	9.6	74.9	0	0	1.03	Marks (1967)
Angiosperms	45.5	5.5	41	0.44	3.3	1.04	Bowen (1966)
Brown Algae	34.5	4.1	37.7	1.2	1.5	1.00	Bowen (1966)
Fungi	49.4	5.5	34	0.4	5.1	1.09	Bowen (1966)
Mean plant	45	5	40	0.5	3	1.02	Bowen (1966)
Bacteria	48.5	7.4	27	0.61	10.7	1.27	Bowen (1966)
Mean Animal	45	6.5	30	1.3	10	1.23	Bowen (1966)
Soil Organic Matter							
Humic acids	56.4	5.5	32.9	1.1	4.1	1.10	Schnitzer and Khan (1972)
	53.8	5.8	36.8	0.4	3.2	1.08	Schnitzer and Khan (1972)
	56.7	5.2	35.4	0.4	2.3	1.05	Schnitzer and Khan (1972)
	56.4	5.8	35.6	0.6	1.6	1.09	Schnitzer and Khan (1972)
	60.4	3.7	33.6	0.4	1.9	0.98	Schnitzer and Khan (1972)
	60.2	4.3	31.9	0	3.6	1.01	Schnitzer and Khan (1972)
Lake sediment HA	53.7	5.8	35.1	0	5.4	1.08	Schnitzer and Khan (1972)
Fluvic acids	42.5	5.9	47.1	1.7	2.8	1.06	Schnitzer and Khan (1972)
	47.6	4.1	47.3	0.1	0.9	0.89	Schnitzer and Khan (1972)
	50.9	3.3	44.8	0.3	0.7	0.87	Schnitzer and Khan (1972)
Water fluvic acid	46.2	5.9	45.3	0	2.6	1.01	Schnitzer and Khan (1972)
Humins	55.4	5.5	33.8	0.7	4.6	1.09	Schnitzer and Khan (1972)
	56.3	6	31.8	0.8	5.1	1.13	Schnitzer and Khan (1972)
Peat	60	6	32	2	0	1.15	Brame and King (1967)

[a]Oxidative ratio

appropriate for describing long-term growth and destruction of the land biosphere are reasonably well constrained. Eventually a more through study of this subject will be required. What is needed is a classification scheme for terrestrial organic matter which distiguishes materials of different oxidative ratios combined with a knowledge of the global distribution and fluxes. Note that short-term O_2/CO_2 exchange ratios could be directly measured through correlation studies of atmospheric CO_2 and O_2. However, such studies may be of little help in defining long-term exchange ratios.

4.6 Natural O_2 Sources and Sinks

We now address the question of whether there are natural long-term sources and sinks for O_2 that are significant compared to burning fossil fuel. Two possibilities are considered: (1) imbalances in weathering and sedimentation rates, and (2) changes in the dissolved O_2 or organic matter in the ocean.

4.6.1 Weathering and Sedimentation

The fluxes of O_2 from weathering and sedimentation listed in Table 4.2 are roughly 60 times smaller than current O_2 consumption from burning fossil fuel. Thus sedimentation and weathering fluxes would have to be underestimated by a factor of five or more in order to be significant compared to the uncertainty in fossil-fuel O_2 consumption. Estimates of present weathering rates based on the particulate load of rivers are not well constrained (see discussion of Holland, 1978, pp. 88–89). However, a factor-of-five uncertainty can safely be ruled out. Human activites have recently accelerated weathering rates in some regions; however, even in areas which one would expect significant human

acceleration e.g. the drainages into the Gulf of Mexico and the Bay of Bengal, the effects appear to be smaller than a factor of 2 (Holland, 1978, p. 89). The organic content of modern sediments of roughly 0.6% is similar to that of ancient sediments (Holland, 1978, p 215-216) which suggests that the operation of the weathering and sedimentation cycles are presently nearly in steady state with respect to production or loss of O_2. The overall uncertainty in the net gain or loss of O_2 due to these cycles is obviously difficult to estimate. If we assume a factor-of-two uncertainty in weathering rates, and a possible difference of 50% between organic content of present sediments and ancient sediments undergoing weathering, we arrive at a maximum net source or sink of $1.2 \cdot 10^{13}$ moles/yr or 2% of present fossil fuel O_2 consumption.

4.6.2 Ocean Net Sources or Sinks

The possible changes in the effective O_2 storage in the ocean can be divided into three catagories: (1) changes in the integrated physical capacity of the ocean for O_2, (2) changes in the amount of organic matter in the ocean, and (3) changes in the deficiency between the integrated O_2 capacity and the actual storage of O_2. The physical capacity is defined here in terms of a completely lifeless ocean in which O_2 is saturated everywhere with respect to the atmospheric partial pressure of O_2 at the ambient potential temperature and salinity, all the carbon in the ocean is fully oxidized (i.e. to carbonic acid, bicarbonate, or carbonate), and all the fixed nitrogen is oxidized to nitrate.

Physical Capacity

The current physical capacity of the oceans for O_2 of $4.2 \cdot 10^{17}$ moles indicated in Table 4.12 amounts to 1.1% of the atmospheric O_2 content. Because O_2

Table 4.12: Ocean Inventories of O_2, Organic C, and P.

	Total (10^{15} moles)	Average (μ mole/kg)[a]
Oxygen (moles O_2):		
Dissolved O_2 capacity[b]	423	302
Dissolved O_2[b]	225	161
Dissolved O_2 deficit (AOU)	198	141
Potential O_2 deficit[c]	359	256
Organic Carbon (moles C):		
Dissolved Organic Carbon[d]	83	69
Particulate Organic Carbon[d]	2.5	1.8
Plankton[d]	0.25	0.18
Phosphorus (moles P):		
Total Phosphorus[e]	2.6	1.9
Preformed Phosphate[f]	1.5	0.8

[a]Based on $1.40 \cdot 10^{21}$ kg total ocean mass (Dietrich et al., 1980 p. 6).
[b]Based on $1.299222 \cdot 10^{9}$ km^3 total ocean volume, 3.90 ml/l average oxygen concentration, and 53.1% average oxygen saturation; from Levitus (1982), page 108.
[c](Total phosphorus)·138.
[d]from Mopper and Degens (1979).
[e]From Richey (1983).
[f]Total phosphorus – AOU/138.

obeys Henry's law (in contrast to CO_2), if there were a sudden reduction in the atmospheric O_2 partial pressure, and there were no change in the physical or biological processes operating in the ocean, the oceans would replenish approximately 1% of the loss in re-establishing equilibrium. This equilibrium would be established on a time scale of 1100 years, the turnover time of the deep sea with respect to the atmosphere (Keeling, 1979). On this basis it can be concluded that any reduction in atmospheric O_2 partial pressure from burning fossil fuel, with a growth time of about 30 years, would drive a flux of O_2 from the ocean which is considerably smaller than 1% of the fossil-fuel O_2 sink.

For a fixed atmospheric O_2 abundance, the physical capacity of the ocean is determined by the total mass of the ocean, and the distribution of temperature and salinity in the ocean. The long residence times of the major ions in sea water of the order of 10^7 years (Holland, 1978, page 154) rule out changes in total salinity of the ocean as a significant source of variability of the physical capacity of the oceans for O_2 on a 10 to 1000 year time scale. Also, the Bunsen solubility coefficients of O_2 (as well as N_2 and Ar) are described very nearly by a linear function of salinity (Weiss, 1970) which means that changes in the statistical distribution of salinity in the ocean for a fixed total salinity will have a neglible effect on the integrated capacity of the ocean. This leaves changes in mass or temperature, as the primary potential sources of changes in physical capacity. Both temperature and mass changes would also cause variations in sea level.

Recent studies of changes in global mean sea level have indicated a statistically significant rise of about 10–15 cm over the last century (Barnett, 1982, Gornitz et al., 1982). There is evidence to suggest that part of this rise has been due to discharges from grounded glaciers and part due to thermal expansion but the relative magnitude of these effects has not been not well determined (Barnett, 1982; Etkins and Epstein, 1982).

Accompanying a rise in sea level caused by the melting of grounded glaciers are three processes which can alter the atmospheric O_2 mole fraction, all of which can be shown to be negligible in the present context. Firstly, air trapped in the ice as bubbles or clathrates is released when the ice melts. Since the trapped air has nearly atmospheric composition, the release can't change the atmospheric O_2 mole fraction, however. Secondly, the rise in sea level caused by the meltwater implies a drop in the mean barometric pressure at sea-level since the volume of air displaced by the water is compensated by volume of air

replacing the ice. By this mechanism, a one-meter rise in sea level decreases the physical capacity of sea water for an atmospheric gas by roughly a factor of (1 meter)/H_{scale}, where H_{scale} is the atmospheric scale height (approximately 8000 m), and thus decreases the total oceans O_2 capacity by

$$\frac{4.23 \cdot 10^{17} \text{ moles}}{8000} = 4.3 \cdot 10^{13} \text{ moles}$$

which amounts to only $1.4 \cdot 10^{-6}$ of the atmospheric O_2 content and which, in terms of the effect on the atmospheric O_2 mole fraction, is partially offset by changes in the capacity for N_2 and Ar. Thirdly, atmospheric gases are dissolved in the meltwater. A one-meter rise in sea level increases the oceans' physical capacity for O_2 by

$$A_o \cdot C_i = (3.6 \cdot 10^{14} \text{m}^2)(0.457 \text{moles/m}^2) = 1.6 \cdot 10^{14} \text{ moles}$$

where A_o is the ocean surface area and C_i is the solubility of the O_2 in moles/m^3 taken here at 0°C (Weiss, 1980). This amounts to only $4 \cdot 10^{-6}$ of the atmospheric O_2 content and, in terms of the effect on the atmospheric O_2 mole fraction, is partially offset by changes in the capacity for N_2 and Ar.

If sea level rises due to thermal expansion, the change in the oceans' physical capacity for a gas can be estimated according to

$$\delta M_i = A_o \cdot \frac{dC_i}{dT} \cdot {K_E}^{-1} \cdot \delta H \tag{4.21}$$

where δM_i is the change in the oceans' physical capacity for species i in moles, C_i is the solubility of species i in the melt water in moles/m^3, K_E is the linear thermal expansion coefficent of sea water, and δH is the change in mean sea level. The sensitivity of the oceans physical capacity to changing temperature is quite sensitive to the temperature of the water undergoing expansion

Table 4.13: Change in ocean capacity for dissolved gases per meter rise in sea level (in units of 10^{15} moles).

	O_2[a]	N_2[a]	Ar[a]	δX_{O_2}[b]
Thermal expansion in 4°C water	−29	−47	−1.4	+72 ppm
Thermal expansion in 8°C water	−17	−33	−0.83	+36 ppm

[a]Calculated based on solubility data of Weiss (1970) for a salinity of 35 permil, thermal expansion data from Dietrich et al. (1980), and an ocean surface area of $3.6 \cdot 10^{14} m^2$ (Dietrich et al.,1980).

[b]Corresponding change in atmospheric O_2 mole fraction. Calculated using a total mass of dry air of $5.124 \cdot 10^{21}$g (Trenberth, 1981), a mean molecular weight of dry air of 28.97 g/mole (US,1976), and an O_2 mole fraction of 0.20946 (Machta and Hughes, 1970).

and increases with decreasing temperature. The capacity change for warming in 4°C water and 8°C water are calculated for O_2, N_2, and Ar in Table 4.13. The capacity change at 4°C which provides a firm upper limit for any capacity changes caused by recent ocean warming, corresponds to a change of 11 ppm/century in the atmospheric O_2 mole fraction based on the 15/century sea level rise. This upper limit is small, but not entirely negligible, compared to fossil-fuel O_2 consumption over the last century. The actual change in physical capacity over the last century was probably considerably smaller than 11 ppm. If we assume, following Revelle (1983), that 25% of the rise in sea level was due to thermal expansion (the remainder being caused by melting of glaciers), and we assume, following Cess and Goldenberg (1981), that the warming has penetrated to an average depth of about 300 m, corresponding to a temperature of approximately 8°C we estimate a change over the last century of +1.35 ppm.

Revelle (1983) predicts that sea level should rise over the next century by

about 30 cm due to warming of upper ocean waters induced by CO_2 greenhouse warming. If the greenhouse effect of other increasing trace gases were taken into account the warming should be roughly double that from CO_2 alone (Ramanthan et al, 1985) so that the predicted rise in sea level due to warming of ocean waters should be 60 cm. The change in ocean capacity based on this rise would increase atmospheric O_2 mole fraction by about 22 ppm. Therefore, although changes in ocean physical capacity over the past century do not appear important for the atmospheric O_2 budget, the changes in physical capacity over the next century may be quite significant.

Ocean Organic Reservoirs

Dissolved organic carbon (DOC) is the primary reservoir of organic matter in the ocean. Most DOC is highly refractory with a mean ^{14}C age of greater than 3400 years (Mopper and Degens, 1979). The ^{14}C age suggests a turnover rate of $2.4 \cdot 10^{13}$ moles C/yr although there is evidence that approximately 20% of the total DOC has a shorter turnover time of approximately 200 years. If we assume that DOC has an oxidative ratio of 1.0 to 1.3 moles O_2 per mole C, the turnover of DOC is estimated to consume $2.4 \cdot 10^{13}$ to $3.1 \cdot 10^{13}$ moles O_2/yr. The present understanding of the sources and sinks for DOC is insufficient to determine whether the DOC reservoir is currently in steady state. It is conceivable, therefore, that changes in DOC are currently a source or sink for as much as $3.1 \cdot 10^{13}$ moles/yr O_2 or 5% of fossil fuel O_2 consumption. There is clearly a need to better define the sources and sinks of DOC and the role of DOC in the global carbon and oxygen cycles.

Dissolved-Oxygen Deficiency

Although the dissolved-O_2 content of surfaces waters is typically within a few percent of equilibrium with the atmosphere, the intermediate and deep waters are substantially undersaturated in O_2. This is illustrated in Fig. 4.3 and in Table 4.12. On average the oceans are 47% undersaturated in O_2.

The oxygen deficiency in the deep sea is controlled by the vertical fluxes of organic matter and ventilation rates of subsurface waters. Most of the organic matter produced photosynthetically in surfaces waters is recycled within the euphotic zone. A small fraction, amounting to roughly 10%, settles out of the euphotic zone before being mineralized. This fraction, known as "new" production, is virtually all oxidized in the underlying waters and leads to the O_2 deficiency of deeper waters. The exported organic matter carries essential nutrients out of the euphotic zone. Continued photosynthesis therefore can only be supported by a continued upwelling of nutrients.

In discussing controls on the oxygen deficiency of the ocean it is convenient first to consider an idealized world ocean under which the following conditions hold:

1. Organic matter is fixed in proportion to the limiting nutrients nitrate and phosphate according to the ratios of Redfield et al. (1963) given in Eq. 4.2.

2. Over the entire euphotic zone the available nutrients are completely exhausted by photosynthesis. This implies that any water parcel which sinks from the surface must leave with a nutrient concentration of zero.

3. The O_2 content of surface waters is in equilibrium with the overlying air. This implies that any water parcel which sinks from the surface has an O_2

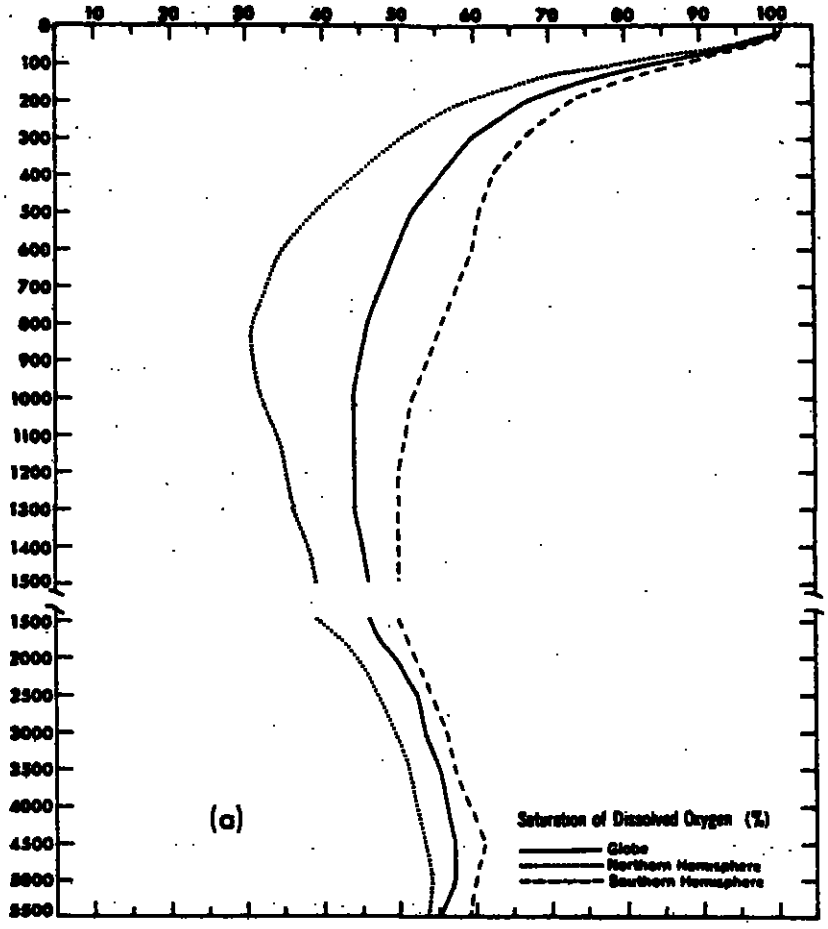

Figure 4.3: Average O_2 profiles in the major ocean basins. From Levitus (1982).

content corresponding to equilibrium with the atmosphere at its particular potential temperature and salinity.

4. Nitrate, phosphate, and organic carbon are remineralized at the same rate, i.e. according to the Redfield ratios in the underlying waters.

In this idealized ocean all the nutrients are in organic form or have been derived from the mineralization of organic matter in isolation from the atmosphere. The oxygen deficiency of the ocean can therefore be calculated according to

$$\Delta M_{O_2} = 138 \cdot M_P \tag{4.22}$$

where M_P is the total number of moles of phosphorous in the ocean. We refer to this as the 'potential' O_2 deficit of the ocean.

The conditions listed above for the ideal ocean describe reasonably the conditions in the central ocean basins in the mid- and low-latitudes. The nitrate and phosphate in these waters are near zero and the O_2 content is near solubility equilibrium with the atmosphere. Nevertheless, the true oxygen deficiency of the ocean as a whole achieves only 55% of the potential deficit as shown in Table 4.12. The principal explanation for this must lie in the mechanism of bottom-water formation. Bottom waters are known to form only over a very limited area of the ocean, principally in the Norwegian Sea in the north Atlantic and the Weddell Sea in the Antarctic (see e.g. Killworth, 1983), where surface waters achieve high densities. The mechanisms of bottom-water formation are not well understood and may involve combined effects of cooling at the surface and the formation of sea ice, both of which increase the density of surface waters. It is clear, however, that bottom-water formation is intermittent, occuring primarily in the coldest winter months, and that the newly-forming bottom waters do not remain long enough at the surface for photosynthesis to deplete the

available nutrients or for dissolved gases to achieve full solubility equilibrium with the atmosphere (Weiss et al. 1979). A substantial fraction of the nutrients carried into the deep sea are carried in inorganic form with the sinking of bottom water. The nutrients carried in inorganic form, known as 'preformed' nutrients, are a conservative property of sea water (Redfield, 1963).

The difference between the true deficit and the 'potential' deficit in the ocean is primarly owing to a failure of the oceans to satisfy condition (2) listed above in the bottom-water formation regions. However, the other three conditions may also be violated at times and places in the oceans. During the formation of Antarctic bottom water in the Weddell sea, for example, dissolved-O_2 content of Winter Water and Western Shelf Water, which are the primary surface component of the newly-forming Weddell Deep Water (which ultimately is a primary source for Antarctic Bottom Water) is approximately 50 μmoles/kg or 15% undersaturated in O_2 (Weiss et al., 1979). Such undersaturation of newly-forming bottom waters would increase the oxygen deficiency of the deeper waters. Also, the rate of mineralization of nutrients from sinking particles may differ substantially from the rate of mineralization of carbon (see e.g. Broecker and Peng, pp 134–139). This could increase the O_2 deficit if nutrients are mineralized at shallower depths than carbon because the nutrients could then be brought back to the surface where they would remove additional organic matter. Note that this type of mechanism must ultimately operate in the formation of DOC.

Much additional research is needed to clarify the controls on the O_2 deficit of the oceans. Nevertheless, it is worth considering what constraints can be imposed on possible changes in the O_2 deficit of the ocean over the past several centuries.

One such constraint comes from the measurements of dissolved O_2, nitrate and phosphate in the North Atlantic thermocline in 1972 (GEOSECS) and

again in 1981 (TTO). On the basis of this data, Peng and Broecker (1984) have argued that changes in nutrient cycling in the ocean have been too small to cause significant variations in atmospheric CO_2 over the past century. The data themselves show that the change in dissolved O_2 over this 9 year period was at most 5 μmoles/kg. Suppose that an alteration in nutrient cycling (the argument doesn't depend on the details of the mechanism) has decreased average dissolved-O_2 content of the thermocline by 0.5 μmoles kg^{-1} yr^{-1} (maximum change compatible with GEOSECS–TTO data). Taking a total thermocline mass of $2.6 \cdot 10^{20}$ kg corresponding to a mean depth of 800 m yields a total decrease of $1.3 \cdot 10^{14}$ moles O_2/yr. Conservation of the overall oxidative state of the atmospheric-thermocline system requires an increase in atmospheric O_2 of 0.6 ppm/yr or 25% of fossil-fuel O_2 depletion. This upper bound to changes imposed by ocean chemistry is significant compared to other terms considered here in the O_2 budget. However, the arguments advanced by Peng and Broecker (1984) indicate that changes of this magnitude are unlikely. From the standpoint of the global O_2 budget it would clearly be desirable to carry out accurate and more frequent measurements of dissolved O_2 in the future. The goal of being able to constrain changes in total oceanic dissolved O_2 to the level of $2 \cdot 10^{13}$ moles O_2/yr seems reasonable.

Another constraint on changes the oceanic O_2 brought about by natural variability in the nutrient cycling in the ocean is implied by measurements of CO_2 in ice cores reported by Oeschger et al. (1985). These measurements show that atmospheric CO_2 did not vary by more than ± 10 ppm ($\pm 1.8 \cdot 10^{14}$ moles) in the 1200 years preceding 1900. It is expected that the fluctuation in atmospheric O_2 (in moles) caused by a fluctuation in the efficiency of nutrient cycling would be roughly $-1.3/(AF)(t)$ times the change in atmospheric CO_2 (in moles) where t is the characteristic time scale of the fluctuation. Here the factor of 1.3 is the

ratio of O_2 produced to CO_2 consumed in marine organic matter (the standard Redfield ratio) and $(AF)(t)$ is the fraction of a pulse of CO_2 initially released into the ocean mixed layer which is present in the atmosphere at a time t later. For times longer than the equilibration time between the mixed layer and the atmosphere (approximately 1 year) releasing a pulse of CO_2 into the mixed layer is equivalent to releasing a pulse of CO_2 into the atmosphere. Thus we can use values for $(AF)(t)$ derived from models used to forcast the uptake of fossil-fuel CO_2 by the ocean. For time scales of 50 to 250 years (AF) is around 0.4 to 0.5 (Siegenthaler and Oeschger, 1978). For time scales as long as the turn-over time of the ocean ($\approx$ 1000 years) $(AF)(t)$ approaches 0.14 (derived from value of 0.86 given for fraction the of CO_2 present in the ocean after full equilibration, from Broecker et al. (1979)). The ice-core CO_2 data therefore constrain the rates of change in atmospheric O_2 brought about by recent changes in marine chemistry to be no greater than $5.8 \cdot 10^{13}$ moles/yr on a 100-year time scale and $5.8 \cdot 10^{12}$ moles/yr on a 1000-year time scale.

4.7 Scenarios for Recent O_2 Depletion

On the basis of the estimates of fossil-fuel O_2 consumption derived above, we can construct scenarios for the probable change in atmospheric O_2 over the last several centuries. If we neglect any sources or sinks for O_2 due to the operation of oceanic and the lithospheric cycles (the discussion in the previous section implies that this is a reasonable assumption) the only additional sources or sinks for O_2 would come from changes in biospheric reservoirs. It remains, therefore, to review the estimates of the net CO_2 source caused by recent biospheric change.

Early attempts at estimating oceanic uptake of fossil-fuel CO_2 ignored possible human impacts on terrestrial biota. These early estimates relied on sim-

plified models of ocean CO_2 uptake which employed parameterizations of ocean transport, such as dividing the ocean into a small discrete number of boxes (Keeling, 1973b), or treating the ocean as a 1–D diffusion system (Oeschger et al., 1975). Once these models were constrained to yield the known distributions of ^{14}C and radon in the oceans, there was little leeway to adjust the rate at which these models could take up atmospheric fossil-fuel CO_2 (see e.g. Broecker et al., 1979). The models suggested that of the $114 \cdot 10^9$ tons C of fossil-fuel CO_2 emitted into the atmosphere by 1970, 51 to 62% of the CO_2 should still be remaining in the atmosphere (Siegenthaler et al., 1978). This prediction was consistent with a preindustrial CO_2 concentration of 288 to 295 ppm (Siegenthaler et al., 1978) and the observed increase in atmospheric CO_2 (Keeling et al. 1976) only if it was assumed that little or no CO_2 was lost or gained by changes in land biospheric reservoirs.

Since the mid 1970's, when most such calculations were carried out, three independent lines of evidence began to indicate that net CO_2 emissions from the land biospheric reservoirs could not be neglected. Firstly, by 1980, a number of studies had been published which suggested that changing land use, brought about primarily by the expansion of agriculture, should be causing significant release of CO_2 from the land biosphere (Bolin, 1977; Adams et al., 1977; Woodwell et al. 1978; Wong, 1978). Owing to the complexity of this problem and the difficulty in compiling accurate global averages, these estimates allowed a wide range of $1 \cdot 10^{15}$ to $18 \cdot 10^{15}$ g C/yr for the net biospheric CO_2 source. It was clear that these estimates were grossly incompatible with the earlier notion that the land biosphere was nearly in steady state. The estimates of net biospheric releases published since 1980 have varied over a slightly narrower range, i.e. from approximately $1 \cdot 10^{15}$ to $4 \cdot 10^{15}$ g C/yr (Olson, 1982, Houghton et al., 1983; Emanual et al., 1984; Houghton et al., 1987). Nevertheless, the inconsistency

between the ocean model studies and the land biospheric studies remains.

Secondly, several studies of $^{13}C/^{12}C$ ratios in tree rings, which under optimal conditions should record the time history of the atmospheric $^{13}CO_2/^{12}CO_2$ ratio, showed a greater change over the period 1750–1980 than was compatible with fossil-fuel production alone (Stuiver, 1978; Freyer, 1978; Peng et al., 1983; Peng, 1985). (The addition of both fossil-fuel and biospheric carbon to the atmosphere decreases the atmospheric $^{13}CO_2/^{12}CO_2$ ratio because both sources are approximately 1.3% depleted in ^{13}C relative to atmospheric CO_2.) These studies lead to estimates of preindustrial CO_2 in the range 230–280 ppm and suggested an integrated CO_2 release from the biosphere amounting to 20% to 250% of the integrated fossil-fuel CO_2 input (Peng, 1985). The wide range of these predictions is mostly a function of the difficulty in selecting trees which truly record atmospheric $^{13}CO_2/^{12}CO_2$ variations. Tree-ring $^{13}C/^{12}C$ ratios vary as a function of the age of the tree and vary with environmental stresses and other factors which are not yet well understood, and it has not been possible to select trees which are unambigously free from these influences. Also, the predicted biospheric CO_2 inputs and preindustrial CO_2 levels are subject to the uncertainties in the carbon-cycle model used to account for the dilution of the atmospheric $^{13}CO_2/^{12}CO_2$ signal through exchange with the land biospheric and ocean carbon reservoirs.

Lastly, measurements of the CO_2 content of air trapped in polar ice cores have provided graphic evidence that the preindustrial CO_2 concentration was lower than 290 ppm. Early measurements of research groups in Bern and Grenoble suggested a preindustrial value of 260 (Barnola et al., 1983). Later measurements using an improved technique for extracting gas from the ices suggested a slightly higher value of 280 ppm (Oeschger et al., 1985). More recent measurements of Neftel et al. (1985) from the station at Siple, Antarctica corroborate

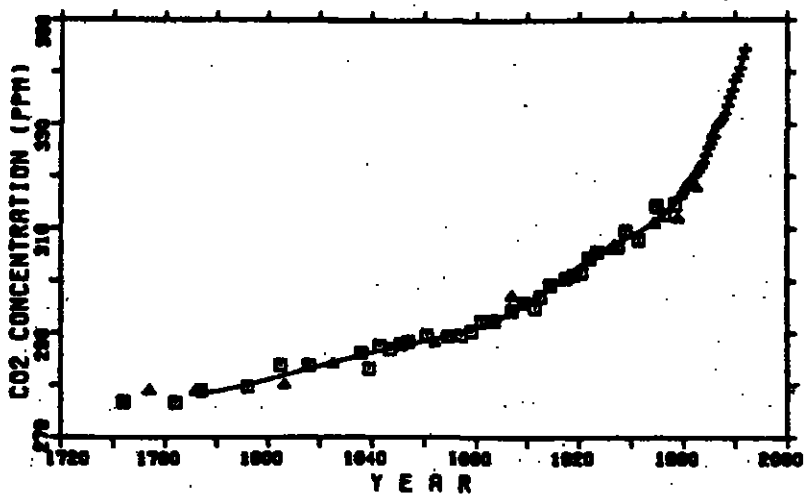

Figure 4.4: Atmospheric CO_2 increase in the past 200 years as indicated by measurements on air trapped in old ice from Siple Station, Antarctica measured by infrared spectroscopy (full triangles), by gas chromatography (open squares), and annual means from Mauna Loa Observatory (crosses). From Siegenthaler and Oeschger (1987).

the higher values and provide a time history of the rise in CO_2 to the present. The most recent version of these data from Siegenthaler and Oeschger (1987) is shown in Fig. 4.4. The Siple ice-core data agree with the Mauna Loa record starting in 1958 and, no doubt, represent a major improvement in our understanding of the increase in atmospheric CO_2 from preindustrial times to the present.

From the Siple/Mauna Loa record it is now possible to solve the inverse problem of estimating the net oxidative source of CO_2 (i.e. fossil-fuel plus biospheric source) which is compatible with the ocean models. The past biospheric source can then be derived by subtracting the fossil-fuel CO_2 sources estimates (e.g. Marland and Rotty, 1984; Keeling, 1973a) from the net oxidative source. The biospheric source derived in this way is subject to uncertainties in the

ocean model, ice-core CO_2 measurements, and fossil-fuel emissions. This procedure has been carried out by Siegenthaler and Oeschger (1987) and the range of compatible biospheric CO_2 sources is shown in Fig. 4.5. Note the range of biospheric CO_2 sources shown in Fig. 4.5 does not allow for possible 10% error (Marland and Rotty, 1984) in the the fossil-fuel CO_2 source. The actual range of biospheric sources is therefore somewhat larger than estimated by Siegenthaler and Oeschger (1987), particularly for the data after 1960. A major implication of the combined Siple/Mauna Loa CO_2 record is that the biosphere must have been a significant CO_2 source in the 19th century. Also, with a lower preindustrial CO_2 value, the ocean models are now compatible with a small net biospheric CO_2 source from 1958 to present (period covered by Mauna Loa record). This is because lowering the value for preindustrial CO_2 increases the excess partial pressure of present atmospheric CO_2 levels relative to sea water, which in turn implies a larger flux of CO_2 into the ocean.

Based on the above biospheric estimates, I have considered the following possible cases for the depletion of O_2 from preindustrial times to the present.

1. The only loss for O_2 is due to burning fossil fuel as estimated above. The land biosphere is in steady state.

2. The change in O_2 is due to burning fossil fuel, estimated above, plus biospheric change, estimated from the inversion of the Siple/Mauna Loa CO_2 record according to Siegenthaler and Oeschger (1987) assuming an oxidative ratio of 1.05 for biospheric carbon. Oceanic uptake is assumed to be the average of the box-diffusion and outcrop-diffusion models used by these authors.

3. The change in O_2 is due to fossil fuel burning, estimated above, plus biospheric change, derived from the CO_2-source estimates of Houghton et

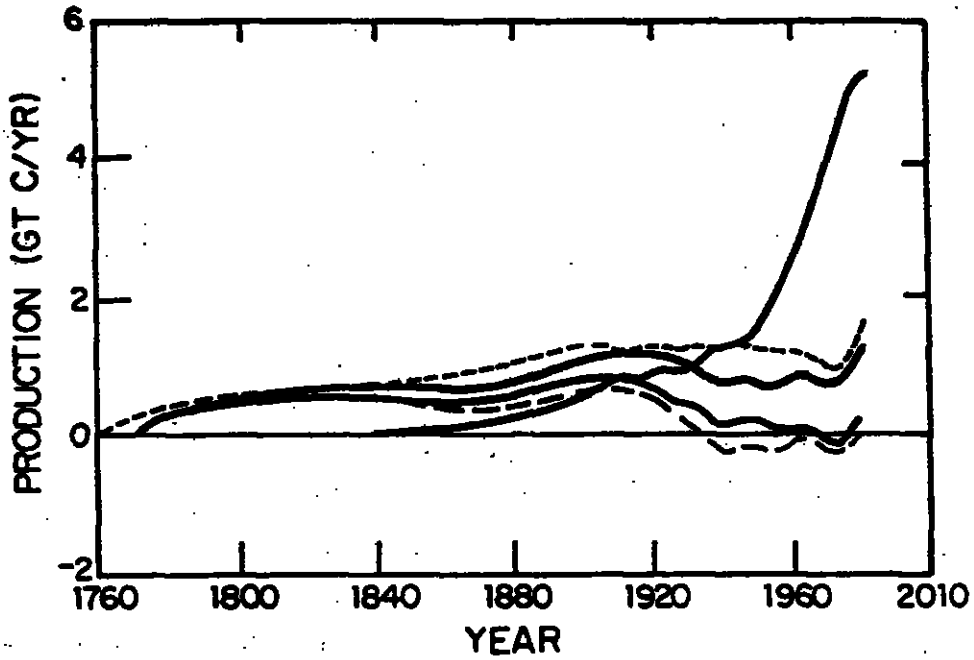

Figure 4.5: Smoothed biospheric CO_2 release rates calculated from inversion of Siple ice-core data. The solid lines correspond to reconstructions based on two different ocean models: 'outcrop-diffusion' model (upper solid line), 'box-diffusion' model (lower solid line) . Dashed lines correspond to reconstructions based on same ocean models but with the Siple CO_2 data shifted within its error limits: Siple data shifted by -6ppm/-10 years (short-dashed), Siple data shifted by +6 ppm/+10 years (long-dashed). From Siegenthaler and Oeschger (1987).

al. (1983) assuming an oxidative ratio of 1.05 for biospheric carbon.

Table 4.7 summarizes the integrated preindustrial-to-present O_2 depletion and the present (1980) O_2 depletion rate for each of the cases. The uncertainty in the O_2 consumption is estimated in each case from the uncertainty of the various input parameters. Note that in Case 2 the uncertainty in fossil-fuel data only makes a small contribution to the uncertainty in the predicted O_2 depletion rate. This is because the net oxidative CO_2 source, as derived from the inversion procedure, accurately ties down the net O_2 sink regardless of whether the CO_2 is derived from fossil-fuel burning or biospheric oxidation. The uncertainty in fossil-fuel burning is relevant in Case 2 only to the extent that it implies uncertainty in the oxidation of elements other than carbon.

An examination of Table 4.14 reveals that measurements of present or past O_2 depletion could be used to distinguish between the possible cases. Specifically, measurements of the current rate of depletion accurate to 10% would decide between biospheric estimates based on ocean models (Case 2) and land use studies (Case 3). If atmospheric O_2 depletion could be measured to better than 10% the O_2 data would constrain the ocean models. Measurements of the integrated past O_2 consumption (e.g. from ice-core air samples) accurate to 15% would primarily test whether or not past biospheric oxidation is as large as called for by both the ocean models and land use studies. Measurements that were more accurate than 15% would primarily provide a consistency check for past CO_2 levels measured in ice cores. If the uncertainty in ice-core CO_2 records is improved the measurements of past O_2 would also constrain the ocean models.

Table 4.14: Scenarios for Recent and Cumulative O_2 Depletion

Cases	1980 Annual[a]	Cumulative Through 1980[a]
(1) Fossil-fuel sink only:	610 ± 60	18050 ± 1700
(2) Prediction from ocean models, fossil-fuel records, and Siple/Mauna Loa CO_2 data:	660 ± 60	28450 ± 4300
(3) Fossil-fuel and biospheric sink[b]:	880 ± 130	33050 ± 4300
Errors in Case (2)		
ocean modelling[c]	± 50	± 2800
fossil-fuel data[d]	± 20	± 600
Siple record[e]	± 26	± 3200
oxidative ratio of biomatter[f]	± 3	± 500
Errors in Case (3)		
fossil-fuel data	± 60	± 1700
biota CO_2 source estimates[g]	± 120	± 3900
oxidative ratio of biomatter[f]	± 14	± 750

[a] In units of 10^{12} moles O_2.

[b] Biospheric O_2 sink modeled from Houghton et al. (1983) assuming 1.05 moles O_2 consumed per mole CO_2 released.

[c] Takes account of difference between CO_2 source estimates of box–diffusion model and outcrop diffusion model from Siegenthaler and Oeschger (1987).

[d] Takes account of uncertainty in excess O_2 consumption from fossil-fuel burning; See text.

[e] Takes account uncertainty in the deconvolution CO_2 source estimates due to uncerainty in ice core data. The reported error limits are consistent with the 'high' and 'low' interpretations of the Siple ice core records from Siegenthaler and Oeschger (1987).

[f] Takes account of 5% uncertainty in oxidative ratio of biosphere.

[g] Error estimates from Houghton et al. (1983).

4.8 Summary

In this chapter I have presented estimates of the current sources and sinks of O_2. Processes which have been considered include the burning of fossil fuel, changes in biomatter reservoirs, sedimentation and weathering of reduced materials, and changes in dissolved O_2 in the oceans.

A major outcome of this chapter has been show that the premise of Machta (1980)—that accurate measurements of changes in atmospheric O_2 mole fraction could be used to document changes in biospheric carbon reservoirs—is basically sound. Burning fossil fuel and changes in land biospheric reservoirs are causing the largest changes in atmospheric O_2 today, so that determination of both the net atmospheric O_2 loss and the estimates of fossil-fuel O_2 consumption would effectively constrain the changes in the biospheric reservoirs. On the basis of the uncertainty in fossil-fuel burning alone, the error in the estimate of biospheric source would be $\pm 6 \cdot 10^{13}$ moles/yr or roughly 30 to 75% of the recent estimate of the biospheric CO_2 source by Houghton et al. (1987).

Other sources and sinks of O_2 may not be negligible. On theoretical grounds one expects secular air–sea exchange fluxes of O_2 to be small. However, the available empirical constraints are compatible with sources and sinks as large as $1.3 \cdot 10^{14}$ moles/yr. An upper limit to changes in atmospheric O_2 associated with changes in dissolved organic carbon is estimated at $\pm 3 \cdot 10^{13}$ moles/yr, and an upper limit associated with imbalances between sedimentation and weathering/volcanism is estimated at $\pm 1.2 \cdot 10^{13}$ moles/yr. Future programs to determine terrestrial biospheric change from atmospheric O_2 data should include better measurements of changes in dissolved O_2, nutrients, and dissolved organic carbon in the ocean.

Probably the most important application of long-term O_2 measurements

would be determining the net oxidative CO_2 source, defined as the sum of biospheric plus fossil-fuel sources. The uncertainty in the net oxidative CO_2 source would depend only on the uncertainty in the net global oxidation of H, S, N, and Fe. For 1980, the net oxidation of these elements from industrial processes can be estimated to $\pm 2 \cdot 10^{13}$ moles/yr or to roughly 4% of the net CO_2 source estimated for that year (Siegenthaler and Oeschger, 1987). The O_2 data combined with data for the build-up of CO_2 in the atmosphere would provide a very tight constraint on the fraction of excess CO_2 being taken up by inorganic processes in the ocean which is essential for forecasting future CO_2 levels and future climate.

4.9 References

Adams, J. A. S., M. S. M. Mantovani, L. L. Lundell, 1977, "Wood versus fossil fuel as a source of excess carbon dioxide in the atmosphere: a preliminary report," *Science* **196**, 54–56.

Atjay, G. L., P. Ketner, P. Duvigneaud, 1979, "Terrestrial primary production and phytomass," in Bolin, B., E. T. Degens, S. Kempe, P. Ketner eds., *The global carbon cycle, SCOPE Report No. 13*, John Wiley & Sons, New York, 129–181.

Barnett, T. P., 1982, "Recent changes in sea level and their possible causes," *Climatic Change* **5**, 15–38.

Barnola, J. M., D. Raynaud, A. Neftel, H. Oeschger, 1983, "Comparison of CO_2 measurements by two laboratories on air from bubbles in polar ice," *Nature* **303**, 410–413.

Bolin, B., 1977, "Changes of land biota and their importance for the carbon cycle," *Science* **196**, 613–615.

Bolin, B., 1983, "The carbon cycle," in B. Bolin and R. B. Cook eds., *The Major Biogeochemical Cycles and Their Interactions*, John Wiley & Sons, Chichester, 41–45.

Bowen, H. J. M., 1966, *Trace Elements in Biogeochemistry*, Academic Press, London.

Brame, J. S. S., J. G. King, 1967 *Fuel: Solid, Liquid and Gaseous, 6th Ed.*, Edward Arnold, London.

Brinkmann, R. T., 1969, "Dissociation of water vapor and evolution of oxygen in the terrestrial atmosphere," *Journal of Geophysical Research* **74**, 5355–5368.

Broecker, W. S., 1970, "Man's oxygen reserves," *Science* **168** 1537–1538.

Broecker, W. S., T. Takahashi, H. J. Simpson, T.-H. Peng, 1979, "Fate of fossil fuel carbon dioxide and the global carbon budget," *Science* **206 (4417)**, 409–418.

Broecker, W. S., T.-H. Peng, 1982, *Tracers in the Sea*, Lamont-Doherty Geological Observatory, Palisades, New York.

Cess, R. D., S. D. Goldenberg, 1981, "The effect of ocean heat capacity upon global warning due to increasing atmospheric carbon dioxide," *Journal of Geophysical Research* **86(C1)**, 489–502.

Chemical Rubber Company, 1974, *Handbook of Chemistry Physics*, CRC Press, Inc., Cleveland.

Clark, W. C., K. H. Cook, G. Marland, A. M. Weinberg, R. M. Rotty, P. R. Bell, L. J. Allision, C. L. Cooper, 1982, "The carbon dioxide question: perspectives for 1982," in W. C. Clark ed., *Carbon Dioxide Review: 1982*, Oxford University Press, New York, 3–44.

Dietrich, G., K. Kalle, W., Kauss, G. Siedler, 1980, *General Oceanography, an Introduction*, New York, Wiley–Interscience.

Emanuel, W. R., G. G. Killough, W. M. Post, H. H. Shugart, 1984, "Modelling terrestrial ecosystems in the global carbon cycle with shifts in carbon storage capacity by land–use change," *Ecology* **65**, 970–983.

Encyclopedia of Chemical Technology, 3rd edition, 1984, Wiley, New York.

Etkins, R., E. S. Epstein, 1982, "The rise of global sea level as an indication of climate change," *Science* **215**, 287–289.

Freyer, H. D., 1978, "Preliminary evaluation of past CO_2 increase as derived from ^{13}C measurements in tree rings," in J. Williams ed., *Carbon Dioxide, Climate and Society*, Pergamon, New York, 69–78.

Garrels, R. M., E. A. Perry, Jr., 1974, "Cycling of carbon, sulfur, oxygen through geologic time," in E. Goldberg ed., *The Sea, Vol. 5*, New York, Wiley Interscience, 303–336.

Garrels, R. M., Lerman, A., 1981, "Phanerozoic cycles of sedimentary carbon and sulfur," *Proc, Natl. Acad. Sci. USA* **78(8)**, 4652–4656.

Gornitz, V., S. Lebedeff, J. Hansen, 1982, "Global sea level trend in the past century," *Science* **215**, 1611–1614.

Holland, H. D., 1978, *The chemistry of the atmosphere and oceans*, New York, John Wiley & Sons.

Holland, H. D., 1984, *The chemical evolution of the atmosphere and the oceans*, Princeton, Princeton University Press.

Houghton, R. A., J. E. Hobbie, J. M. Melillo, B. Moore, B. J. Peterson, G. R. Shaver, G. M. Woodwell, 1983, "Changes in the carbon content of terrestrial biota and soils between 1860 and 1980: a net release of CO_2 to the atmosphere," *Ecological Monographs* **53(3)**, 235–262.

Houghton, R. A., R. D. Boone, J. R. Fruci, J. E. Hobbie, J. M. Melillo, C. A. Palm, B. B. Peterson, G. R. Shaver, G. M. Woodwell, B. Moore, D. L. Skole, N. Meyers, 1987, "The flux of carbon from terrestrial ecosystems to the atmosphere in 1980 due to changes in land use: geographical distribution of the global flux," *Tellus* **39B**, 122–139.

Jenkins, W. J., and J.C. Goldman, 1985, "Seasonal oxygen cycling and primary production in the Sargasso Sea," *Journal of Marine Research* **43**, 465–491.

Keeling, C. D., 1973a, "Industrial production of carbon dioxide from fossil fuels and limestone," *Tellus* **25(2)**, 174–198.

Keeling, C. D., 1973b, "The carbon cycle: reservoir models to depict the exchange of atmospheric carbon dioxide with the oceans and land plants," in S. Rasool, ed., *Chemistry of the Lower Atmosphere*, 251–329.

Keeling, C. D., R. B. Bacastow, A. E. Bainbridge, C. A. Ekdal, P. R. Guenther, L. S. Waterman, J. F. S. Chen, 1976, "Atmospheric carbon dioxide variations at Mauna Loa Observatory, Hawaii," *Tellus* **28(6)**, 538–551.

Keeling, C. D., 1979, "The Suess Effect: ^{13}Carbon-^{14}Carbon Interrelations, *Environ. Int.*, **2**, 229–300.

Keeling, C. D.,R. B. Bacastow, T. P. Whorf, 1982, "Measurements of the concentration of carbon dioxide at Mauna Loa Observatory, Hawaii," in W. C. Clark ed., *Carbon Dioxide Review: 1982*, Oxford University Press, New York, 377–385.

Killworth, P. D., 1983, "Deep convection in the ocean," *Reviews of Geophysics and Space Physics* **21(1)**, 1–25.

Komhyr, W. D., R. H. Gammon, T. B. Harris, L. S. Waterman, T. J. Conway, W. R. Taylor, K. W. Thoning, 1985, "Global atmospheric CO_2 distribution

and variations from 1968–1982 NOAA/GMCC flask sample data," *Journal of Geophysical Research* **90(D3)**, 5567–5596.

Levitus, S., 1982, *Climatological Atlas Of the World Ocean, NOAA Professional Paper 13*, U. S. Department of Commerce and National Oceanic and Atmospheric Administration, Rockville, Md.

Lovelock, J. E., J. P. Lodge, Jr., 1972, "Oxygen in the contemporary atmosphere," *Atmospheric Environment* **6**, 575–578.

Machta, L., E. Hughes, 1970, "Atmospheric oxygen 1967–1970," *Science* **168**, 1582–1584.

Machta, L., 1980, "Oxygen Depletion," in G. C. Jacoby ed., *Carbon Dioxide Effects Research and Assessment Program; Proceedings of the International Meeting on Stable Isotopes in Tree-Ring Research*, United States Department of Energy, 125–127.

Marks, L. S., 1967, *Standard Handbook for Mechanical Engineers, 7th ed.*, New York, McGraw–Hill.

Marland, G., R. M. Rotty, 1984, "Carbon dioxide emissions from fossil fuels: a procedure for estimation and results for 1950–1982," *Tellus* **36B**, 232–261.

McElroy, M. B., 1976, "Chemical processes in the solar system: a kinetic perspective," in Chemical Kinetics (International Review of Science) Physical Chemistry, series **2** vol. 9, Butterworth, London.

Mopper, K., E. T. Degens, 1979, "Organic carbon in the ocean: nature and cycling," in Bolin, B., E. T. Degens, S. Kempe, P. Ketner eds., *The Global Carbon Cycle, SCOPE Report No. 13*, John Wiley & Sons, New York, 293–316.

Neftel A., E. Moor, H. Oeschger, B. Stauffer, 1985, "Evidence from polar ice cores for the increase in atmospheric CO_2 in the past two centuries," *Nature* **315**, 45–47.

Oeschger, H., U. Siegenthaler, U. Schotterer, A. Gugelmann, 1975, "A box diffusion model to study the carbon dioxide exchange in nature," *Tellus* **27(2)**, 168–192.

Oeschger, H., B. Stauffer, R. Finkel, C. C. Langway, Jr., 1985, "Variations of the CO_2 concentration of occluded air and of anions and dust in polar ice cores," in E. T. Sundquist and W. S. Broecker eds. *The Carbon Cycle and Atmospheric CO_2: Natural Variations Archean to Present*, American Geophysical Union, Washington D. C., 132–142.

Olson, J. S., 1982, "Earth's vegetation and atmospheric carbon dioxide," in W. C. Clark ed., *Carbon Dioxide Review: 1982*, Oxford University Press, New York, 388–398.

Peng, T.-H., W. S. Broecker, H. D. Freyer, S. Trombore, 1983, "A deconvolution of the tree ring based $\delta^{13}C$ record," Journal of Geophysical Research **88(C6)**, 3609–3620.

Peng, T.-H., W. S. Broecker, 1984, "Ocean life cycles and the atmospheric CO_2 content," *Journal of Geophysical Research* **89(C5)**, 8170–8180.

Peng, T.-H., 1985, "Atmospheric CO_2 variations based on the tree–ring ^{13}C record," in E. T. Sundquist and W. S. Broecker eds. *The carbon cycle and atmospheric CO_2: natural variations archean to present*, American Geophysical Union, Washington D. C., 123–131.

Peterson, B. J., J. M. Melillo, 1985, "The potential storage of carbon caused by eutrophication of the biosphere," *Tellus* **37B**, 117–127.

Ramamathan, V., R. J. Cicerone, H. B. Singh, J. T. Kiehl, 1985, "Trace gas trends and their potential role in climate change," *Journal of Geophysical Research* **90(D3)**, 5547–5566.

Redfield, A. B., B. H. Ketchum, F. A. Richards, 1963, "The influence of organisms on the composition of seawater," M. N. Hill ed., *The Sea, Vol. 2*, New York, Wiley Interscience, 26-77.

Revelle, R. R., 1983, "Probable future changes in sea level resulting from increased atmospheric carbon dioxide," in *Changing Climate, Report of the Carbon Dioxide Assessment Comittee*, National Academy Press, 433–448.

Richey, J. E., 1983, "The phosphorous cycle," in B. Bolin and R. B. Cook eds., *The Major Biogeochemical Cycles and Their Interactions*, John Wiley & Sons, Chichester, 51–56.

Rossini et al., eds., 1952, *Tables of selected values of chemical thermodynamic properties*, Nat. Bur. Std. Circ. No. 500.

Rotty, R. M., 1983, "Distribution of and changes in industrial carbon dioxide production," *Journal of Geophysical Research* **88(C6)**, 1301–1308.

Schnitzer, M., S. U. Khan, 1972, *Humic substances in the environment*, Marcel Dekker, New York.

Siegenthaler, U., H. Oeschger, 1978, "Predicting future atmospheric carbon dioxide levels," *Science* **199**, 388–395.

Siegenthaler, U., H. Oeschger, 1987, "Biospheric CO_2 emissions during the past 200 years reconstructed by deconvolution of ice core data," *Tellus* **38B**, 140–154.

Schlesinger, W. H., 1984, "Soil organic matter: A source of atmospheric CO_2," in G. M. Woodwell ed., *The Role of Terrestrial Vegetation in the Global Carbon Cycle: Measurement By Remote Sensing, SCOPE Report No. 23*, John Wiley, New York.

Söderlund, R., B. H. Svensson, 1976, "The global nitrogen cycle," in Svensson, B., and Söderlund, R., eds., *Nitrogen, Phosphorous, and Sulfur—Global Cycles, SCOPE Report No. 7, Ecol. Bull. (Stockholm)*, **22**, 23–73.

Stuiver, M., 1978, "Atmospheric CO_2 increases related to carbon reservoir changes," *Science* **199**, 253–258.

Sundquist, E. T., 1985, "Geological perspectives on carbon dioxide and the carbon cycle," in E. T. Sundquist and W. S. Broecker eds. *The Carbon Cycle and Atmospheric CO_2: Natural Variations Archean to Present*, American Geophysical Union, Washington D. C., 5–59.

Trenberth, K. E., 1981, "Seasonal variations in global sea level pressure and the total mass of the atmosphere," *Journal of Geophysical Research* **86(C6)**, 5238–5246.

UN, 1951–1969, *World Energy Supplies*. Statistical Papers, Series J., United Nations Department of International Economic and Social Affairs, Statistical Office, New York.

UN, 1955, *World Energy Requirements in 1975 and 2000*, International Conference on Peaceful Uses of Atomic Energy, United Nations Department of Economic and Social Affairs, Statistical Office, New York.

UN, 1981, *United Nations Statistical Yearbook, 1981* Department of International Economic and Social Affairs, Statistical Office, New York.

UN, 1982, *1980 Yearbook of World Energy Statistics*, United Nations Department of International Economic and Social Affairs, Statistical Office, New York.

US, 1976, *U. S. Standard Atmosphere, 1976*, National Oceanic and Atmospheric Administration, National Aeronautics and Space Administration and United States Air Force, U. S. Printing Office, Washington D. C.

Van Valen, L., 1971, "The history and stability of atmospheric oxygen," *Science* **171(3970)**, 439–443.

Veizer J., W. H. Holzer, C. K. Wilgus, 1980, "Correlation of $^{13}C/^{12}C$ and $^{34}S/^{32}S$ secular variations," *Geochemica et Cosmochemica Acta* **44**, 579–587.

Walker, J. C. G., 1977, *Evolution of the Atmosphere*, Macmillan, New York.

Watts, J. A., 1982, "The carbon dioxide question: a data sampler," in W. C. Clark ed., *Carbon Dioxide Review: 1982*, Oxford University Press, New York, 422–469.

Weiss, R. F., 1970, "The solubility of nitrogen, oxygen, and argon in water and seawater," *Deep Sea Research* **17**, 721–735.

Weiss, R. F., H. G. Östlund H. Craig, 1979, "Geochemical studies of the Weddell Sea," *Deep–Sea Research* **26A**, 1093–1120.

Wollast, R., 1983., "Interactions in estuaries and coastal waters," in B. Bolin and R. R. Cook eds. *The Major Biogeochemical Cycles and Their Interactions, SCOPE Report No. 21*, New York, John Wiley and Sons, 385–407.

Wong, C. S., 1978, "Atmospheric input of carbon dioxide from burning wood," *Science* **200**, 197–200.

Woodwell, G. M., R. H. Whittaker, W. A. Reiners, G. E. Likens, C. C. Delwiche, D. B. Botkin, 1978, "The biota and the world carbon budget," *Science* **199**, 141–146.

WEC (World Energy Conference), 1980, *Survey of Energy Resources*, Federal Institute for Geosciences and Natural Resources, Hanover, Federal Republic of Germany, 1980.

Chapter 5

Concluding Remarks

We are living in a pivotal time in the evolution of the earth. The latter half of the twentieth century marks the end of an epoch in which the biogeochemical evolution of the planet has been driven by "natural" causes, and marks the beginning an epoch in which the biogeochemical evolution of the earth will be significantly altered, perhaps even controlled, by human actions.

The rapidity of global change anticipated in the next decades and centuries presents both opportunities and responsibilities to the earth sciences. The opportunities arise from the possibility of studying dynamic variables of the earth as they respond to new types of inputs and forcings. Thus, Roger Revelle has termed the buildup of CO_2 in the atmosphere as "Man's great geophysical experiment" (see Bryan, 1987). The responsibilities arise from the urgency of assembling, as rapidly as possible, a viable understanding of complex interactions of the ocean, atmosphere, and biosphere so that politicians and other policy planners can be forewarned of future changes.

Compared to the changes which are anticipated in the next century, such as global warming of several degrees Celsius, 5 to 15% reductions in stratospheric

ozone, a meter or more rise in mean sea level, it seems as though little has happened. Some will argue that because the earth is still basically "healthy" there's little cause for vigorous action. However, the very fact that the most significant changes are still to come underscores the importance of biogeochemical measurements which are currently being conducted or will be conducted in the next few decades. One cannot possibly understand disease unless one understands what it means to be healthy. We probably only have a few more decades to study a "healthy" earth.

The assembling of a viable understanding of the earth as an integrated ecosystem must involve the study of phenomena occurring on spatial scales ranging from the molecular to the global. One area of study which has played a central role in our current understanding of man's perturbation of the earth is the measurement of long-lived atmospheric trace gases, CO_2, CH_4, N_2O, and the freons. All of these are greenhouse gases, and may cause direct or indirect changes in stratospheric ozone; thus they are among the primary agents of climatic change. The prominence of these gases also lies, in part, in their role as indicators of global change. Any pronounced trend in the concentration of an atmospheric species with a lifetime longer than the characteristic mixing time of the atmosphere (approximately 1 year) indicates a trend on a global scale. The fact that all of these gases are accumulating in the atmosphere at an accelerating pace comprises some of the strongest *prima facie* evidence that the burning of fossil fuel, the expansion of agriculture, and other human activities have already significantly altered the overall chemistry of the earth.

The purpose of this thesis has been to establish a method for measuring another long-lived tracer, atmospheric O_2. High-resolution measurements of atmospheric O_2 would address some of the most difficult and profound questions now faced in biogeochemistry. Two such questions were discussed in Chapter 1:

(1) The question of the magnitude of the "new" production in surface waters, and (2) the question of the impact of human activities and climatic changes on the living and dead reservoirs of carbon in the land biosphere. The first of these issues could be addressed by measuring the amplitude of seasonal variations in atmospheric O_2 and CO_2 at well-chosen sights around the world which would constrain estimates of the seasonal air-sea exchange of O_2. As was discussed in Chapter 1 and further substantiated in Chapter 4, the second question could be addressed by measurements of secular changes in atmospheric O_2, i.e. the residual changes in O_2 after averaging over seasonal or other short-term variability. For both of these issues the O_2 measurements would comprise a crucial complement to local ecosystem studies or satelite-based studies.

Measuring changes in the trace gases CO_2, CH_4, and N_2O, which vary annually at the 0.1 to 1% level, has not been achieved without a great deal of careful work. Measuring changes in O_2, which is expected to vary at only the 0.001% level, has appeared like such a formidable undertaking that few scientists have given the question serious thought.

Chapters 2 and 3 of this thesis have described tests which demonstrate the feasibility of measuring short-term changes in atmospheric O_2 to the level of 0.5 parts per million in the mole fraction. This level of resolution should be adequate for resolving all but the subtlest features of atmospheric O_2 variability. Nevertheless, there are still significant technical issues to be addressed before the method can be directly applied to background-air measurements.

The most significant of these is the question of how to store or transfer air samples without corrupting the O_2 mole fraction. The difficulties may be considerable. O_2 mole fraction could be altered both by homogeneous fractionation (by differential diffusion of O_2 and N_2) and by heterogeneous fractionation (differential adsorption of O_2 and N_2 on surfaces).

Several mechanisms could cause homogenous fractionation of O_2/N_2 at ppm levels. These include (1) differential conductance of O_2 and N_2 through small orifices such as pin-hole leaks or flow around the seat of pressure regulators, (2) thermal-diffusive fractionation, caused by temperature gradients, and (3) gravimetric fractionation, which could cause differences of several ppm O_2 between between the top and bottom of high-pressure cylinders. I do not expect, however, that homogeneous fractionation will present serious difficulties at pressures above 1 atmosphere. The time scales for diffusive fractionation are quite long (as an extreme example; note that the characteristic time constant to approach gravimetric equilibrium over a vertical length of one meter at 2000 PSIG is longer than a year) and it is likely that convection caused by ambient temperature changes and the turbulence created in the transfer of gas through small orifices are sufficient to ensure adequate mixing. Also, homogeneous fractionation could be eliminated in most circumstances by introducing turbulence artificially, e.g. by placing a small ball in the container and agitating it magnetically.

Heterogeneous fractionation could be caused either by differential physisorption of N_2 and O_2 or by chemisorption of O_2. A number of tests which I have conducted suggest the importance of heterogeneous fractionation: in transferring a fraction of the contents of a high-pressure cylinder to a second, well evacuated, smaller container at 1000 PSIG, I have found that the content of the second cylinder is generally depleted in O_2 by 10 to 20 ppm relative to the source cylinder. I attribute the O_2 loss to differential physisorption of O_2 and N_2 onto the walls of the smaller container because the magnitude of the loss was largely independent of transfer rate and because the lost O_2 appeared to be recovered as the pressure of the smaller container dropped below a few hundred PSIG. Other explanations are possible, however.

One approach to reducing fractionation in samples is to maintain virtually constant pressure within the sample vessel at all times. This could be accomplished by using sample containers with stopcocks or valves at either end which are flushed thoroughly with air at a constant pressure before closure. The contents of the flask could then be analyzed by flushing the sample through the O_2 analyzer with a background flow gas at the same pressure and integrating the deviation in the response of the O_2 analyzer. A very similar procedure is commonly used to analyze samples by gas chromatography. This approach ensures that the walls of the sample vessel are always conditioned to essentially constant O_2 and N_2 partial pressures and it eliminates any problems from homogeneous fractionation within the sample vessel because the entire sample content is integrated.

In general, the reducing of fractionation in different circumstances will require careful testing of different types of storage containers and different methods of transferring samples. The interferometric oxygen analyzer is the ideal tool for testing and proving viability of different methods.

A major additional requirement is development of highly-stable standards or reference gases. Ideally, one would like to have air standards for which the oxygen mole fraction is tied to an absolute scale (it is not necessary to know the O_2 mole fraction absolutely, only to have fixed reference point). This is likely to require the development of gravimetric, volumetric, or other methods of standardization.

One method of absolute standardization which may be worth exploring is to use the relative refractivity as an absolute measure of O_2. To accomplish this, one would need to eliminate or fully characterize all systematic errors contributing the observed fringe-count ratio to a few parts in 10^8. Based on my current understanding of the experiment, I would expect the principal difficulties to be

(1) maintaining very accurate alignment between the two wavelength components so that the optical-path-difference ratio reflects only the refractivity ratio of the gas and not density differences, e.g. caused by temperature gradients or path-length differences between the two beams, and (2) reducing or accounting for the optical path difference caused by stress-induced index variations in the cell windows which, for the present sample cell, amount to roughly 10^{-5} times the optical path difference changes in the gas. Both types of systematic error could be greatly reduced by basing the standardization on the difference in the relative refractivities of air and pure N_2 because the systematic errors for N_2 would largely cancel the errors for air.

The accurate determination of long-term changes in atmospheric O_2 probably must await the development of absolute standards. In the mean time, however, it will be possible to explore variation in O_2 over a broad range of temporal and spatial scales. Most short-term variations could be referenced against a suite of compressed-air reference gases which, with care, should be stable to 1 ppm O_2/yr.

One of the first applications of the present oxygen measurement capability should be the establishment of a global sampling network consisting of several well-chosen sites around the world where air samples are gathered on a weekly or biweekly basis and shipped to a central laboratory for analysis of O_2, CO_2, and other trace gases. Even as little as two or three years of data from such a network would provide a wealth of information on the coupled global oxygen and carbon cycles.

One feature which is expected to be prominent in such data is a large seasonal signal in the high northern latitudes. The amplitude of the seasonal CO_2 signal above 60° N is roughly 16 parts per million, and since the signal is mostly due to exchanges with land plants and soils, an equally large O_2 signal is ex-

pected. It will be very interesting to see whether the O_2 signals is larger or smaller than the CO_2 signal. If air-sea exchange of O_2 is as large as expected, the seasonal O_2 signal could be as much as 30 to 50% larger on a per-mole basis than the CO_2 signal. It will also be interesting to see how the amplitude of the seasonal signals varies with latitude. The CO_2 signal in the southern hemisphere is very weak owing to the small extent of seasonally-active land plants in the southern hemisphere. The oxygen variations, however, could be 3 to 5 times larger than the CO_2 signals if seasonal air-sea exchange processes are important. The difference in the amplitude of the CO_2 and O_2 signals should be a valuable indicator of air-sea exchange processes and marine biological productivity.

Another feature which should emerge from such a data set is a variation in the annual-mean O_2 mole fraction with latitude. CO_2 measurements show an excess of approximately 2 ppm in the northern hemisphere relative to the southern hemisphere. This gradient is attributable, in part, to the uneven distribution of fossil-fuel burning because most fuel is consumed in the northern hemisphere. However, the gradient is also influenced by the uptake of fossil-fuel CO_2 by the ocean, the natural transport of CO_2 within the ocean, and net sources and sinks from the land biosphere (Heimann et al. 1986). If this profile were sufficiently well understood it could be used, for example, to discern the extent of deforestation or forest recovery in different latitude zones. Knowledge of the meridional O_2 gradient would improve our understanding of the meridional CO_2 gradient because the two profiles are governed by many of the same factors but with differing relative contributions. For example the distribution of fossil-fuel and land-biosphere sources and sinks must match the corresponding O_2 sources and sinks, however, the distribution of the fossil-fuel CO_2 sink in the ocean has no analogous O_2 component. Also, the net north-south transport of O_2 within the ocean is probably less significant than north-south transport of

CO_2, as can be seen, for example, in the North-Atlantic Deep Water where the net southward transport of O_2 is partly offset by oxidation of particulate organic carbon (POC), whereas the net southward transport of CO_2 is augmented by the decay of POC.

Another important application for O_2 measurements, in addition to ground-based sampling, is measuring the verticle profile of O_2 within the stratosphere. Stratospheric samples could be collected using an existing cryogenic whole-air sampling apparatus (Lueb et al., 1975) which has been used successfully for CO_2, N_2O, CH_4 and other trace gases. As discussed in the introduction, the stratospheric verticle profiles of O_2 and CO_2, taken together with independent constraints on verticle mixing, would place constraints on the net loss rate of O_2 over the past five years. In fact, stratospheric measurements might provide the only reliable method for determining the net O_2 loss rate before absolute standards are developed.

Numerous other geochemical applications of the O_2 measurements come to mind. Many of these would depend on using the instrument directly in the field. Based on the simplicity and robustness of the method, this appears to be a very reasonable proposition. One application for a field instrument is studying O_2/CO_2 correlations within or beneath a forest canopy. Since O_2/CO_2 exchange ratios are characteristic of different exchange processes, O_2/CO_2 correlation studies might provide insights into the sub-units of the ecosystem participating in photosynthesis and respiration at any particular time, the flow of organic matter within the plants and soil, or the extent of anaerobic activity. Another application is mounting the instrument on an airborne platform to measure vertical profiles of O_2 in the marine boundary layer. Knowledge of this profile, when combined with other constraints on turbulent mixing, would determine air-sea exchange fluxes of O_2. Yet another application is to install an O_2 analyzer

at a remote station for continuous monitoring of O_2 as a function of time. This approach would yield a much more detailed time series than could be achieved with flask sampling.

The effort invested in measuring changes in atmospheric CO_2 has expanded rapidly in the last few years. It now includes some 35 sampling stations worldwide and involves the efforts of six or more nations. This effort is justified by the growing importance of understanding the complex interactions of the biosphere, the atmosphere, and the ocean, and the role of CO_2 both as an agent and indicator of climatic change. Through the increase in CO_2 over time, and the evolving distribution of CO_2 in the atmosphere, these data have told us a very interesting story of the growing human population and how it has begun to alter the natural biological cycles of the earth.

The CO_2 data, taken alone, have only told part of the story. An important piece of the story has been written in the variations of O_2, a language which we have not been able to read. In the next few decades, as fossil-fuel usage increases, as vast areas of tropical forest are destroyed, as gases which destroy the ozone layer and cause the greenhouse effect continue to accumulate in the atmosphere, and as other human actions begin to noticeably change the natural flow of energy, water, and carbon on the earth, the plot of this story will surely thicken. We need to begin recording the oxygen story as well.

One might look into the future to a time when the effort invested to measure changes in CO_2 is matched by comparable effort to measure changes in atmospheric O_2. The accomplishment of this thesis has been to show that this goal is not as remote as one might have thought a few years ago.

Bryan, K., 1987, "Man's great geophysical experiment: can we model the consequences?", *Oceanus* **29(4)**, 36–42.

Heimann, M., C. D. Keeling, I. Y. Fung, 1986, "Simulating the atmospheric carbon dioxide distribution with a three dimensional tracer model," in J. R. Trabalka, and D. E. Reichle eds., *The Changing Carbon Cycle A Global Analysis*, New York, Springer–Verlag.

Lueb, R. A., D. H. Ehhalt, L. E. Heidt, 1975, "Balloon–borne low temperature air sampler," *Review of Scientific Instruments* **46(6)**, 702–705.

Appendix A

Derivation of Sensitivity Relation

Eq. 2.5 is most simply derived for the case of a binary mixture. We let X_a and X_b denote the mole fractions of constituents a and b such that

$$X_a + X_b = 1. \tag{A.1}$$

The refractivity of the mixture is then given by

$$r_{mix} = r_a X_a + r_b X_b \tag{A.2}$$

where r_a and r_b denote the refractivities of constituents a and b. The relative refractivity is then given by

$$\tilde{r} = \frac{r_{mix}(\lambda_1)}{r_{mix}(\lambda_2)}. \tag{A.3}$$

Substituting Eq. A.2 into Eq. A.3 and eliminating X_b via Eq. A.1 yields

$$\tilde{r} = \frac{[r_a(\lambda_1) - r_b(\lambda_1)]\, X_a - r_b(\lambda_1)}{[r_a(\lambda_2) - r_b(\lambda_2)]\, X_a - r_b(\lambda_2)}. \tag{A.4}$$

Differentiating with respect to X_a

$$\frac{1}{\tilde{r}}\frac{d\tilde{r}}{dX_a} = \frac{r_a(\lambda_1) - r_b(\lambda_2)}{r_{mix}(\lambda_1)} - \frac{r_a(\lambda_2) - r_b(\lambda_2)}{r_{mix}(\lambda_2)} \tag{A.5}$$

and eliminating r_b using Eqs. A.2 and A.1 yields

$$\frac{1}{\tilde{r}}\frac{d\tilde{r}}{dX_a} = \frac{1}{1 - X_a}\left[\frac{r_a(\lambda_1) - r_{mix}(\lambda_1)}{r_{mix}(\lambda_1)} - \frac{r_a(\lambda_2) - r_{mix}(\lambda_2)}{r_{mix}(\lambda_2)}\right] \tag{A.6}$$

or

$$\frac{1}{\tilde{r}}\frac{d\tilde{r}}{dX_a} = \frac{1}{1 - X_a}\left[\frac{r_a(\lambda_1)}{r_{mix}(\lambda_1)} - \frac{r_a(\lambda_2)}{r_{mix}(\lambda_2)}\right]. \tag{A.7}$$

Substituting from Eq. A.3 into Eq. A.7 we have

$$\frac{d\tilde{r}}{dX_a} = \frac{1}{1 - X_a}\frac{r_{mix}(\lambda_1)}{r_{mix}(\lambda_2)}\left[\frac{r_a(\lambda_1)}{r_{mix}(\lambda_1)} - \frac{r_a(\lambda_2)}{r_{mix}(\lambda_2)}\right] \tag{A.8}$$

or

$$\frac{d\tilde{r}}{dX_a} = \frac{1}{1 - X_a}\frac{r_a(\lambda_2)}{r_{mix}(\lambda_2)}\left[\frac{r_a(\lambda_1)}{r_a(\lambda_2)} - \frac{r_{mix}(\lambda_1)}{r_{mix}(\lambda_2)}\right] \tag{A.9}$$

or

$$\frac{d\tilde{r}}{dX_a} = \frac{n_a(\lambda_2) - 1}{n_{mix}(\lambda_2) - 1}\frac{\tilde{r}_a - \tilde{r}}{1 - X_a} \tag{A.10}$$

where $\tilde{r}_a = r_a(\lambda_1)/r_a(\lambda_2)$ is the refractivity ratio of constituent a.

Eq. A.10 can also be applied directly to a mixture containing more than two components and thus Eq. 2.5 follows directly. In this case component b is identified with the of sum of all species other than a. The use of Eq. A.10 to describe changes in refractivity ratio in a multicomponent mixture requires that the transformation which alters the mole fraction of species a does not alter the relative proportions of the other constituents.

Appendix B

Relative Refractivity Measurements

B.1 Introduction

This appendix describes ancillary refractivity measurements performed in order to assess the sensitivity of the relative refractivity of air to changes in trace-gas concentrations, density, and temperature. Measurements of relative refractivities between 4359.56Å and 2537.27Å are reported for air, N_2, Ar, CO_2, CH_4, CO, N_2O, and H_2O. For all gases except H_2O the first-order variation of the relative refractivity with density is resolved. The results are described in terms of the first and second virial coefficients of the relative refractivity. Also reported are measurements of the sensitivity coefficient S_{O_3} of the relative refractivity of air to traces of O_3 and measurements of temperature dependence of the refractivity of nitrogen over the range 22–33°C.

The refractive index of a gas is most generally expressed as a power expan-

sion for the Lorentz–Lorenz function LL in density

$$LL = \frac{n^2 - 1}{n^2 + 2}\frac{1}{\rho} = A_R + B_R\rho + C_R\rho^2 + \cdots \tag{B.1}$$

where n is the refractive index, ρ is the molar density, and A_R, B_R, and C_R are, respectively, the first, second, and third virial coefficients of the refractivity. These coefficients are functions of frequency and temperature but not of density. The first virial coefficent A_R is related to the polarizibility α of an isolated molecule according to

$$A_R = \frac{4\pi}{3}\alpha. \tag{B.2}$$

The second virial coefficient B_R is related to the excess polarizibility of interacting pairs of molecules (Buckingham and Graham, 1974; Buckingham and Pople, 1955).

One can also expand $(n-1)$ directly as a function of density according to

$$(n-1)/\rho = A_n + B_n\rho + C_n\rho^2 + \cdots. \tag{B.3}$$

The virial coefficients of Eqs. B.1 and B.3 are related according to

$$A_R = \frac{2}{3}A_n \tag{B.4}$$

$$B_R = \frac{2}{3}B_n - \frac{1}{9}{A_n}^2 \tag{B.5}$$

$$C_R = \frac{2}{3}C_n - \frac{2}{9}A_nB_n - \frac{4}{27}{A_n}^3 \tag{B.6}$$

Based on Equation B.1, it is clear that the relative refractivity, defined according to

$$\tilde{r}(\lambda_1, \lambda_2) = r(\lambda_1)/r(\lambda_2) \tag{B.7}$$

where $r = n - 1$, is generally also a function of density. Thus we can write

$$\tilde{r}(\lambda_1, \lambda_2) = a(\lambda_1, \lambda_2) + b(\lambda_1, \lambda_2) r(\lambda_2) + c(\lambda_2, \lambda_2) r(\lambda_2)^2 + \cdots \tag{B.8}$$

where $r(\lambda_2)$ is used as the independent variable instead of ρ. The coefficients of Eq. B.8 and B.1 are related according to

$$a(\lambda_1, \lambda_2) = A_R(\lambda_1)/A_R(\lambda_2) \tag{B.9}$$

$$b(\lambda_1, \lambda_2) = \tfrac{27}{8} A_R(\lambda_2)^{-3} \left[B_R(\lambda_1) A_R(\lambda_2) - B_R(\lambda_2) A_R(\lambda_1)\right] + \tfrac{1}{6} \tfrac{A_R(\lambda_1)}{A_R(\lambda_2)} \left[\tfrac{A_R(\lambda_1)}{A_R(\lambda_2)} - 1\right]. \tag{B.10}$$

Using $r(\lambda_2)$ as the independent variable is advantageous because it is easier to measure refractive indicies to high accuracy than to measure densities to high accuracy.

In the measurements reported here, $\tilde{r}(\lambda_1, \lambda_2)$ is measured over a range of values $0 < r(\lambda_2) < 0.003$. The precision of the measurements is sufficient for determining the first and second virial coefficients, a and b in Eq. B.8, but not for determining higher coefficients, c etc.

B.2 Relative Refractivity Virial Coefficients

The interferometer used in these measurements is described in Section 2.2. The scan gas, used for modulating the fringe signals, was derived from the same source as the sample gas. The dynamic fringe signals, generated in scans from 0 to 20 torr, were analyzed according to the algorithm in Appendix C.

Initially, $\tilde{r}(\lambda_1, \lambda_2)$ is determined from dynamic pressure scans in the scanning cell with the sample cell evacuated. $\tilde{r}(\lambda_1, \lambda_2)$ is determined according to

$$\tilde{r}(\lambda_1, \lambda_2) = \frac{\lambda_1}{\lambda_2}\frac{f_1}{f_2}$$

where f_1/f_2 is the frequency ratio of the λ_1 and λ_2 fringe signals. The dynamic fringe scans are also used to determine the fractional fringe offset $\epsilon^{(0)}$ between a particular λ_1 fringe maximum and an adjacent λ_2 fringe maximum.

Subsequently, the sample cell is slowly filled while counting the elapsed λ_2 fringes to a particular fringe count. Dynamic scans are then continued in order to determine the relative offset ϵ of another pair of λ_1 and λ_2 fringes. The relative refractivity is related to the fringe offsets according to

$$\tilde{r}(\lambda_1, \lambda_2) = \frac{\lambda_1}{\lambda_2}\frac{p_1 + \epsilon - \epsilon^{(0)}}{p_2} \tag{B.11}$$

where p_1 and p_2 are exact integers which represent the integral order of the optical path difference at λ_1 and λ_2 between the first and second pair of fringes. The absolute refractivity $r(\lambda_2)$ is given by

$$r(\lambda_2) = n(\lambda_2) - 1 = \frac{p_2\lambda_2}{2L}. \tag{B.12}$$

where L is the cell length (61.17 ± 0.01 cm). The fractional fringe corrections to Eq. B.12 are not significant in the present context. Under suitable conditions, a unique solution to Eq. B.11 can be found by starting with the following information: (1) the measured values for a ϵ and $\epsilon^{(0)}$, (2) an estimate for p_2 determined by the number of λ_2 fringes which elapsed during the filling of the sample cell, and (3) an estimate for $\tilde{r}$ based on extrapolating previous measurements of $\tilde{r}(\lambda_1, \lambda_2)$ to the current value of $r(\lambda_2)$.

Both Eq. B.11 and B.12 assume that the optical path difference, p_2, is due only to the change in sample-gas density and thus they neglect any contributions due to differences in scanning-gas density. For these measurements the scanning-gas contribution to p_2 was always less than one fringe which leads to errors in $(n(\lambda_2)-1)$ and $\tilde{r}(\lambda_1,\lambda_2)$ of at most $3.6 \cdot 10^{-7}$ and $1 \cdot 10^{-8}$ respectively.

All measurements were carried out at ambient lab temperature which varied, at most, from 20 to 24°C.

The minimum guaranteed purity of the gases as supplied by the vendor was: nitrogen (99.999%), argon (99.999%), carbon dioxide (99.995%), methane (99.99%), carbon monoxide (99.99%), nitrous oxide (99.99%). These gases were used without further purification. Compressed air was obtained from a cylinder which was filled from an intake at the Scripps Pier in La Jolla, California and scrubbed of CO and hydrocarbons. Water vapor was derived from a laboratory source of distilled water. The water was transferred to a glass bulb connected both to the inlet of the scanning cell and a separate vacuum line where the residual air was pumped away first by freezing the water, and then by warming the water so that it boiled. During the measurements, the water was warmed to yield a source pressure of approximately 40 torr. Measurements on water vapor were carried out using the dynamic scanning method only.

Measurements of the relative refractivity $\tilde{r}(\lambda_1,\lambda_2)$ of air, N_2, Ar, CO_2, CH_4, N_2O, and CO, plotted against $n(\lambda_2)-1$ are shown in Figures B.1 through B.7. The data are well described by a linear relationship. The measurements on air and N_2 contain errors caused by secondary reflections within the cell windows which interfere with the phase of the primary beams. These errors were largely eliminated in measurements of other gases which were carried out after the plane-parallel cell windows were replaced with windows with a small (2 arcmin) wedge angle.

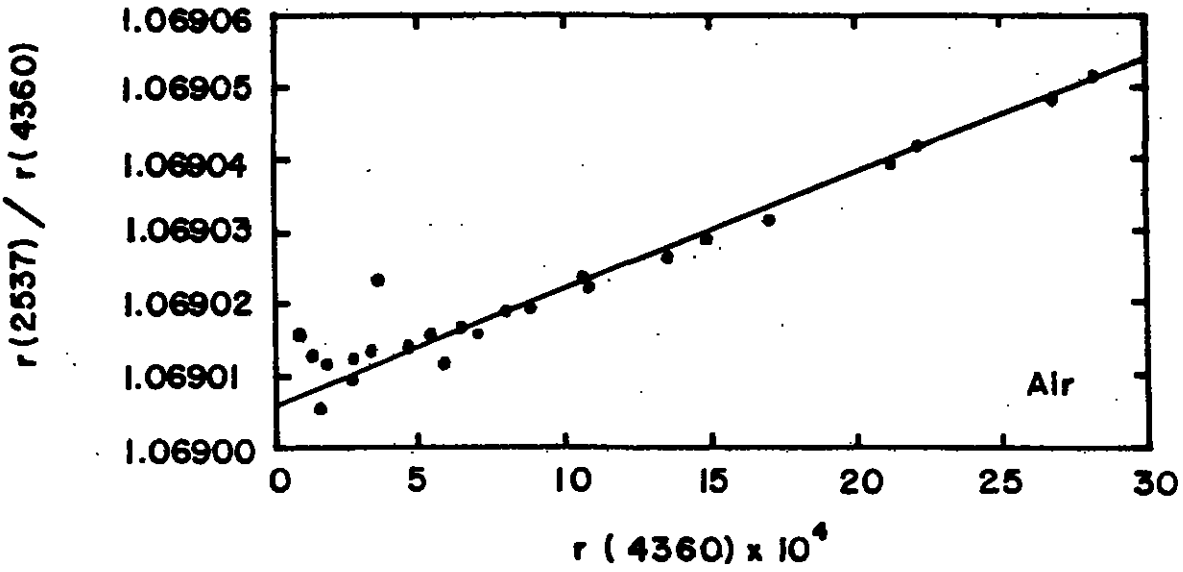

Figure B.1: Variation of the Relative Refractivity of Air vs $n-1$

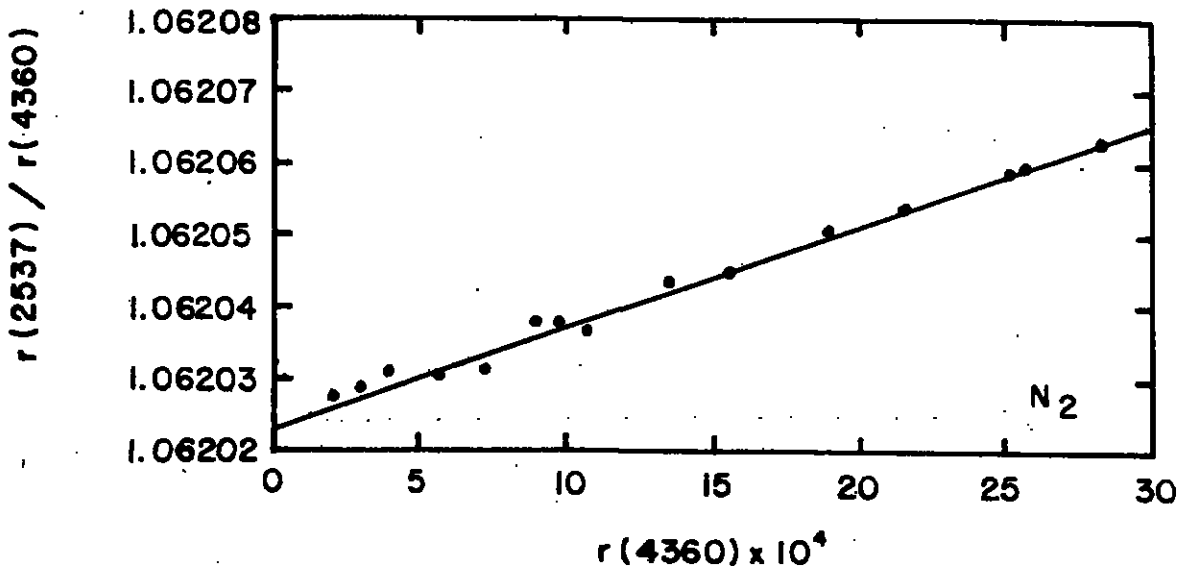

Figure B.2: Variation of the Relative Refractivity of N_2 vs $n-1$.

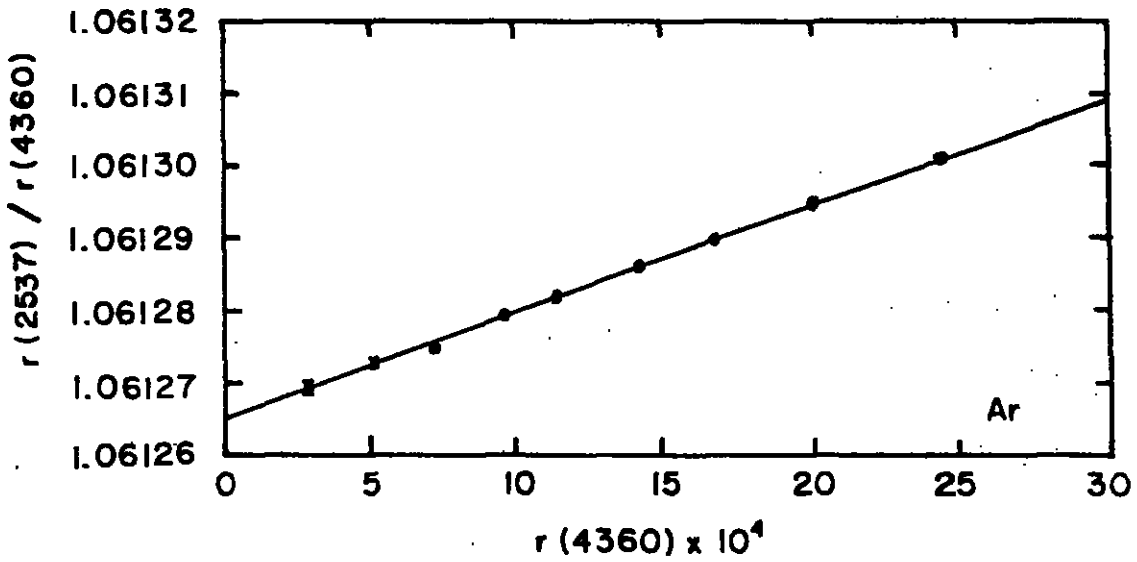

Figure B.3: Variation of the Relative Refractivity of Ar vs $n-1$.

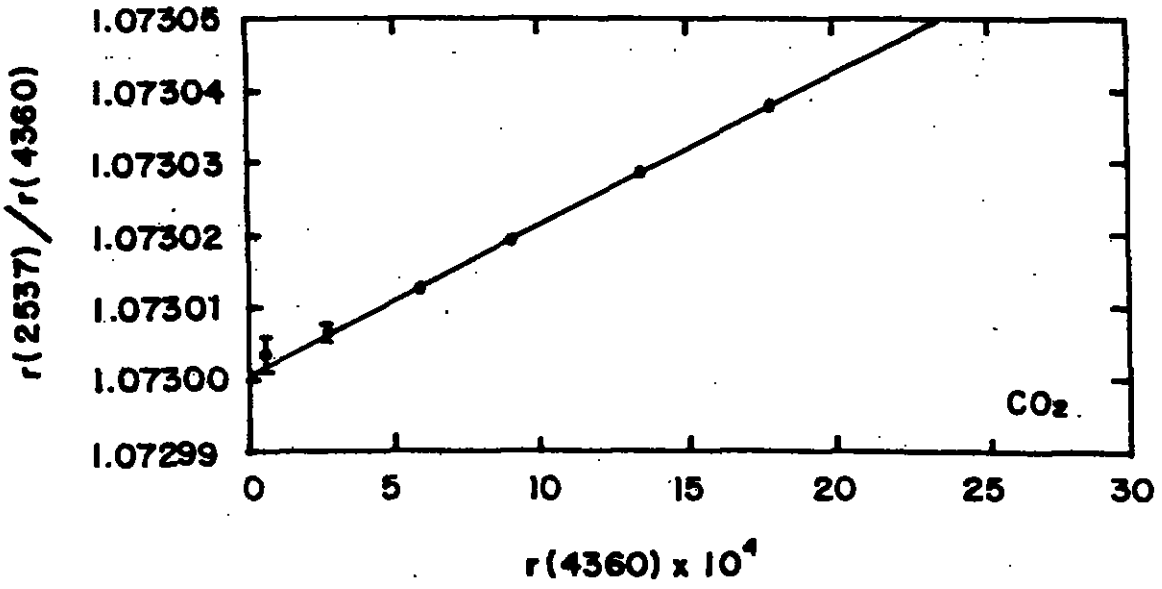

Figure B.4: Variation of the Relative Refractivity of CO_2 vs $n-1$.

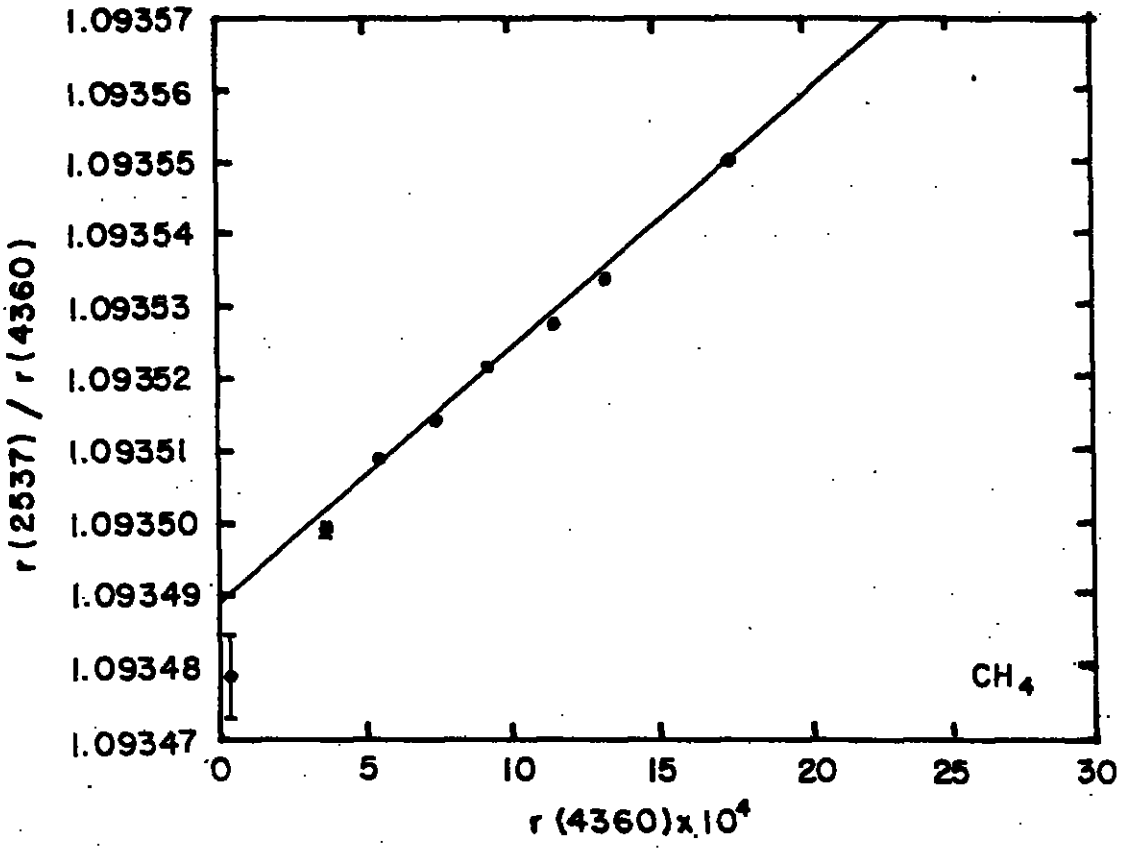

Figure B.5: Variation of the Relative Refractivity of CH_4 vs $n-1$.

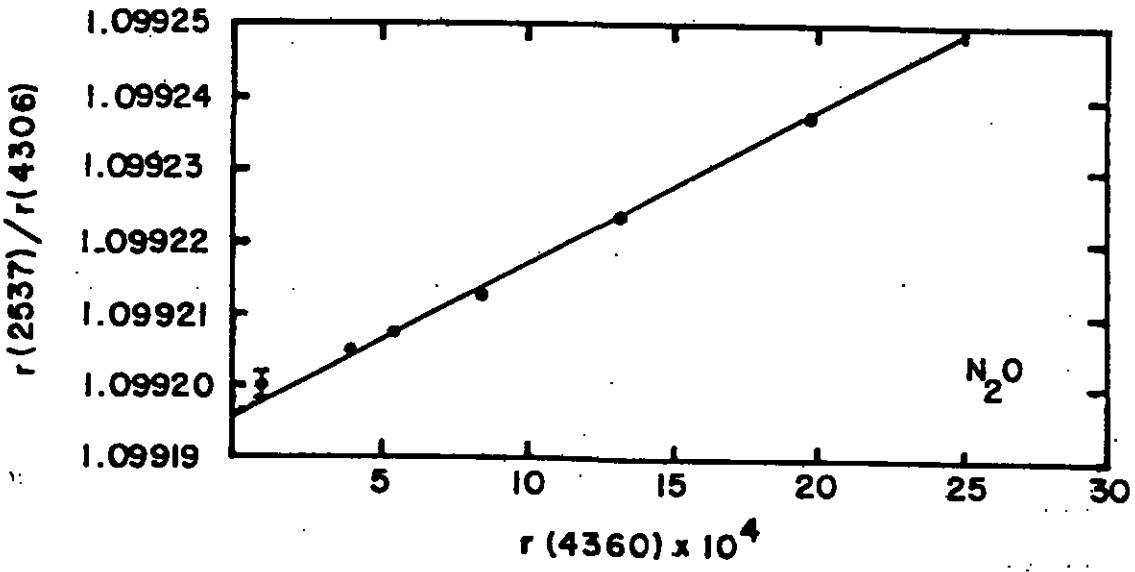

Figure B.6: Variation of the Relative Refractivity of N_2O vs $n-1$.

The coefficients $a(\lambda_1, \lambda_2)$ and $b(\lambda_1, \lambda_2)$ are derived respectively from the intercept and slope of a weighted least squares fit to the data in Figures B.1 to B.6 with weights proportional to $(n-1)^2$. Results are compared with previous measurements in Table B.1. Quoted uncertainties are 2σ precision to the least squares fit.

For water vapor two sets of measurements are reported, the first with scans from 0.5 to 10 torr, which yielded $a(\lambda_1, \lambda_2) = 1.10654 \pm 0.00005$, the second set 0.5 to 5 torr, which yielded $a(\lambda_1, \lambda_2) = 1.10645 \pm 0.00010$. Because the source presure was only 40 torr, the pressure scan-rate decreased exponentially during these scans. Simulations of the fringe-analysis routine applied to sine-waves with an exponentially decreasing frequency indicated that this lead to a systematic error in $a(\lambda_1, \lambda_2)$ of at most $1.5 \cdot 10^{-4}$.

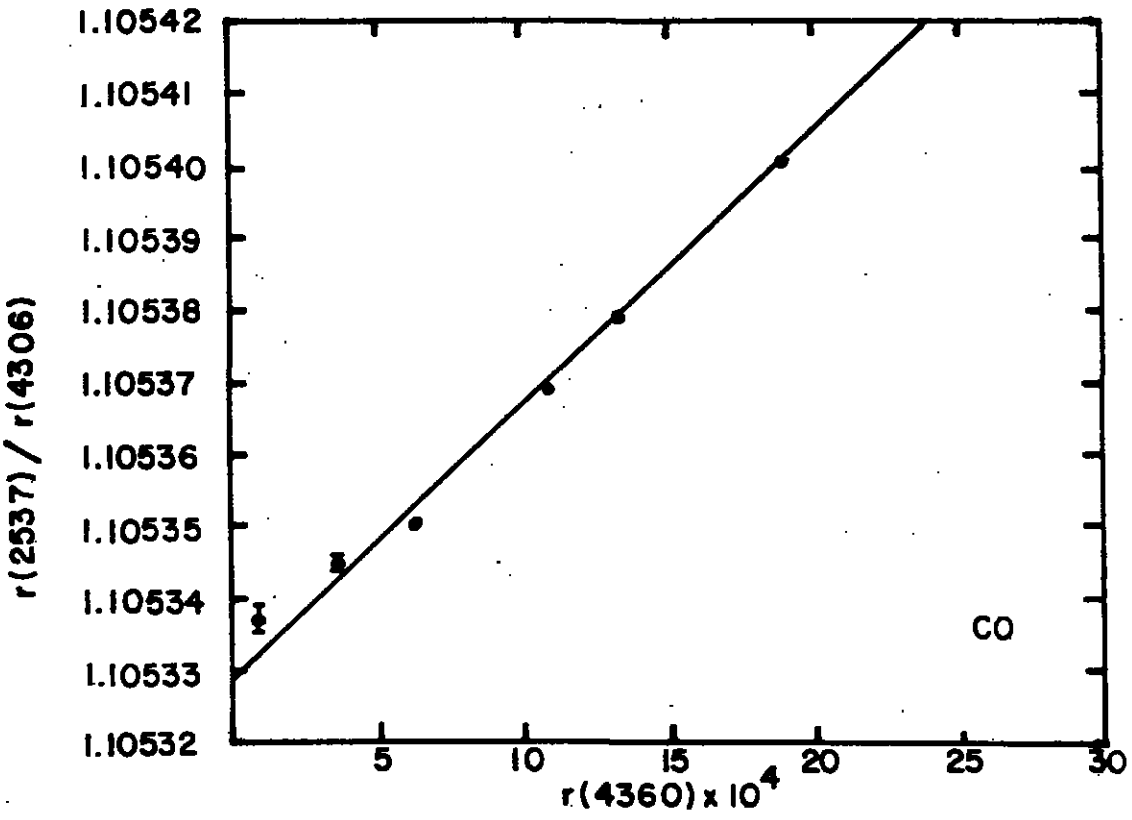

Figure B.7: Variation of the Relative Refractivity of CO vs $n - 1$.

Table B.1: First and second virial coefficients of the relative refractivity of air, N_2, Ar, CO_2, CH_4, CO, and N_2O.

	a(2537,4360)	b(2537,4360)	reference
Air	1.069006 $\pm 2 \cdot 10^{-6}$	0.0157 ±0.0006	This work
	1.06902	—	Edlen (1966)
N_2	1.062024 $\pm 2 \cdot 10^{-6}$	0.0134 ±0.0006	This work
	1.06216	—	Koch (1913)
Ar	1.0612649 $\pm 5 \cdot 10^{-7}$	0.01478 ±0.00022	This work
	1.06119	—	Larsden (1934)
CO_2	1.0730001 $\pm 5 \cdot 10^{-7}$	0.02084 ±0.00036	This work
	1.07304	—	Koch (1914)
CH_4	1.0934889 $\pm 1.5 \cdot 10^{-6}$	0.0347 ±0.0011	This work
CO	1.1053292 $\pm 2.6 \cdot 10^{-6}$	0.0373 ±0.0016	This work
	1.10501	—	Koch (1914)
N_2O	1.0991955 $\pm 9 \cdot 10^{-7}$	0.02109 ±0.00055	This work
H_2O	1.10654 $\pm 1.5 \cdot 10^{-4}$	—	This work
	1.1089	—	Zeiss and Meath (1975)[a]

[a]Calculated from differential photoabsorption data, high energy inelastic scattering data, and visible and ultra-violet refractivity data.

B.3 Ozone Sensitivity Coefficient in Air

The sensitivity coefficient $S_{O_3}^{(air)}$ of air to traces of O_3 was measured by producing trace quantities of O_3 in a stream of air passing though the sample cell of the interferometer and observing the changes in the fringe positions as the ozone concentration was varied. Ozone was produced photolytically in a quartz cell irradiated with 1849 Å emission from a "penray" type Hg lamp. The air used in these measurements was a synthetic mixture of 21.40% O_2 in N_2. The difference in the sensitivity coefficient for this mixture and for natural air is not significant.

The O_3 concentration was measured directly in the optical path of the interferometer through the attenuation of 2537Å fringe signal. The amplitude of modulation of the fringe signal in an interferometer is given by

$$M = 4\sqrt{I_1\ I_2} \tag{B.13}$$

where M is the intensity difference between fringe maximum and fringe minimum, and I_1 and I_2 are the intensities of the coherent beams in the two arms of the cell in the absence of interference. If an absorber, such as O_3, is introduced into one arm of the interferometer, we have from Beer's law

$$\ln\left(\frac{M}{M_0}\right) = \frac{\sigma_{O_3}\ \rho\ X_{O_3}\ (2L)}{2} \tag{B.14}$$

where M_0 is the modulation amplitude in the absence of O_3, σ_{O_3} is the absorption cross section ($1.146 \cdot 10^{-17}$ cm^2 at 2537Å from Mauersberger et al., 1986), ρ is the total number density, X_{O_3} is the O_3 mole fraction, and $2L$ is the active optical path length.

The sensitivity of the relative refractivity of air to traces of O_3, where total O remains constant, is given by

$$\frac{d\bar{r}}{dX_{O_3}} = S_{O_3}^{(air)} - \frac{3}{2}\left[1 - X_{O_2}\right] S_{O_2}^{(air)} \tag{B.15}$$

where

$$S_{O_3}^{(air)} = [\tilde{r}_{O_3} - \tilde{r}_{air}] \frac{n_{O_3}(\lambda_2) - 1}{n_{O_2}(\lambda_2) - 1} \tag{B.16}$$

and

$$S_{O_2}^{(air)} = \frac{\tilde{r}_{O_3} - \tilde{r}_{O_2}}{1 - X_{O_2}} \frac{n_{O_3}(\lambda_2) - 1}{n_{O_2}(\lambda_2) - 1}. \tag{B.17}$$

The second term on the r.h.s. of Eq. B.15 accounts for the O_2 loss which must stoichiometrically balance the O_3 formed.

Fig. B.8 shows the measured changes in $\tilde{r}$ as a function of the O_3 mole fraction. $\delta\tilde{r}$ was derived from the change in the 2537Å fringe remainder

$$\delta\tilde{r}(\lambda_1, \lambda_2) = \frac{\delta\epsilon}{p_2} \tag{B.18}$$

where p_2 was estimated from the known cell pressure and temperature. A linear least-squares fit to the data yields a slope of $(4.23 \pm 0.22) \cdot 10^{-7}$ ppm^{-1} (all quoted uncertainties are 2σ precision). From Eq. B.15 we have

$$S_{O_3}^{air} = 4.23 \cdot 10^{-7} + (3/2)(1 - 0.20946)(3.10 \cdot 10^{-8}) = (4.59 \pm 0.22) \cdot 10^{-7}. \tag{B.19}$$

Similar measurements are reported using pure O_2 as the source gas. The sensitivity of the relative refractivity of O_2 to traces of O_3 is given by

$$\frac{d\tilde{r}}{dX_{O_3}} = S_{O_3}^{(O_2)} \tag{B.20}$$

where

$$S_{O_3}^{(O_2)} = [\tilde{r}_{O_3} - \tilde{r}_{O_2}] \frac{n_{O_3}(\lambda_2) - 1}{n_{O_2}(\lambda_2) - 1}. \tag{B.21}$$

Data with O_2 as the source gas are shown in Fig. B.9. The linear least-squares fit yields $S_{O_3}^{(O_2)} = (4.55 \pm 0.16) \cdot 10^{-7}$ ppm^{-1}.

From Eqs. B.16 and B.21 it follows that

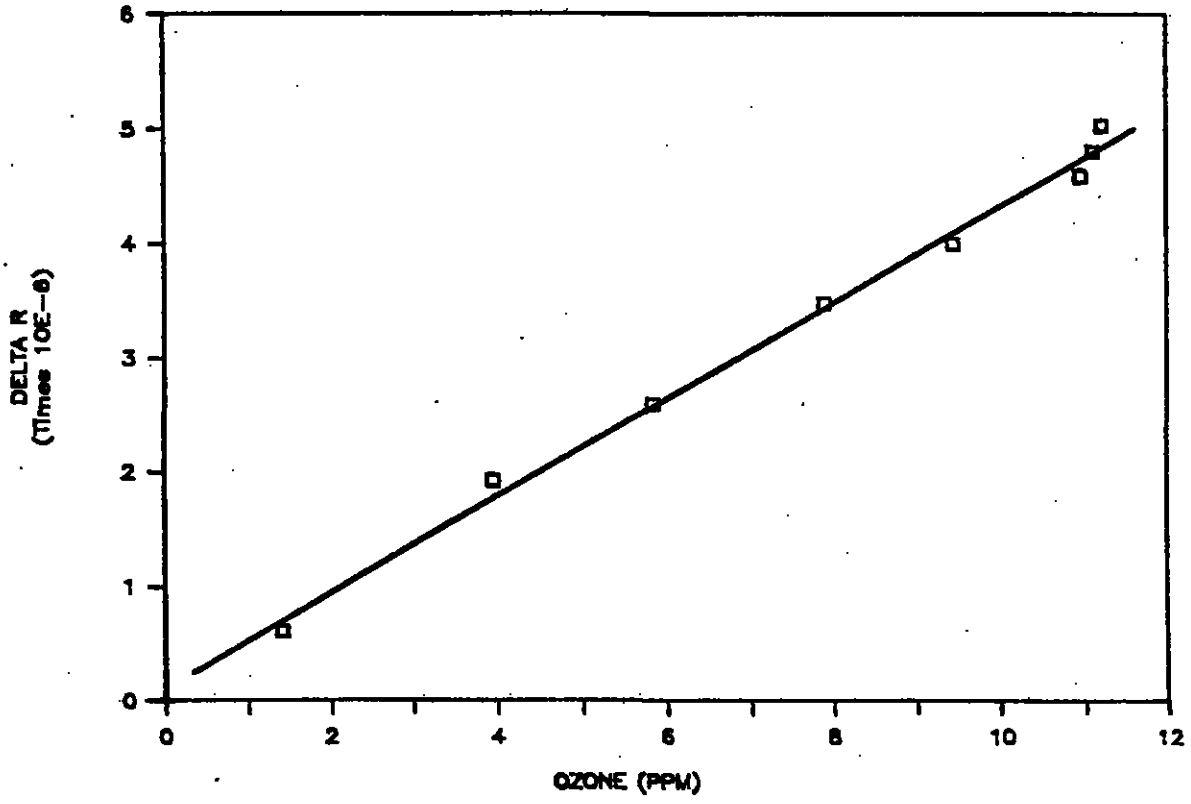

Figure B.8: Variation of the relative refractivity of air with trace O_3.

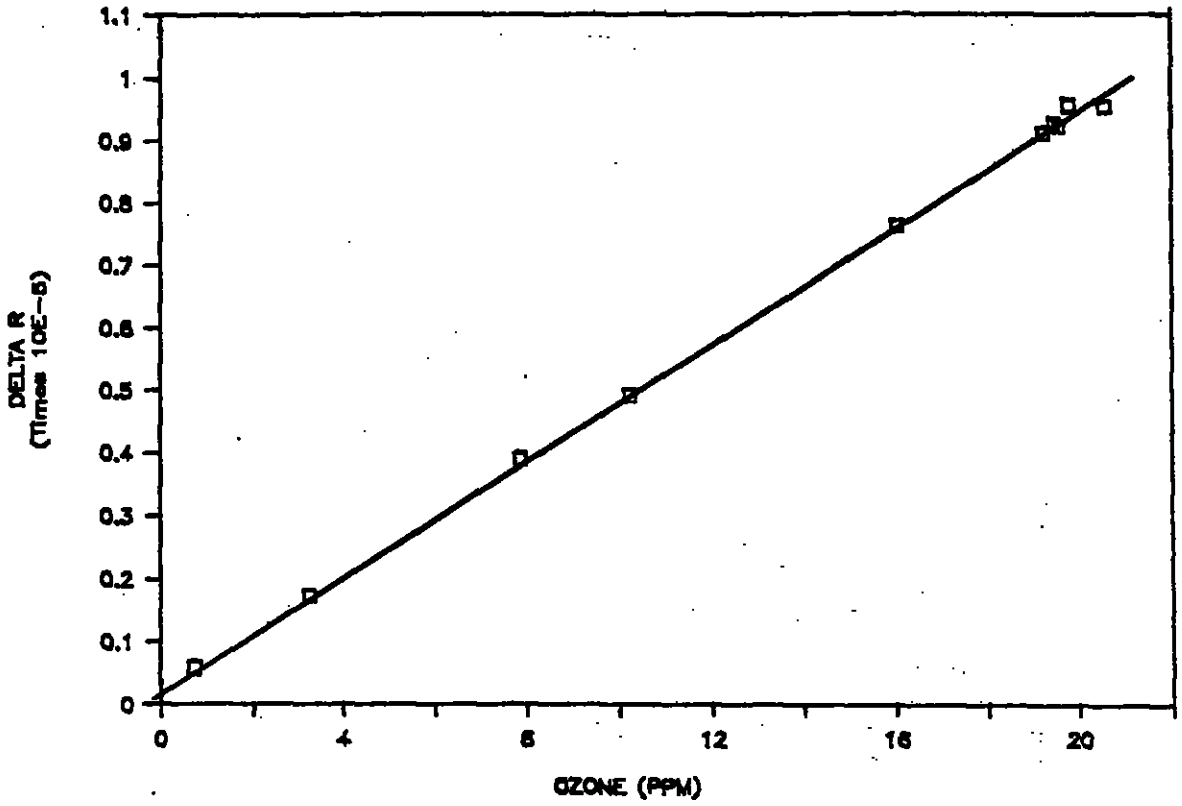

Figure B.9: Variation of the relative refractivity of O_2 with trace O_3.

$$S_{O_3}^{(air)} = S_{O_3}^{(O_2)} \cdot \frac{n_{O_2}(\lambda_2) - 1}{n_{air}(\lambda_2) - 1} + [\bar{r}_{O_2} - \bar{r}_{air}] \cdot \frac{n_{O_3}(\lambda_2) - 1}{n_{air}(\lambda_2) - 1} \qquad \text{(B.22)}$$

which provides a consistency check for the value of measurement of $S_{O_3}^{(air)}$ derived above if $n_{O_3}(\lambda_2)$ is known.

It appears that the only reported refractivity measurements of O_3 are those of Cutherbertson and Cutherbertson (1912) carried out over the wavelength range 4800 to 6708 Å. Extrapolating their data to 4360 Å, I estimate

$$n_{O_3}(4360) - 1 = 5.8 \cdot 10^{-4}$$

which yields from, Eq. B.22,

$$S_{O_3}^{(air)} = (4.80 \pm 0.1) \cdot 10^{-7} \text{ppm}^{-1}$$

where the uncertainty allows for both the uncertainty in $S_{O_3}^{(O)_2}$ and a 30% uncertainty in the extrapolated value of $n_{O_3}(4360)$. This result agrees to within the error limits with the result derived above from measurements in air.

B.4 Temperature Sensitivity of N_2

The interferometer cell block was heated inside an insulated enclosure (cardboard walls filled with glass wool) to approximately 40 °C, and measurements of the relative refractivity of N_2 were carried out as the cell temperature relaxed back to ambient temperature. The characteristic time for the system to relax to room temperature was approximately 15 hours. A pair of thermistors, which were placed near opposite ends of the cell block, recorded the cell temperature. The thermistors were calibrated against a pair of glass thermometers which were accurate to 0.1 °C.

The thermistor data indicated that throughout these measurements there was a persistent 0.5°C difference in the temperature at opposite ends of the cell block. This was probably due to the power dissipation of two capacitance pressure gauges which were inside the enclosure nearer the warmer end. Other than this constant offset, the temperature differences recorded by the two thermistors were smaller than 0.2 °C.

The relative refractivity was determined according to

$$\tilde{r}(\lambda_1, \lambda_2) = \frac{\lambda_1}{\lambda_2} \frac{p_1 + \epsilon - \epsilon^{(0)}}{p_2}$$

where p_1 and p_2 are integers which represent the integral order of the optical-path-difference at λ_1 and λ_2 caused by introducing N_2 into the sample cell, ϵ and $\epsilon^{(0)}$ are the fractional orders at λ_1 (relative to the integral λ_2 order) for the filled cell and evacuated cell, respectively. All measurements were carried out at a constant value of $p_2 = 2000$ corresponding to $n(\lambda_2) - 1 = 7.13 \cdot 10^{-4}$. Sequential measurements of ϵ and $\epsilon^{(0)}$ were taken by alternately filling and evacuating the sample cell. The difference $\epsilon - \epsilon^{(0)}$ was calculated by interpolation.

Two separate temperature runs were carried out. The measured relative refractivities for both runs are shown in Fig. B.10 plotted against the cell temperature, taken as the mean of the two thermistor readings. A least-squares fit of the data yields a slope of $2.7 \pm 0.8 \cdot 10^{-7}$ (2σ) °C^{-1}. Because of the difficulty in ruling out possible systematic errors caused, for example, by temperature gradients in the gas or cell windows, the data should be interpreted as an upper limit to the possible temperature dependence. Thus, the maximum temperature dependence compatible with the data is $4 \cdot 10^{-7}$ °C^{-1}.

B.5 References

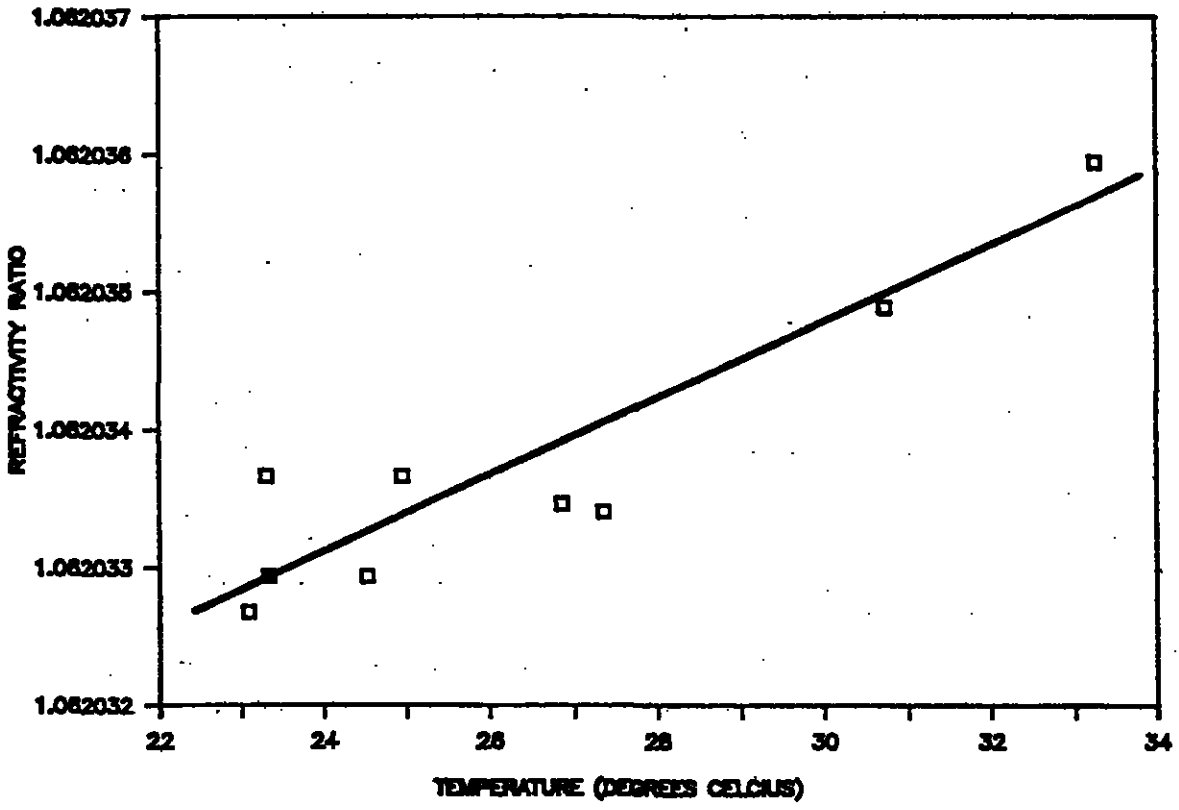

Figure B.10: Variation of the relative refractivity of N_2 vs temperature

Buckingham, A. D., Graham, C., 1974, "The density dependence of the relative refractivity of gases," *Proceedings of the Royal Society of London. A.* **336**, 275–291.

Buckingham, A. D., Pople, J. A., 1955, "The statistical mechanics of imperfect polar gases part 1.– second virial coefficients," *Transactions of the Faraday Society* **51**, 1173–1179.

Cuthbertson C., M. Cuthbertson, 1913, "On the refraction and dispersion of the halogens, halogen acids, ozone, steam, oxides of nitrogen and ammonia," *Philosophical Transactions of the Royal Society, Series A* **213**, 1-26.

Edlen, B., 1966, "The refractive index of air," *Metrologica* **2(2)**, 71–80.

Larsden, T., 1934, *Z. Physik* **88**, 389.

Longhurst, R. S., 1973., *Geometrical and Physical Optics, Third Ed.* Hong Kong, Commonwealth Printing Press Ltd.

Koch, J., 1913, "Über die Dispersion des Lichtes in gasförmigen Körpern innerhalb des ultravioletten Spektrums. Zweite Mitteilung.," *Arkiv för Matematik, Astronomie och Fysik* **9(6)**, 1-11.

Koch, J., 1914, "Über die Dispersion des Lichtes in gasförmigen Körpern innerhalb des ultravioletten Spektrums. Dritte Mitteilung.," *Arkiv för Matematik, Astronomie och Fysik* **10(1)**, 1-10.

Mauersberger, K., J. Barnes, D. Hanson, J. Morton, 1986, "Measurement of the ozone absorption cross-section at the 253.7 nm mercury line," *Geophysical Research Letters* **13(7)**, 671–673.

Zeiss, G. D., W. J. Meath, 1975, "The H_2O–H_2O dispersion energy constant and the dispersion of the specific refractivity of dilute water vapour," *Molecular Physics* **30(1)**, 161–169.

Appendix C

Digital Fringe Analysis Algorithm

We start with a discrete representation of the raw fringe signals

$$S_k^{(1)} = 1 + cos(\frac{2\pi k}{T^{(1)}} + \phi^{(1)}) + \text{"noise"}$$

$$S_k^{(2)} = 1 + cos(\frac{2\pi k}{T^{(2)}} + \phi^{(2)}) + \text{"noise"}$$

where k is the sampling index. Our goal is to derive from these signals an estimate of the phase of $S^{(1)}$ at a particular maximum of $S^{(2)}$.

The first step is to filter the fringe signals according to

$$\bar{S}_k^{(1)} = \sum_{l=-n^{(1)}}^{n^{(1)}} F_l \cdot S_{k+l}^{(1)}$$

$$\bar{S}_k^{(2)} = \sum_{l=-n^{(2)}}^{n^{(2)}} F_l \cdot S_{k+l}^{(2)}$$

where the symmetry filter F_l is given by

$$F_l = \begin{cases} -1 & \text{if } l > 0 \\ 0 & \text{if } l = 0 \\ 1 & \text{if } l < 0 \end{cases} .$$

The filter half widths, $n^{(1)}$ and $n^{(2)}$ are chosen to yield, to within round-off error, the relations $n^{(1)} = T^{(1)}/2$ and $n^{(2)} = T^{(2)}/2$. The symmetry filter serves to attenuate the high frequency noise and to transform the extrema of $S_k^{(1)}$ and $S_k^{(2)}$ into zero-crossings in $\tilde{S}_k^{(1)}$ and $\tilde{S}_k^{(2)}$. These zero-crossings are located by Newton's method, i.e. by interpolating on the basis of the adjacent positive and negative values. This results in arrays $Z^{(1)}(i)$ and $Z^{(2)}(j)$ where i and j index the successive maxima and minima of the orginal signals and where Z expresses the "time" of occurrence of the zero-crossing in units of the original sampling index k. Since $T^{(1)}$ and $T^{(2)}$ are not known initially, they are derived iteratively. From a default guess for $n^{(1)}$ and $n^{(2)}$ we calculate the arrays $Z^{(1)}(i)$ and $Z^{(2)}(j)$ which then are least-squares fitted against the independent variables i and j. The fringe periods $T^{(1)}$ and $T^{(2)}$, which are given by twice the slope of the fitted lines, are used then for a revised estimate of $n^{(1)}$ and $n^{(2)}$. The iteration converges rapidly, and needs only to be performed for the first run since $T^{(1)}$ and $T^{(2)}$ vary insignificantly between runs.

The next step is to express the "times" of occurrence of the zero-crossings of $\tilde{S}_k^{(2)}$ using zero-crossings of $\tilde{S}_k^{(1)}$ as an effective clock. This is done by a point by point interpolation; i.e., for each zero-crossing $Z_j^{(2)}$ we calculate

$$Z_j = \frac{Z^{(2)}(j) - Z^{(1)}(i_j)}{Z^{(1)}(i_j + 1) - Z^{(1)}(i_j)} + i_j$$

where i_j is the index for the zero-crossing $Z^{(1)}(i_j)$ which occurred most recently prior to the zero-crossing $Z^{(2)}(j)$. This interpolation yields an approximately

linear relation between the zero-crossings of $\bar{S}_k^{(1)}$ and $\bar{S}_k^{(2)}$ even in the presence of non-uniformities in the original fringe scan rate. The array Z_j is fitted in an ordinary linear least-squares fitting routine against the independent variable j. The relative frequency of the two fringe signals is given by the slope b of the fitted line, and the phase $\phi_0^{(1)}$ of $S_k^{(1)}$ measured relative to the "first" maximum of $S_k^{(2)}$ is related to the intercept a of the fitted line according to

$$\frac{\phi_0^{(1)}}{2\pi} = \begin{cases} a/2 & \text{if } p^{(1)} > 0;\ p^{(2)} > 0 \\ (a-b)/2 & \text{if } p^{(1)} > 0;\ p^{(2)} < 0 \\ (a+1)/2 & \text{if } p^{(1)} < 0;\ p^{(2)} > 0 \\ (a+1-b)/2 & \text{if } p^{(1)} < 0;\ p^{(2)} < 0 \end{cases}$$

where $p^{(1)}$ and $p^{(2)}$ denote the polarity of the first zero-crossing $(i,\ j = 0)$ of $\bar{S}_k^{(1)}$ and $\bar{S}_k^{(2)}$ where positive polarity denotes a fringe maximum. If the condition $p^{(2)} > 0$ holds, the "first" maximum of $S_k^{(2)}$ is the maximum at $j = 0$; otherwise the "first" maximum is the virtual maximum at $j = -1$.

The least-squares fit achieves the highest precision in the relative phase of the signals for fringes occurring near the center of the scan. Thus it is advantageous to select a centrally located reference fringe rather than e.g. the "first" fringe. The relative phase of signals at the reference fringe is given by

$$\frac{\phi_{\text{ref.}}^{(1)}}{2\pi} = \frac{\phi_0^{(1)}}{2\pi} + a \cdot \Delta p^{(2)}$$

where $\Delta p^{(2)}$ is the difference in the fringe order at the 'first' fringe and the reference fringe. The fringe remainder ϵ_1 is given by

$$\epsilon_1 = \frac{mod_{2\pi}(\phi_{\text{ref.}}^{(1)})}{2\pi}$$

where $mod_{2\pi}(x)$ denotes x modulus 2π.

Appendix D

Hg Lamp: Use in Interferometry

D.1 Introduction

The relative refractivity measurements described in this thesis rely on the interference fringes generated by the 4359.56 and 2537.27Å lines of a low pressure Hg lamp. Although the Hg lines have long been used for interferometry (see e.g. Michelson and Morley, 1889), few previous applications have called for such high fractional fringe resolution (10^{-3} to 10^{-4} of a fringe). At this level there are many subtle features in the emission spectrum of Hg lamps (e.g. secondary lines, continuum background, hyperfine splittings) which can contribute to the apparent fringe positions. The contributions may vary depending on the lamp type, on the operating conditions, and on the method of spectral filtering. The purpose of this Appendix is to summarize measurements of the various contributions.

I have used two types of Hg lamps throughout these investigations. The first is an electrodeless lamp supplied by Ophthos Instruments. This lamp contains about 1 mg of ^{198}Hg and 3 torr of Ar. The lamp is exited in a Broida cavity with

5 watts of net input power at 2.42 GHz. The lamp is supplied with a quartz jacket which is intended to be used for water cooling the lamp. Because liquid water tends to absorb the microwave power, I found it convenient to cool the lamp by forcing a flow of N_2 through the jacket. N_2 cooling achieves adequate output-power stability and seems to extend the lamp life.

The second type of lamp is a standard "penray"-type lamp which consists of a capillary "U" tube with electrodes at either end. These lamps contain a trace of natural Hg and 50 to 100 torr of Ar. I operate these lamps at 7 milliamperes of DC current using 500 V in series with a 50Ω ballast resistor and using only passive cooling (e.g. embedding the lamp in an aluminum block). Lamp life is extended by occasionally reversing the polarity of the power supply.

D.2 Interfering Spectral Lines

The energy level diagram of Hg I and the wavelengths of the more intense emission lines are shown in Figure D.1. The 2537.27Å ($6s^2\ ^1S_0 - 6p\ ^3P_1$) line is well isolated from other prominent Hg lines. In a background gas of Ar, however, a weak Ar line is present at 2535.47Å. The 4359.56Å ($6p\ ^3P_1 - 7s^3S_1$) line has potential interfering lines due to Hg at 4340.44Å ($6\ ^1P_1 - 7d\ ^3D_2$) and 4348.72Å ($6p^1\ ^1P_1 - 7d\ ^1D_2$). All of these lines are transmitted through "stock" 100Å bandpass (FWHM) Hg-line interference filters. The potentially significant adjacent lines and relative intensities are summarzed in table D.1.

In the presence of interfering lines the "sinusoidal" fringes of a two-beam interferometer consist of a superposition of the fringes of the primary line with fringes of the interfering lines. Considering first the effect of a single weak

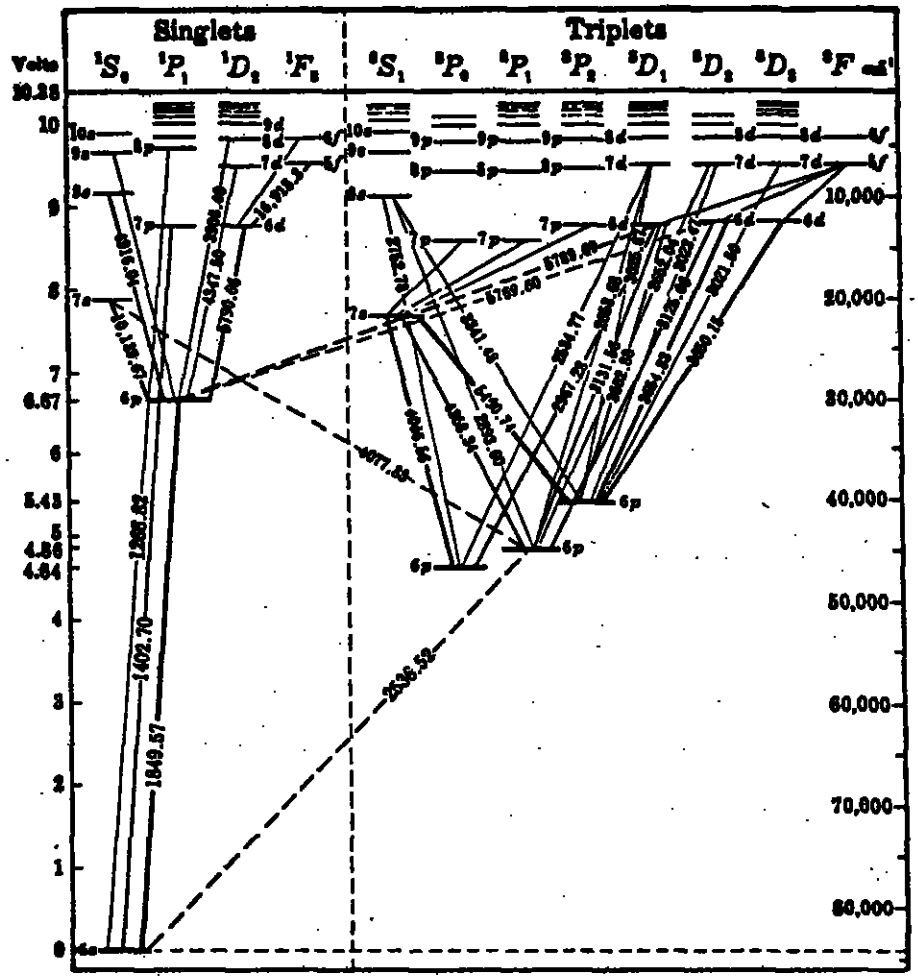

Figure D.1: Energy level diagram of Hg I. The wavelengths of the more intense Hg lines are given. The symbols 6p, etc., written near each level, indicate the true principal quantum number and the l value of the emission electron. From Herzberg (1944).

Table D.1: Hg lines near 2537.27 Å and 4359.56 Å.

Wavelength, Å (vac)	2535.47 (Ar II)	4340.44 (Hg I)	4348.72 (Hg I)
Transition		$6p\ ^1P_1 - 7d\ ^3D_2$	$6p\ ^1P_1 - 7d\ ^1D_1$
Relative Intensity for ^{198}Hg electrodeless lamp	0.0024[a]	0.0057[b]	0.014[b]
Relative Intensity for natural Hg penray-type lamp	0.0001[a c]	0.0010[b]	0.0040[b]

[a]Relative to 2537Å line.
[b]Relative to 4360Å line.
[c]Measured with 2537Å blocked by Hg–Ar absorption cell.

adjacent line, we can represent the total detector signal by,

$$S(x) = cos(2\pi x/\lambda_0) + \epsilon\ cos(2\pi x/\lambda') \tag{D.1}$$

where x denotes the optical path difference in cm and where ϵ is the ratio of the intensity of the weaker line λ' to the primary line λ_0. To first order in ϵ it follows that

$$S(x) = A\ cos(\frac{2\pi x}{\lambda_0} - \Phi) \tag{D.2}$$

where

$$A = 1 + \epsilon \cdot cos(2\pi x(\frac{1}{\lambda_0} - \frac{1}{\lambda'})) \tag{D.3}$$

and

$$\Phi = \epsilon \cdot sin(2\pi x(\frac{1}{\lambda_0} - \frac{1}{\lambda'})) \tag{D.4}$$

Considering, for example, the interference of the 4348.72Å line with the 4359.56Å line for which $\frac{1}{\lambda_0}/(\frac{1}{\lambda'} - \frac{1}{\lambda_0}) = 402$ and $\epsilon = 0.014$, we find from Eq. D.4 that the

phase of the fringe signal is shifted by as much as $\epsilon/(2\pi) = 2.2 \cdot 10^{-3}$ of a fringe with a periodicity of 402 fringes.

The fringe shifts due to multiple interfering lines are additive. The effect of multiple lines on the relative phase of the 4359.56Å and 2537.27Å fringes is illustrated in Fig. D.2 where the fractional 2537.27Å fringe count is plotted versus the 4359.56Å fringe count (relative to the zeroth order fringe) as nitrogen gas is bled into the sample cell (a linear regression to the 2537.27 Å fringe count versus 4359.56Å fringe count has been subtracted from the data to allow the small fringe shifts to be displayed graphically). An air-cooled electrodeless ^{198}Hg lamp with 100Å interference filters was employed. The short-term oscillations are consistent with Eq. D.4 for the combined effects of the interfering lines listed in Table D.1. (The overall curvature is due to the non-linear density dependence of refractive index discussed in Appendix B.)

Interfering lines cause errors in the differential gas measurements if their relative intensities are unsteady. I have found that the relative intensity of some of the lines listed in Table D.1 can vary by as much as a factor of two during the first hour after turning on the lamp. The relative intensity of these lines is also sensitive to the lamp excitation conditions. For example, I have observed a 50% increase in the relative intensity of the 4347.5Å line caused by increasing the net forward microwave power into the lamp from 6 watts to 22 watts.

Such errors can be greatly reduced by employing a custom 10Å FWHM filter which is angle-tuned to eliminate the 4340.44 and 4348.72 Å lines. I have shown that this procedure alone reduces the maximum errors in the relative phase of the 2537.27 Å and 4359.56Å fringes to less than $5 \cdot 10^{-4}$ of a 2537.27Å fringe.

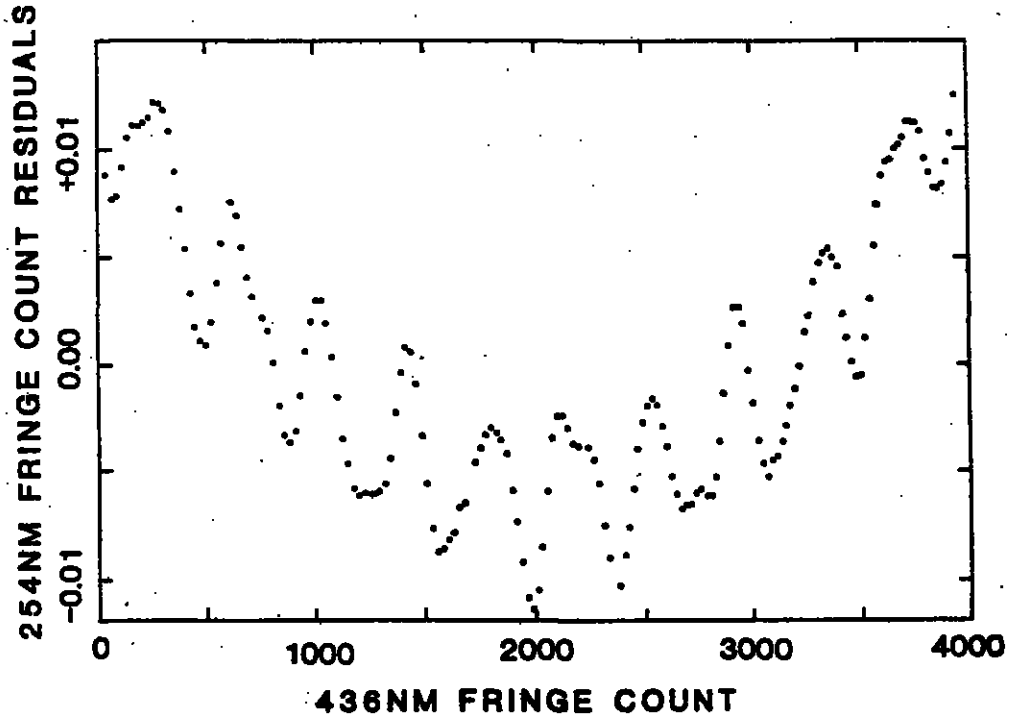

Figure D.2: 2537Å fringe order residuals versus 4360Å fringe order.

D.3 Continuum Background

Broad-band and continuum emissions, which have been attributed to Hg–Hg or Hg–{inert gas} dimers, have been observed in electrically discharged or optically excited mixtures of Hg and inert gases (Mitchell and Zemansky, 1971 pp 87–89). Because continuum emissions which happen to lie within the band-pass of the Hg-line filters could lead to errors in fringe position (particularly at low optical path differences), I undertook to measure the continuum background of both the electrodeless- and "penray"-type lamps in the vicinity of the 2537.27 and 4359.56 Å lines.

The lamp emission was examined with a grating spectrometer and photomultiplier detector. In order to reduce scattered light in the spectrometer caused by Hg-line emissions, an interference filter was placed between the lamp and the spectrometer. For measurements in the vicinity of the 4359.56Å line, a 10Å bandwidth angle-tuned interference filter was employed which could be tuned to either side of the 4359.56Å line. For measurements in the vicinity of the 2537.27Å line, a 100Å filter was used which effectively rejected all prominent Hg lines except the 2537.27Å line. The intensity of the 2537.27Å line was then further reduced (by a factor of 15 and 150 for the ^{198}Hg and natural Hg lamps respectively) relative to adjacent spectral regions by interposing between the lamp and the filter a 10 cm absorption cell saturated with Hg vapor and filled with 1 atm Ar. The spectrometer was then scanned over the transmission band of the filter, and the difference between the photomultiplier count rate and the photomultiplier dark count was recorded.

The measurements confirmed that the continuum-background emissions from these lamps are very weak. Upper limits to the continuum-background intensities were estimated based on the photomultiplier dark-current and other noise

Table D.2: Continuum background intensities of Hg lamps.

lamp type	4410-4420 Å[a]	2500-2600Å[b]
Electrodeless lamp ^{198}Hg[c]	$< 1 \cdot 10^{-5}$Å^{-1}	$< 2.5 \cdot 10^{-5}$Å^{-1}[d]
Penray lamp, natural Hg[e]	$< 6.5 \cdot 10^{-5}$Å^{-1}[e]	$< 2.5 \cdot 10^{-5}$Å^{-1}

[a]Intensity per Å bandwidth relative to total intensity of 4359.56Å line.
[b]Intensity per Å bandwidth relative to total intensity of 2537.27Å line.
[c]Net 3 watts into lamp cavity.
[d]Valid outside of ±5 Å of the 2537 Å line.
[e]7mA DC lamp current.

sources (e.g. the uncertainty in the intensity of the wings of the Hg lines caused by the spectrometer slit function) and are indicated in Table D.2. The upper limits are sufficiently small that the continuum background emission cannot lead to significant errors in fringe position even if stock interference filters (100Å FWHM) are used to isolate the 2537.27Å and 4359.56Å lines.

D.4 Hyperfine Structure

Natural Hg consists of four even and two odd isotopes as summarized in Table D.3. The hyperfine splittings of the 2537.27 and 4359.56 Å emission lines contain contributions from both the mass isotope effect and nuclear spin interactions. The splittings have been measured and terms identified by Schüler and Keystone (1932) and are summarized in Table D.3. The even isotopes, with $I = 0$, each contribute a single component. The odd isotopes, ^{199}Hg and ^{201}Hg, each contribute a multiplet of components because of nuclear-spin interactions.

The use of a natural Hg lamp as an interferometric source has two limita-

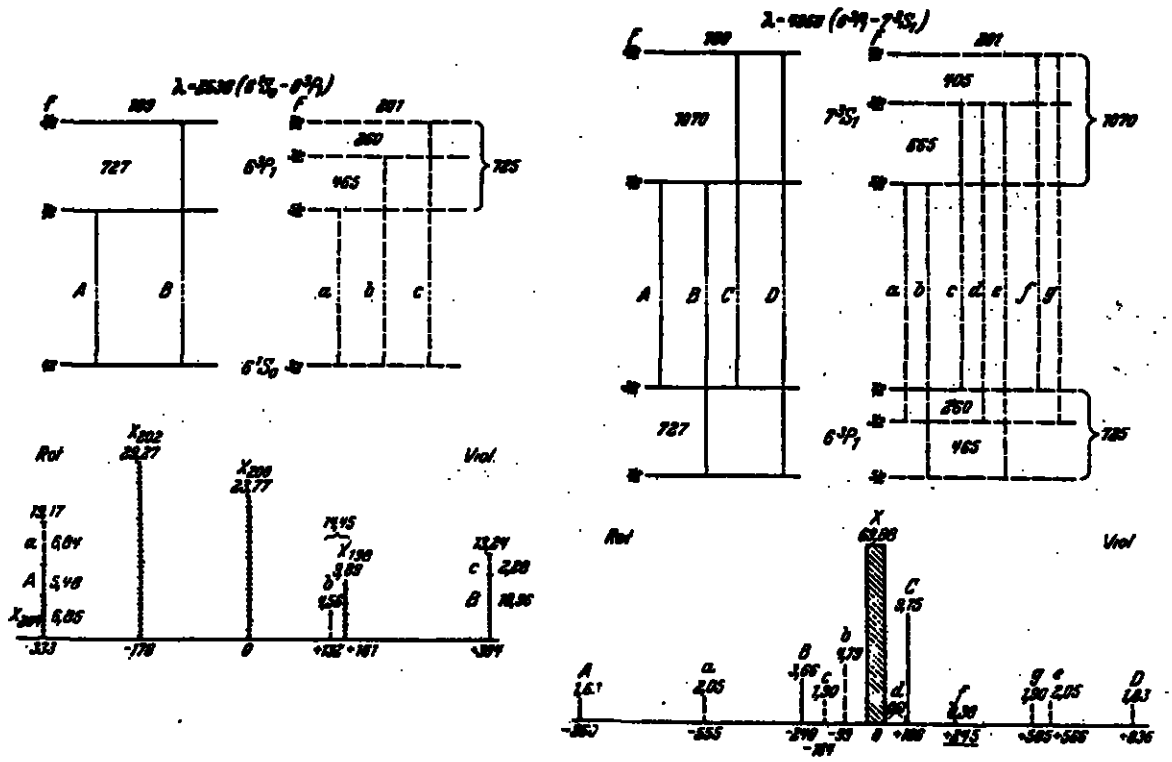

Figure D.3: Hyperfine spectrum of the 2537Å and 4358Å lines of natural Hg from a water cooled DC discharge lamp from Schüler and Keyston (1932). Components of ^{199}Hg are labeled with capital letters A, B, etc., components of ^{201}Hg are labeled with small letters a, b, etc., and components of even isotopes are labeled by X. Hyperfine splittings are in units of 10^{-3} cm^{-1}.

Table D.3: Hg stable isotopes, natural abundances, and nuclear spin[a]

Atomic no.	Natural Abundance, %	Spin, I
198	10.02	0
199	16.84	$\frac{1}{2}$
200	23.13	0
201	13.22	$\frac{3}{2}$
202	29.80	0
204	6.85	0

[a]Chemical Rubber Company, 1974.

tions:

- The coherence length of the lines is limited by hyperfine structure. For the present application this is not a serious limitation because the effective optical-path-length used for the relative refractivity measurements is typically 0.4 cm, which is short compared to the coherence length of natural Hg. The coherence length limitation of natural Hg would preclude the extension of the method to longer optical paths, however.

- The mean frequency of the emission lines varies with lamp operating conditions because of variations in the relative intensity of the different hyperfine components. This is a more serious difficulty because it leads directly to shifts in the relative position of the 2537.26 and 4359.56Å fringes. I have found that the ratio of the mean frequency the 2537.26 and 4359.56 Å lines is sensitive at the $5 \cdot 10^{-7}$ level to changes in the anode current of "penray" lamps filled with natural Hg.

D.5 Broadening and Frequency Shifts of ^{198}Hg

The coherence limitations of natural mercury have long been recognized (Michelson, 1892). Although it was obvious by the 1930's that these limitations could be overcome by preparing Hg artificially with a single even isotope, this was not realized until the 1940's when it became possible to prepare sufficient quantities of ^{198}Hg by neutron bombardment of gold (Weins, 1946). The preparation of ^{198}Hg proceeds according to

$$^{197}\mathrm{Au} + n \longrightarrow ^{198}\mathrm{Au}$$
$$^{198}\mathrm{Au} \longrightarrow ^{198}\mathrm{Hg} + \beta^{-1}.$$

A slight impurity of ^{199}Hg has been detected in such artificially prepared Hg which probably results from neutron capture of the ^{198}Au and subsequent decay to ^{199}Hg (Meggers and Westfall, 1950).

The spectral lines of isotopically pure ^{198}Hg are broadened predominantly by two mechanisms: (1) Doppler broadening due to the motion of the molecules relative to the laboratory frame of reference, and (2) Lorentz broadening due to collisions with background gas molecules. Associated with Lorentz broadening is a shift in the spectral emission frequency.

Doppler broadening leads to a frequency distribution of emission given by (see e.g. Mitchell and Zemansky, 1971, pp. 99-100)

$$F(\nu) = F_0 e^{-\left[\frac{2(\nu-\nu_0)}{\Delta\nu_D}\sqrt{\ln 2}\right]^2}$$

where $\Delta\nu_D$ is the Doppler breadth given by

$$\Delta\nu_D = 2\sqrt{2\ln 2}\frac{\nu_0}{c}\sqrt{\frac{RT}{M}}.$$

The simplest theory of Lorenz broadening which takes account of both broadening and frequency shifts leads to a frequency distribution of emission given by

$$F(\nu) = \frac{1}{(\nu_0 + \Delta\nu_0 - \nu)^2 + \left(\frac{\Delta\nu_L}{2}\right)^2}$$

where $\Delta\nu_0$ is the frequency shift and $\Delta\nu_L$ is the Lorentz half–breadth of the line. A more accurate theory would also take account of possible assymmetry in the emission lines (see e.g. Lenz, 1924), which can be neglected in the limit of low pressure. Experiments on Lorentz broadening show that the Lorentz half–breadth and the frequency shift $\Delta\nu_0$ is proportional to the background gas pressure. It is common to express the Lorentz half–breadth in terms of a collision cross section σ_L according to

$$\Delta\nu_L = \frac{2}{\pi}{\sigma_L}^2 \, N\sqrt{2\pi RT\left(\frac{1}{M_1} + \frac{1}{M_2}\right)}$$

where M_1 amd M_2 are the atomic weights of the emitting species and background gas respectively and N is the background gas number density in molecules per cm^3.

Table D.4 lists values for the Doppler widths, Lorentz widths, and Lorentz shifts for the 4359.56Å and 2537.27Å lines in Ar at 300 K.

High contrast fringes have been achieved with the 4359.56 Å lines as well as most other ^{198}Hg lines with optical path lengths as large as 30 cm (Kaufman, 1962). This is consistent with the limitation imposed by Doppler broadening. The 2537.27Å intercombination line, which is subject to self reversal, does not achieve such high coherence lengths, although useful etalon fringes have been attained at a 5 cm spacing (Kaufman, 1962).

Kaufman (1962) has measured the emission lines of a water-cooled ^{198}Hg lamp to an accuracy of ±0.0001Å, and he considers the following lines to be

Table D.4: Broadening and frequency shifts in ^{198}Hg

Hg lines	2537.27Å (39412 cm^{-1})	4359.56Å (22938cm^{-1})
Doppler width @ 300K	0.035 cm^{-1}	0.020 cm^{-1}
Lorentz broadening in Ar		
width $\Delta\nu_L$ per torr Ar	0.0004 cm^{-1}[a]	—
shift $\Delta\nu_s$ per torr Ar[b]	0.00016 cm^{-1}[a]	—
	0.0003 cm^{-1}[c]	0.0004[c]

[a]High pressure measurements of Füchtbauer et al. (1923).
[b]Shifts are towards longer wavelength.
[c]Based on ^{198}Hg lamps filled with 0.4 to 10 torr Ar (Kaufmann, 1962).

acceptable as length standards: 2537, 2652 , 2753, 2894, 2968, 3022, 3126, 3342, 3651, 4047, 4359, 5462, and 5771 Å. Based on the magnitude of the Lorentz shift, one would expect the emission frequencies of these lines from a lamp filled with 3 torr of Ar to be stable at the 10^8 level even in the presence of a 100°C change in lamp temperature.

D.6 References

Chemical Rubber Company, 1974, *Handbook of Chemistry Physics*, CRC Press, Inc., Cleveland.

Füchtbauer, C., Joos, G. Dinkelacker, O., 1923, *Ann. D. Phys.* **71** 204.

Herzberg, G., 1944, *Atomic Spectra and Atomic Structure*, New York, Dover Publications.

Kaufman, V., 1962, "Wavelengths, Energy Levels, and Pressure Shifts in Mercury 198," *Journal of the Optical Society of America* **52(8)**, 866–870.

Lenz, W., 1924, *Zeitschrift för Physik* **25**, 299.

Meggers, W. F., F. O. Westfall, 1950, "Lamps and Wavelengths of Mercury 198," *Journal of Research of the National Bureau of Standards*, **44**, 447–455.

Michelson A. A., E. W. Morley, 1889, *American Journal of Science* **38**, 181.

Michelson A. A., 1892, *Phil. Mag.* **34**, 280.

Mitchell, A. C. G., M. W. Zemansky, 1971, *Resonance Radiation and Exited Atoms*, Cambridge, Cambridge University Press.

Schüler, H., J. E., Keyston, 1931, "Hyperfeinstrukturen und Kernmomente des Quecksilbers," *Zeitschrift för Physik* **72**, 423–441.

Weins, J. H., 1946, "Production of ^{198}Hg as a possible source of an improved wave-length standard," *Physical Review* **70**, 910–914.